elektronisches
dokument
ULB Sachsen-Anhalt

Theoretical investigations on the structure and aggregation of bent-core mesogenic compounds

Dissertation

zur Erlangung des akademischen Grades

doctor rerum naturalium (Dr. rer. nat.)

vorgelegt der

Naturwissenschaflichen Fakultät II – Chemie und Physik

der Martin-Luther-Universität Halle-Wittenberg

von Herrn M. Sc. (Applied Chemistry) Ananda Rama Krishnan Selvaraj

geb. am 12.10.1978 in Vridhachalam (India)

Gutachter:

1. Priv, -Doz. Dr. Rudolf Friedemann
2. Professor Dr. Tim Clark

Halle (Saale), Datum: 08.08.2007

urn:nbn:de:gbv:3-000013108
[http://nbn-resolving.de/urn/resolver.pl?urn=nbn%3Ade%3Agbv%3A3-000013108]

To my beloved parents

Acknowledgements

This dissertation has been prepared from 20.01.2004 to 20.01.2007 under the guidance of Priv. -Doz. Dr. Rudolf Friedemann.

I am grateful to Priv. -Doz. Dr. Rudolf Friedemann for his valuable scientific guidance on my dissertation work, motivating words, correcting our publications and my dissertation. I am also grateful to his family members for their pleasing attitude.

I am grateful to Professor Dr. Carsten Tschierske for the useful scientific discussions, appreciation for the B_7 mesophase model, encouragement and help on my dissertation work.

I am grateful to Professor Dr. Wolfgang Weissflog for his scientific guidance and his appreciation on my dissertation work.

I am pleased to Professor Dr. René Csuk and Professor Dr. Dirk Steinborn for the computational resources and encouragements.

I am grateful to Deutschen Forschungsgemeinschaft (DFG) within the graduate study program No. 894/1 for the financial support and all the members of the program for the cooperation. I am also grateful to Professor Dr. Alfred Blume and Deutschen Akademischen Austauschdienstes (DAAD) for the financial support in the last six months.

My sincere gratitude to Professor Dr. Gerhard Pelzl and Professor Dr. Horst Kresse for their valuable scientific discussions, the correlation between theoretical results with mesophase properties and for the correlation between theoretically calculated dipole moments with experimental dielectric constant values.

I am grateful to my colleagues Dr. R. Amaranatha Reddy and Dr. H.N. Srinivasa Murthy for the useful scientific advices and references. I am also grateful to Dr. Michi Nakata for her valuable appreciation towards the B_7 mesophase model.

I am thankful to Ms. Zinaida Vakhovskaya for the experimental data of dielectric constants.

I am thankful to Dr. Hans-Juergen Walter, Dr. Gerald Möbius and Mr. Frank Broda for their help to work with Gaussian and AMBER programs and continuous cooperation.

I am pleased to Priv. -Doz. Dr. Hans-Herrmann Rüttinger, Professor Dr. Wolf-Dieter Rudolf, Professor Dr. Günter Israel and Professor Dr. Hans-Peter Abicht for their encouraging words.

I am thankful to my colleagues Mrs. Liane Schmidt, Mrs. Diana Schöenbrodt, Dr. Claudia Körb, Dr. Christina Keith, Dr. Marko Prehm, Dr. Christian Albrecht, Ms. Sonja Findeisen, Ms. Diana Ster, Mr. Robert Kieffer and Mr. Volker Schönewerk for their help.

I am grateful to my parents Mr. Selvaraj .M, Mrs. Ranjitham .S and my brother Mr. Karthikeyan .S for their caring words and blessings.

Table of contents

Chapter 1 Introduction 1

1.1 Bent-core or banana-shaped compounds - a new sub-field of liquid crystals 1
1.2 Reports of theoretical investigations on bent-core mesogenic systems 4
1.3 Aim of this work 5

Chapter 2 Theory and methods 7

2.1 *Ab initio* and density functional theory methods 7
2.2 Molecular mechanics and molecular dynamics procedures 9
2.3 Analysis of molecular dynamics results 11
2.3.1 Radial atom pair distribution function 11
2.3.2 Orientational correlation function 12
2.3.3 Diffusion coefficients 12

Chapter 3 Polar substituents on bent-core compounds 13

3.1 Systems and explanations 13
3.2 Computational details 16
3.3 DFT and HF results 18
3.3.1 Substituents on the central unit 18
3.3.1.1 Planar and twisted conformations - superposition with X-ray structure 18

3.3.1.2 One-fold scans 20
3.3.1.3 Two-fold potential energy surface scans 22
3.3.1.4 Dipole moments, ESP group charges and polarizabilities 24
3.3.2 Polar substituents on the external phenyl rings 27
3.3.2.1 Relaxed rotational barriers - ϕ_7 27
3.3.2.2 Dipole moments and ESP group charges 30
3.4 MM results - dimers 32
3.5 MD results - monomers 33
3.5.1 Trajectories of torsion angle - ϕ_1 33
3.5.2 Average structure from MD - superposition with X-ray structure 36
3.5.3 B-factors 37
3.5.4 Bending angles and molecular lengths 38
3.6 MD results - clusters 40
3.6.1 Radial atom pair distribution function and orientational correlation function 41
3.6.2 Diffusion coefficients and root mean square deviations 42

Chapter 4 Influence of the orientation of ester linkage groups on bent-core compounds 45

4.1 Systems and explanations 45
4.2 Computational details 47
4.3 DFT and HF results 48
4.3.1 Relaxed rotational barriers - ϕ_1 and ϕ_7 48
4.3.2 Effect of an external electric field on the rotational barrier 51
4.3.3 Two-fold potential energy surface scans 52
4.3.4 Dipole moments, bending angles and ESP group charges 53

4.3.5 Correlation between dipole moments and dielectric constants 57
4.4 MM results - dimers 59
4.5 MD results - monomers 60
4.5.1 Trajectories of torsion angles - ϕ_1 60
4.5.2 Bending angles and molecular lengths 62
4.6 MD results - clusters 65
4.6.1 Radial atom pair distribution function 65
4.6.2 Pressure effect on g(r) 65
4.6.3 Size effect on g(r) 66
4.6.4 Orientational correlation function 67
4.6.5 Diffusion coefficients 68

Chapter 5 Bent-core vs. linear mesogens 69

5.1 Systems and explanations 69
5.2 Computational details 70
5.3 DFT results 70
5.3.1 Relaxed rotational barriers - ϕ_1 70
5.3.2 Dipole moments, polarizabilities, bending angles and ESP group charges 71
5.4 MD results - monomers 74
5.4.1 Trajectories of torsion angle - ϕ_1 74
5.4.2 Bending angle and molecular length 76
5.5 MD results - clusters 78
5.5.1 Radial atom pair distribution function 78
5.5.2 Density/pressure plots 79
5.5.3 Diffusion coefficients 80

Chapter 6 Cyclic urea - a new central unit in bent-core compounds 82

6.1 Systems and explanations 82
6.2 Computational details 83
6.3 DFT results 83
6.3.1 Relaxed rotational barriers - ϕ_1 83
6.3.2 Two-fold potential energy surface scans 84
6.3.3 Dipole moments, bending angles and diagonal components of polarizability 86
6.3.4 ESP group charges 88
6.4 MM results - dimers 89
6.5 MD results - monomers 92
6.5.1 Trajectory of the torsion angle - ϕ_1 92
6.5.2 Bending angle and molecular length 93
6.6 Two-fold potential energy surface scans of different central units 93

Chapter 7 Hydrogen bonding in bent-core compounds 96

7.1 Systems and explanations 96
7.2 Computational details 97
7.3 HF and DFT results 97
7.3.1 Relaxed rotational barriers - ϕ_1 97
7.3.2 Two-fold potential energy surface scans 98
7.3.3 Dipole moments and bending angles 100
7.3.4 ESP group charges 102
7.3.5 Proton transfer on the bent-core units 103
7.4 MD results - dimers 104

7.4.1 Trajectory of torsion angles - ϕ_1, ϕ_1' and ϕ_4' 104

Chapter 8 Ferroelectric, antiferroelectric and B_7 mesophase model 108

8.1 Systems and explanations 108
8.2 Computational details 109
8.3 The energies of structural models 109
8.4 The proposed helical model for the B_7 mesophase 112
8.5 Proposed new bent-core structures 114
8.5.1 Halogen bonding in bent-core mesogens 114

Chapter 9 Summary 116

Bibliography 122
Abbreviations and symbols 130
Curriculum Vitae 132
Erklärung 133

Chapter 1 Introduction

1.1 Bent-core or banana-shaped compounds - a new sub-field of liquid crystals

Thermotropic liquid crystals are essential molecular electronic materials of the current research due to their technological applications. From the shape of such molecules, they were mainly classified into three types. They are rod-shaped (calamitic), disc-shaped and banana-shaped or bent-core mesogenic molecules. The mesophases formed by the liquid crystalline systems are strongly controlled by molecular shape, reduced symmetry, microphase segregation, self assembly and self-organisation. Chirality is an important phenomenon in such compounds. The introduction of chirality into the liquid crystalline materials has led to interesting non-linear effects like thermochromism, electroclinism, ferroelectricity, antiferroelectricity and pyroelectricity [1-7].

One of the recent interesting kind of thermotropic liquid crystalline systems are bent-core mesogens because these achiral molecules are able to form helical chiral macrostructures. Due to their bent shape, the molecules can tightly pack along the bent direction which led to a long range correlation of the lateral dipole moments and therefore to a macroscopic polarization of the smectic layers.

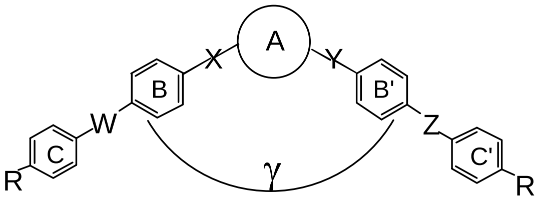

Fig. 1 General structure of bent-core molecules. A: central unit, B,B': middle rings, C,C': outer rings, W,X,Y,Z: connecting groups, R: terminal chains, γ: bending angle.

In tilted smectic layers the achiral bent-core molecules can generate chiral superstructures. Thus, polar order in the smectic layers induces the chirality. The individual packing of the mesogenic molecules led to different symmetries like C_{2V}, C_2, C_{1h} and C_1 in their polar smectic mesophases [3-7].

The general structure of five-ring bent-core mesogenic molecules is illustrated in Fig. 1. The central unit A is mostly represented by 1,3-phenylene unit, 2,7- naphthalene unit, 3,4'- biphenyl segments or five-membered heterocyclic rings. The connecting groups W, X, Y and Z are often ester, azomethine and amide groups in different orientations. Moreover, the bent-core molecules are modified by small polar substituents at the central unit, the middle and outer rings as well as at the terminal chains which determine significantly the mesophase behaviour of these compounds. The bending angle γ is a key parameter of banana-shaped compounds and therefore a subject of experimental and theoretical investigations.

Vorlander who is the pioneer in the field of liquid crystals and reported about mesogenic properties of bent-core molecules already in 1929 stating that the thermal stability of the mesophases formed by such molecules is low compared with corresponding rod-like molecules [8,9]. After around 60 years, Matsunaga and coworkers revived the synthesis of bent-core molecules in 1991 [10]. But they did not realize the physical important polar switching of these molecules. Later on T.Niori *et al.* in 1996 discovered the polar switching in these molecules [11] and D. R. Link *et al.* explained that the opposite tilt direction of the achiral molecules in the smectic layers induce the opposite chirality in their adjacent smectic layers [12]. Further, D. Kruerke *et al.* and T.Sekine *et al.* have shown the spontaneous chiral resolution in a non-tilted mesophases [13-15]. The mesogenic phases formed by bent-core molecules were characterized by X-ray diffraction, polarizing microscope, electrooptics and dielectric spectroscopy [3]. Thus, the polarity and chirality of domains formed by achiral bent-core molecules made them to a new sub-field in liquid crystal research. The possible arrangements of the bent-core molecules in the polar smectic layers in presence of external electric field and the explanation of chirality by bent-core molecule is illustrated in Fig. 2.

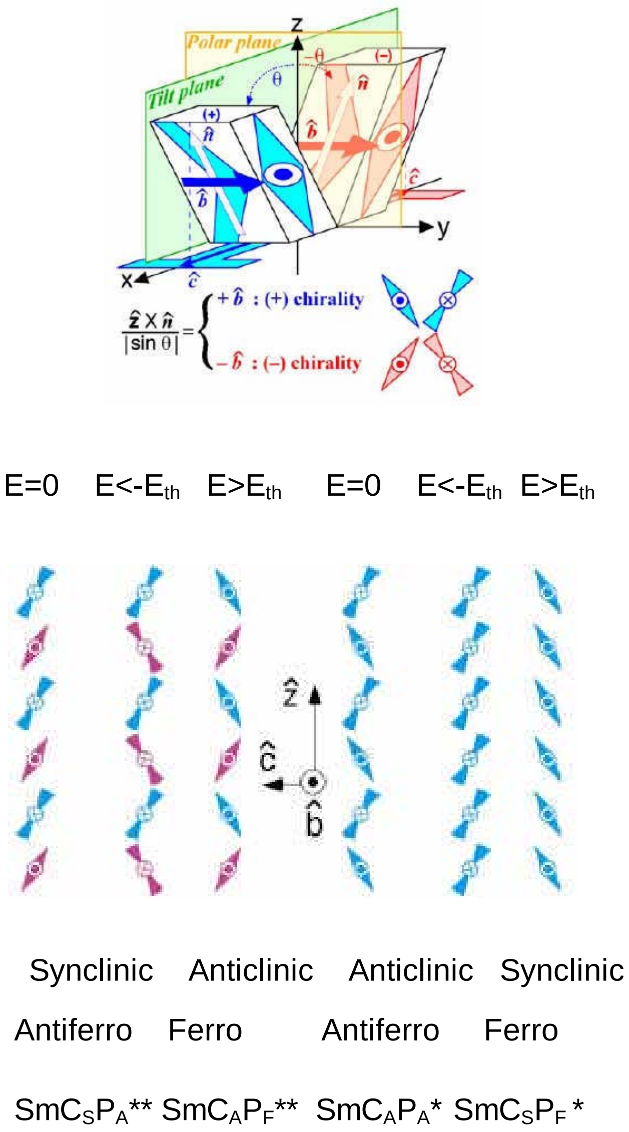
Polar plane
Tilt plane
z
y
x
θ
−θ
(+)
(−)
n̂
b̂
ĉ
ẑ × n̂ / |sin θ| =
+b̂ : (+) chirality
−b̂ : (−) chirality
E=0 E<-E_th E>E_th E=0 E<-E_th E>E_th
ẑ
ĉ
b̂
Synclinic Anticlinic Anticlinic Synclinic
Antiferro Ferro Antiferro Ferro
SmC_SP_A** SmC_AP_F** SmC_AP_A* SmC_SP_F *

Fig. 2 Arrangements of smectic layers in the SmCP phase [12],

(*: chiral, **: racemic models, E: electric field, th: threshold.)

In Fig. 2, the molecular long axis n tilts by θ from the smectic layer normal Z because of the existence of a third axis, i.e. bent direction b, each layer where the bent-core molecule are closely packed with uniform bent and tilt senses, possess chirality which is defined by

$$\frac{\hat{\mathbf{z}} \times \hat{\mathbf{n}}}{\sin\theta} = \pm\hat{\mathbf{b}}.$$

According to the interlayer correlation of polarization which is assumed to be parallel to b and tilt direction, the possible four states are also shown in the Fig. 2. $SmC_{S,\ A}$ $P_{F,\ A}$ subscripts $_S$ and $_A$ for C indicate the synclinic and anticlinic tilt in adjacent layers and subscripts $_F$ and $_A$ for P indicate ferroelectric and antiferroelectric states. In ferroelectric state polarizations in the adjacent layers are in the same direction. In antiferroelectric state the polarizations in the adjacent layers are in the opposite direction. Alternation of layer chirality observed in the SmC_SP_A and SmC_AP_F phases led to the racemic layer structure. But in the SmC* and SmC_A* phases formed by chiral rod-like molecules, the polarizations and tilt directions does not correlate. Therefore, racemic layer arrangement is not possible. Thus the polarization of the bent-core molecules is allowing them to differ from other types of liquid crystalline compounds.

The structure of bent-core compounds can be divided into three major parts. These are the central unit, wings including aromatic rings, connecting groups and terminal chains. The mesogenic properties of such compounds are mainly determined by the central unit, number of aromatic rings in the wings, direction and nature of the connecting groups as well as the length and type of the terminal chains. Moreover, the role of small polar substituents in bent-core molecules is more significant than in calamitic molecules [16-24] because the phase behavior of such molecules is more sensitive to even small structural modifications in comparison with rod-shaped mesogenic molecules. Therefore, it is useful to investigate structure property relations including modifications on different parts of banana-shaped molecules by theoretical methods.

1.2 Reports of theoretical investigations on bent-core mesogenic systems

Up to now, there are only limited theoretical studies on bent-core systems on the atomic level. Theoretical investigations on isolated bent-core molecules are mostly restrained on three ring systems or five-ring systems without terminal chains using density functional theory (DFT) as well as semi-empirical methods [25-29]. The aim of these studies mainly insisted in the investigation of the conformational properties of the isolated bent- core molecules including significant torsion angles of the bent-core. Moreover, molecular statistics simulations were performed on bent-core molecules including Monte Carlo (MC) and molecular dynamics (MD) methods. Within the MC techniques global patterns for the shape and polarity of the molecules were mostly used [30-41]. Recently, the results of a molecular dynamics simulation of an isolated bent-core molecule of the five-ring 1,3-phenylene type on a water surface using the Amber force field was published [42]. The calculations were performed to investigate the influence of the water molecules on the conformational behavior of the banana-shaped molecule.

1.3 Aim of this work

The main aspect of this work is the investigation of structure property relations of bent-core compounds on the atomic level by theoretical methods.

First, *ab initio* and density functional methods were used to study conformational and polar properties of the isolated molecules in a systematic way. The influence of small substituents like F, Cl and NO_2 both at the central unit and at the outer phenyl rings was studied. Moreover, the role of connecting groups like ester, azomethine and amide segments and their orientation were investigated. Bent-core compounds with a different central unit were included to check the function of this essential part of the molecule. From the calculated properties of the isolated bent-core molecules like relaxed rotational barriers, molecular lengths, and bending angles as well as electro static potential group (ESP) charges, dipole moments and polarizabilities try to find some relations to the mesophase behavior of the compounds.

Second, calculations on bent-core molecules formed by intermolecular hydrogen bonds as well as on dimers with alternative orientations of the monomers were carried out to get some hints on the stability of these systems.

Third, MD simulations both on the isolated molecule in vacuum and clusters with up to 128 monomers were performed using the AMBER program to study the aggregation effect in the bent-core compounds. The analysis of significant MD parameters both for the isolated molecule and a molecule in the aggregated state opens the possibility to study the effect of intermolecular interactions on structural and energetic properties of the bent-core systems. Moreover, by considering room temperature and clearing temperatures of the compounds as well as clusters with a different number of monomers in the MD simulations temperature and size effects were analyzed. The pressure effect on the shape of the mesogens is considered by including increasing pressure up to 500 bars in the MD simulations of bent-core molecules with its corresponding linear isomer. The correlation of the MD results with the mesophase properties of the bent-core compounds is tested to find some insights on the phase behavior of this interesting kind of liquid crystals.

Chapter 2 Theory and methods

In this chapter, some hints about the *ab initio* and density functional theories, molecular mechanics and molecular dynamics methods were given and the analysis of the molecular dynamics results was discussed.

2.1 *Ab initio* and density functional theory methods

For the calculation of the structural and energetic properties of the isolated bent-core molecules in the ground state at first *ab initio* methods on the Hartree Fock level including the procedure of the self-consistent-field (HF-SCF/STO-3G) were used [43-53]. This method with a very small basis set was selected to handle the relative large organic molecules with a maintainable effort especially for the rather costly two-fold potential energy scans.

The conventional HF method is based on the first principles of quantum mechanics and applied in the Roothaan-Hall equation [50] for the calculation of molecules. Approximations such as time separation, Born-Oppenheimer assumption, independent particle model, iterative SCF procedure and basis set limitations are taken into account to reduce the effort of the method. No adjusting parameters are necessary in this method.

The HF method starts from the electronic Schrödinger equation given in short form in eq. 2.1.

$$\mathbf{H_{el}}\Psi = \mathbf{E_{el}}\Psi \qquad \text{……….}(2.1)$$

$\mathbf{H_{el}}$ is the electronic Hamiltonian operator, Ψ is the wave function and $\mathbf{E_{el}}$ is the electronic energy of the system. Within the Born Oppenheimer approximation the interaction of the nuclei can be considered in a separated way. The wave function Ψ for a closed shell molecular system with 2n electrons is approximated by a Slater determinant.

$$\Psi(1,2,\ldots\ldots 2n) = \det \|\phi_1(1)\alpha\ \phi_1(2)\beta \ldots\ldots\ldots \phi_n(2n-1)\alpha\ \phi_n(2n)\beta\| \quad \ldots\ldots\ldots\ldots(2.2)$$

which is build up from the one-electron functions ϕ_i. The determinant function fulfills the antisymmetry requirement on the wave function and partly includes correlation effects. In the standard Roothaan-Hall method the one-electron functions ϕ_i are described by convenient basis functions χ_r in the form

$$\phi_i = \Sigma_r\, c_{ri}\, \chi_r \qquad \ldots\ldots.(2.3)$$

The optimal linear parameters c_{ri}, the wave function and the energy of the system are obtained by an iterative variation process (SCF procedure). In the conformational analysis of molecules this procedure has to be performed in every step of the geometry optimization to find the most stable conformers. The following literatures give the basics of *ab initio* HF-SCF methods [43-53].

The investigations on the monomers were extended by DFT calculations on the B3LYP/6-31G(d) level. The DFT method is based on the theorem of Hohenberg and Kohn [53] that the energy of the ground state of an electronic system is completely described by the electron density ρ. This means that the energy is a definite functional of the electron density $E = E[\rho]$. The problem of the method is that the functional is not known and there is no easy way to find it. In the last years, especially by the works of Kohn and Sham [54], Becke, Lee, Yang and Parr [55-58], Perdew and Wang [59,60] and others functionals were designed for the calculation of larger molecular systems. The three parameter functional of Becke (B3) and the gradient corrected functional of Lee, Yang and Parr (LYP) are combined in the popular B3LYP hybrid functional to describe the exchange correlation term. The parameters were determined by fitting to experimental data. The advantage of the DFT method in comparison to the corresponding HF-SCF procedure is a more complete cover of correlation effects and the good relation between effort and quality of the results. In the past, the B3LYP functional with the standard basis set 6-31-G(d) was successful applied for larger organic molecules as well as hydrogen bond systems [61-63].

Therefore, the DFT method on the B3LYP/6-31G(d) level was used for the systematic calculations on structural and electronic properties of the isolated bent-core molecules. Both the HF-SCF/STO-3G and the DFT calculations on the B3LYP/6-31G(d) level were carried out by using the GAUSSIAN98 package [64] on the SUN FIRE 6800/3800 of the computational center of the Martin-Luther-University Halle-Wittenberg as well as on SGI workstations of our group.

2.2 Molecular mechanics and molecular dynamics procedures

Molecular mechanics or force field methods are used for the calculation of very large systems with more than 10000 atoms in the field of material and life sciences. The handling of such large systems is only possible by a rigorous simplification in comparison to the *ab initio* and DFT methods. The force field energy is written as a sum of terms describing the energy for distorting the molecule, the van der Waals energy, the electrostatic energy and special additional terms by empirical potentials [65-68].

$$\mathbf{E_{FF} = E_{str} + E_{bend} + E_{tors} + E_{vdw} + E_{el} + E_{cross} + E_{spec}} \quad \text{........}\mathbf{(2.4)}$$

E_{FF} = Force field energy, E_{str} = bond stretching energy, E_{bend} = angle stretching energy, E_{tor} = energy of torsional motion, E_{vdw} = energy of the van der Waals interactions, E_{el} = energy of electrostatic term such as non bonded interactions, E_{cross} = cross term which is the energy of stretch-bend terms, E_{spec} = special additional terms by empirical potential. The parameters of the potentials are adjusted by experimental values and by results of very accurate *ab initio* calculations. Atoms were modeled as mass points including a defined net charge. In the last years a number of force fields were developed such as AMBER [69], CHARMM [70], GROMOS [71], MM [72] and others with a special aim for their application. For the molecular mechanics calculations on the bent core systems we have used the “gaff” (generalized amber force field) force field in the AMBER program which is adapted for organic molecules [73].

Molecular dynamics is a simulation of the time-dependent behaviour of a molecular system, such as vibrational motion or Brownian motion. It requires a way to compute the energy of the system, most often using molecular mechanics calculation. It includes the calculation of the so called trajectory in the following steps. The first step is choosing the initial positions of the atoms. Second, choose an initial set of atom velocities. Thirdly, compute the momentum of each atom from its velocity and mass. Finally, compute the forces on each atom from the energy expression by a molecular mechanics force field. Compute the new positions for the atoms in a short time interval, called time step Δt, typically 1-10 fs by numerical integration of Newton's equations

$$\mathbf{d^2r_i\,(t)/dt^2 = m_i^{-1}\,F_i} \qquad \text{……(2.5)}$$

$$\mathbf{F_i = -\,\partial V(r_i,\, r,\ldots r_N)/\partial r_i} \qquad \text{……(2.6)}$$

(Where the force on atom $_i$ is denoted by F_i and time is denoted by t; the potential energy is V, r_i atomic coordinates, m_i is the mass of the atom $_i$)

of motion using the information obtained from the previous steps and computes the new velocities and accelerations for the atoms. The length of the time step is restricted by the requirement that Δt should be small compared to the period of the highest frequency motions being simulated. Static equilibrium quantities can be obtained by averaging over the trajectory, which must be of sufficient length to form a representative ensemble of the state of the system. In addition dynamic information can be extracted [74-78].

In the simulation of a cluster of molecules, the periodic boundary conditions are applied to minimize edge or wall effects. If the irregularity of the system is incompatible with periodicity, edge or wall effects may be reduced by treating part of the system as an extended wall region in which motion of the atoms is partially restricted. Simulation of isolated molecules was carried out in vacuum that is without any wall or boundary effects. In the vacuum boundary condition all possible conformations of the molecules can be realized.

The MD simulations on the clusters of the molecules with 64 and 128 molecules were carried out using periodic boundary conditions because the classical way to minimize edge effects in a cluster of molecular system is to use periodic boundary conditions. The atoms of the system which is to be simulated are put into a cubic or more generally into any periodically space-filling shaped box which is treated as if it is surrounded by $26(3^3–1^3)$ identical translated images of itself. When an infinite sum of the interactions is to be performed, the interactions of an atom in the central computational box with all its periodic images are computed. In most cases this is not desirable. The only interactions with nearest neighbors are taken into account.

The non-bonded coulomb interactions can be implemented in MD simulations by the cutoff values. In this way, interactions between atom pairs only with a distance shorter than a given cutoff length are considered, and effects from more distant pairs are neglected. This cutoff treatment was tested for various systems. It has been revealed that the cutoff approximation can severely affect their properties.

The cutoff value should be less than or equal to the half of the minimum length of the simulation box. The SHAKE algorithm (otherwise known as the constrained Verlet method) has been used for hydrogen and heavy atom bond lengths. Thus, algorithms, such as SHAKE, that constrain the bonds to their equilibrium lengths are useful in saving the computational efforts and increasing the simulation time.

2.3 Analysis of molecular dynamics results

The molecular dynamics results were analyzed by trajectories of significant torsion angles, radial atom pair distribution functions, orientational correlation function, diffusion coefficients and root mean square deviations plots.

2.3.1 Radial atom pair distribution function

In the condensed phase, the microscopic structure can be characterized by a set of pair distribution functions for the atomic positions. The simplest of them is the radial atom pair distribution function $g(r)$. Radial distribution function can be measure experimentally using X-ray diffraction which can be compared with that obtained from the MD simulations.

2.3.2 Orientational correlation function

Orientational correlation functions are another method of examining the local structure of the isotropic state. The relative orientation of the two neighboring central 1,3-phenylene units of bent-core molecules can be described by the cosine angle between the two bond vectors. The dependence of this angle on the distance between the atoms C2 and C5 in the central units can be discussed in terms of the orientational correlation function *g(o).*

2.3.3 Diffusion coefficient

The molecular self-diffusion coefficients are important observables to quantify the molecular mobility which are calculated by invoking the Einstein relationship [79-80]. In which the diffusion coefficient D is related to the mean square displacement $\langle \Delta r^2 \rangle$ in a time t by the following equation.

$$\langle \Delta \mathbf{r}^2 \rangle = \mathbf{6Dt}$$

Chapter 3 Polar substituents on bent-core compounds

Introduction of small polar substituents both into the central 1,3-phenylene unit and the external phenyl rings cause significant changes in the phase behaviour of bent-core mesogens [3-7,16-24]. Obviously, such substitutions influence the shape, polarity and flexibility of the molecules and cause a different aggregation of the bent-core mesogens. In order to study the effect of substitution on the properties of bent-core molecules in a systematic way, we have performed HF/STO-3G and DFT B3LYP/6-31G(d) calculations on 1,3-phenylene bis [4-(4-n-hexyloxyphenyliminomethyl) benzoates] type systems (P-6-O-PIMB).

3.1 Systems and explanations

The main structure of the considered bent-core molecules and definition of the torsion angles with numbering of the atoms were illustrated in Fig. 3 and Table 1. In Fig. 4, the orientation of the coordinate system is shown related to the central 1,3-phenylene unit to define the direction of the dipole moment and its components. The sense of direction of the dipole moment corresponds from the negative to the positive centre of charge as generally considered.

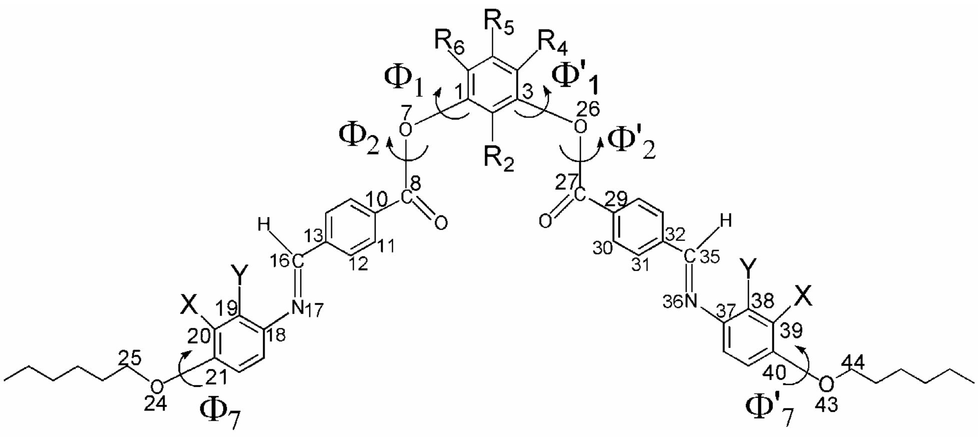
R5
R6
R4
Φ1
Φ'1
1
3
7
26
Φ2
Φ'2
R2
8
27
10
29
13
32
11
12
30
31
H
H
16C
C35
Y
Y
X
X
19
38
N17
36N
37
20
18
39
25
44
21
40
24
43
Φ7
Φ'7

Fig. 3 The main structure of the considered substituted bent-core mesogens.

Table 1 Acronyms of the systems with clearing temperatures.

System		R_2	R_4	R_5	R_6	X	Y	T [b] [16]
S1	**P-6-O-PIMB**	H	H	H	H	H	H	$\mathrm{SmCP_A}$ 174° I
S2	**P-6-PIMB**[a]							
S3	**4-Cl-P-6-O-PIMB**	H	Cl	H	H	H	H	$\mathrm{SmCP_A}$ 133° I
S4	**DCl-P-6-O-PIMB**	H	Cl	H	Cl	H	H	N 148° I
S5	**DCl-P-6-O-PIMB-X-F/**	H	Cl	H	Cl	F	H	SmA 129° I
S6	**DCl-P-6-PIMB-X-F**[a]							
S7	**DCl-P-6-O-PIMB-Y-F**	H	Cl	H	Cl	H	F	N 128° I
S8	**DCl-P-6-O-PIMB-X-Cl**	H	Cl	H	Cl	Cl	H	N 109° I
S9	**F-P-6-O-PIMB**	H	H	F	H	H	H	$\mathrm{SmCP_A}$ 180° I
S10	**F-P-6-O-PIMB-X-F**	H	H	F	H	F	H	$\mathrm{SmCP_A}$ 164° I
S11	**F-P-6-O-PIMB-Y-F**	H	H	F	H	H	F	Cr 144° I
S12	**NO_2-P-6-O-PIMB**	NO_2	H	H	H	H	H	$\mathrm{SmCP_F}$ 177° I
S13	**NO_2-P-6-O-PIMB-Y-CH_3**	NO_2	H	H	H	H	CH_3	Cr 137° I
S14	**NO_2-P-6-O-PIMB-Y-CF_3**	NO_2	H	H	H	H	CF_3	Cr 140° I

[a] Indicates systems with hexyl terminal chains. [b] Clearing temperature for systems with octyloxy terminal chains; Clearing temperatures in degree Celsius.

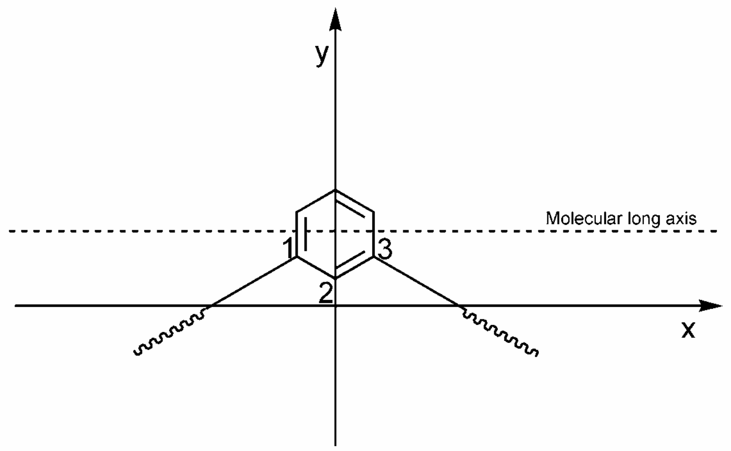

Fig. 4 Coordinate system for the explanation of the components of the dipole moment in 1,3-phenylene type molecules

The ESP group charges are localized at the centres of the rings as well as at the centres of the C-O and the C=N bonds of the connecting groups, respectively. In this way the ESP group charges and their positions are comparable in the most stable conformers of the five-ring bent-core mesogens of the 1,3-phenylene type.

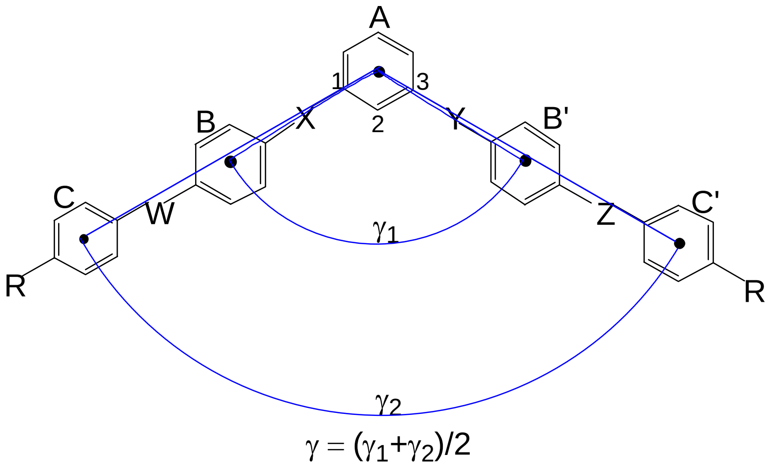

Fig. 5 Simple model for the calculation of the bending angle γ

A simple model was introduced to define the bending angle γ for the five-ring systems with a central 1,3-phenylene unit. The procedure is illustrated in Fig. 5. The centers of the five aromatic rings are calculated for the corresponding conformers.

From the central points of the rings BAB' and CAC' the angles γ_1 and γ_2 are obtained, respectively. The bending angle γ is indicated as the mean value of γ_1 and γ_2. This model allows a simple quantification of the bent property of conformations for such type of banana-shaped mesogens [81].

3.2 Computational details

Ab initio and DFT calculations in the HF/STO-3G and B3LYP/6-31G(d) levels were performed using the program package Gaussian98 [64]. For a systematic study on the conformational behaviour of the bent-core molecules, the relaxed rotational barriers and two-fold PES scans (Ramachandran-like plots) were calculated for significant torsion angles of the legs (please see Fig. 3). The energetically preferred structures were obtained by a full optimisation from different starting structures including twisted and planar ones. The one- and two-fold PES scans were generated by fixing the corresponding torsion angles and a complete optimisation of the other parameters in a stepwise manner. The planar structures result from a partial optimisation with fixed values for the relevant torsion angles. The dipole moment and its components as well as the diagonal elements of the polarizability were calculated for the most stable conformations and their dependency with respect to torsion angle ϕ_1 was analyzed. A simple procedure was used for the calculation of a global pattern of charge distribution along the legs of the molecule. The atomic net charges of a molecule were calculated from the fit to reproduce its electrostatic potential (ESP charges). For the phenyl rings the ESP group charges are defined by summarizing the charges of the corresponding carbon atoms and localizing the values at the centers of the rings. In this way, the ESP group charges and their positions are comparable for the most stable conformations of the five-ring mesogens of the 1,3-phenylene type.

Moreover, molecular dynamics (MD) simulations have been carried out with an implemented AMBER7 version using gaff force field [82]. Atomic net charges for the molecules were adapted from the fit to reproduce electrostatic potential within

HF/6-31G(d) level. The procedure is consistent with the defined atomic charges for amino acid fragments in the AMBER program [83]. Classical MD simulations have been performed on the isolated molecules in vacuum at 300 K and their clearing temperatures with a simulation time of 1ns. A time step of 0.5 fs was used in all the simulations and the non-bonded interactions were calculated with a cutoff radius of 10000 pm. The MD simulations on the clusters were performed with 64 monomers using an antiferroelectric starting structure model [3] for three systems (**S1**, **S4** and **S12**). For the treatment of the clusters a total simulation time of 3 ns and a time step of 0.5 fs were used at two different temperatures including heating phases. Equilibration phases of 1 ns were taken into account for the analysis of the MD data both at 300 K and at the clearing temperature. The MD simulations were carried out with constant pressure (n, p, T) conditions. The SHAKE algorithm was used only for hydrogen atoms. The non-bonded interactions in the clusters were calculated with a cutoff radius of 1000 pm. The MD results were analyzed by a graphics tool developed in our group at an Octane workstation and already utilized for mesogenic and biochemical systems [84, 85] and the AMBER7 standard tool for MD analysis PTRAJ. From the MD results the trajectory of the torsion angle ϕ_1 was calculated. The B-factor value for the connecting group atoms was considered as a good indicator of conformational flexibility and thermal motion of the molecules [86]. The connecting groups have a major influence on the flexibility and polarity of banana-shaped molecules. Therefore, the B-factor values were calculated for connecting group atoms. The histograms for the bending angle distribution were analyzed. From the full width at half maximum (FWHM) values of the bending angle its range can be evaluated. The molecular length was considered as core length (L_C) which is the distance between oxygen atoms of the alkoxy groups and total length (L_T) is the distance between terminal carbon atoms of the alkoxy chains. The structure formation in the clusters can be analyzed by the calculation of radial atom pair distribution function g(r) [79, 80, 87]. The g(r) values were related to the reference atom C2 of the central ring. Further information on the arrangement of the molecules in the cluster can be estimated from the evaluation of the orientation correlation function g(o). The g(o) data are obtained from the calculation of the radial dependence of the absolute cosines between the vectors of the reference atoms C2 and C5 which determine the orientation of the central unit. Hints on the mobility of the molecules in the cluster can be achieved from the calculation of the diffusion coefficients D using the Einstein model within the molecular dynamics procedure [79-80]. From the averaged mean square displacement (MSD) of the center of mass $<\Delta \mathbf{r}^2> = 6Dt$ the diffusion coefficients D can be obtained by a linear fit.

3.3 DFT and HF results

3.3.1 Substituents on the central unit

3.3.1.1 Planar and twisted conformations – superposition with X-ray structure

The results of the conformational studies on the systems **S1** and the 4,6-dichloro substituted **S4** are summarized in Table 2. Both the HF and the DFT methods indicate that the twisted conformers are energetically preferred in comparison to the

Table 2 Comparison of HF and DFT results on the conformers of P-6-O-PIMB and DCl-P-6-O-PIMB

System	Conformer	HF [a]					DFT [a]				
		E_r	μ	γ	Φ_l	Φ'_l	E_r	μ	γ	Φ_l	Φ'_l
S1	**twisted**	**0**	**3.67**	**129**	**239**	**239**	**0**	**4.76**	**121**	**249**	**252**
		(-2299.1504)[b]					**(-2342.6816)[b]**				
	Planar	**21**	**4.09**	**118**	**179**	**179**	**7**	**6.80**	**114**	**179**	**179**
S4	**twisted**	**0**	**5.98**	**126**	**59**	**59**	**0**	**4.15**	**115**	**50**	**54**
		(-3207.1500)[b]					**(-3261.8643)[b]**				
	planar	**19**	**3.50**	**123**	**0**	**0**	**11**	**2.26**	**125**	**0**	**0**
	X-ray	**2604**	**0.40**	**140**	**73**	**94**	**2187**	**0.79**	**140**	**73**	**94**
	X-ray like[c]	**12**	**0.90**	**135**	**73**	**94**	**17**	**1.18**	**134**	**73**	**94**

[a] E_r – kJmol^{-1}, μ – Debye, γ, Φ_1, Φ'_1– degree, [b] total energy (hartree) of the most stable conformers in parentheses, [c] all torsion angles are fixed like in X-ray but bond length and bond angles are optimised.

planar ones by about 20 kJ mol^{-1} (HF) and 10 kJ mol^{-1} (DFT). From X-ray investigation of **S4** in the solid state a twisted structure was also found [88]. In both methods the relative energy of the X-ray conformer is very high. The partial optimized conformers of **S4** with fixed torsion angles as in the X-ray structure but optimised bond lengths and angles (X-ray like conformers) are relatively stable twisted forms 12 kJ mol^{-1} (HF) and 17 kJ mol^{-1} (DFT). The high relative energy of the X-ray conformer results mainly from deviations in the bond length, especially of the C-H bonds.

The calculations on the isolated molecules indicate the conformational flexibility of the bent-core mesogens. The values of the dipole moment and the bending angle (γ) depend significantly on the conformers and the substituents at the central ring. It is remarkable that the X-ray [88] and X-ray like conformers show very small dipole moments and relatively large bending angles related to the most stable one which is obviously caused by packing effects. This is illustrated by a superposition of the preferred HF and DFT conformers as well as the X-ray structure in Fig. 6.

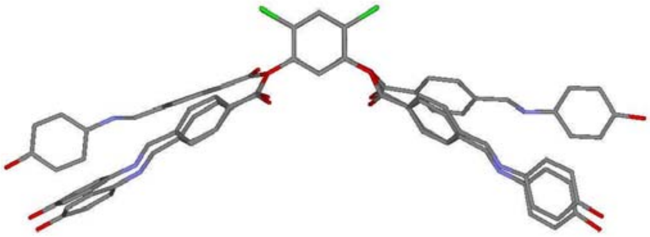

Fig. 6 Superposition of system **S4** conformers related to the 1,3-phenylene central unit (above: X-ray, middle: DFT, below: HF).

3.3.1.2 One-fold scans

The influence of a substitution in the central 1,3-phenylene unit on the flexibility of the isolated bent-core molecules was investigated by a systematic analysis of the relaxed rotational barriers related to the significant torsion angles ϕ_1 and ϕ_2 (please see Fig. 3). First, the relaxed rotational barrier of the leg with respect to the torsion angle ϕ_1 = C2-C1-O7-C8 was calculated. The results for the unsubstituted as well as for the dichloro- , fluoro- and nitro- substituted molecules are illustrated in Figs. 7(a) and 8(a).

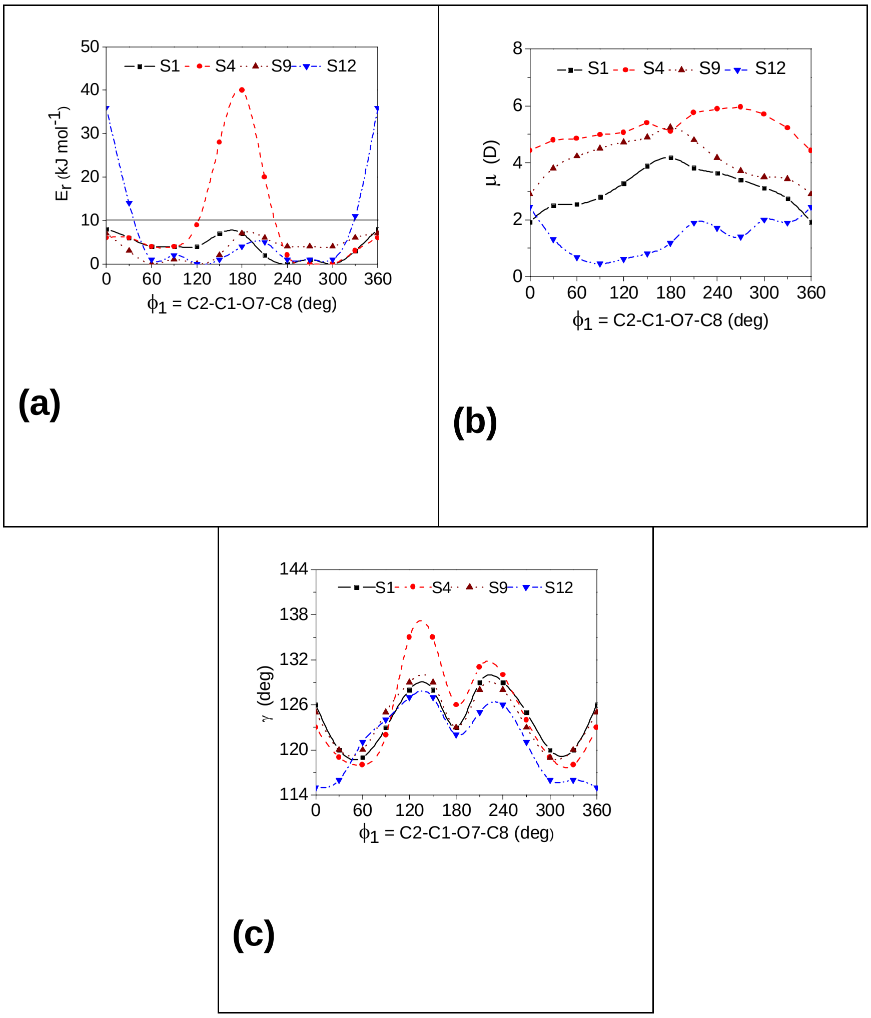

Fig. 7 One-fold scans (HF) related to the torsion angle ϕ_I. [(a): relative energy E_r, (b): dipole moment μ, (c): bending angle (γ).]

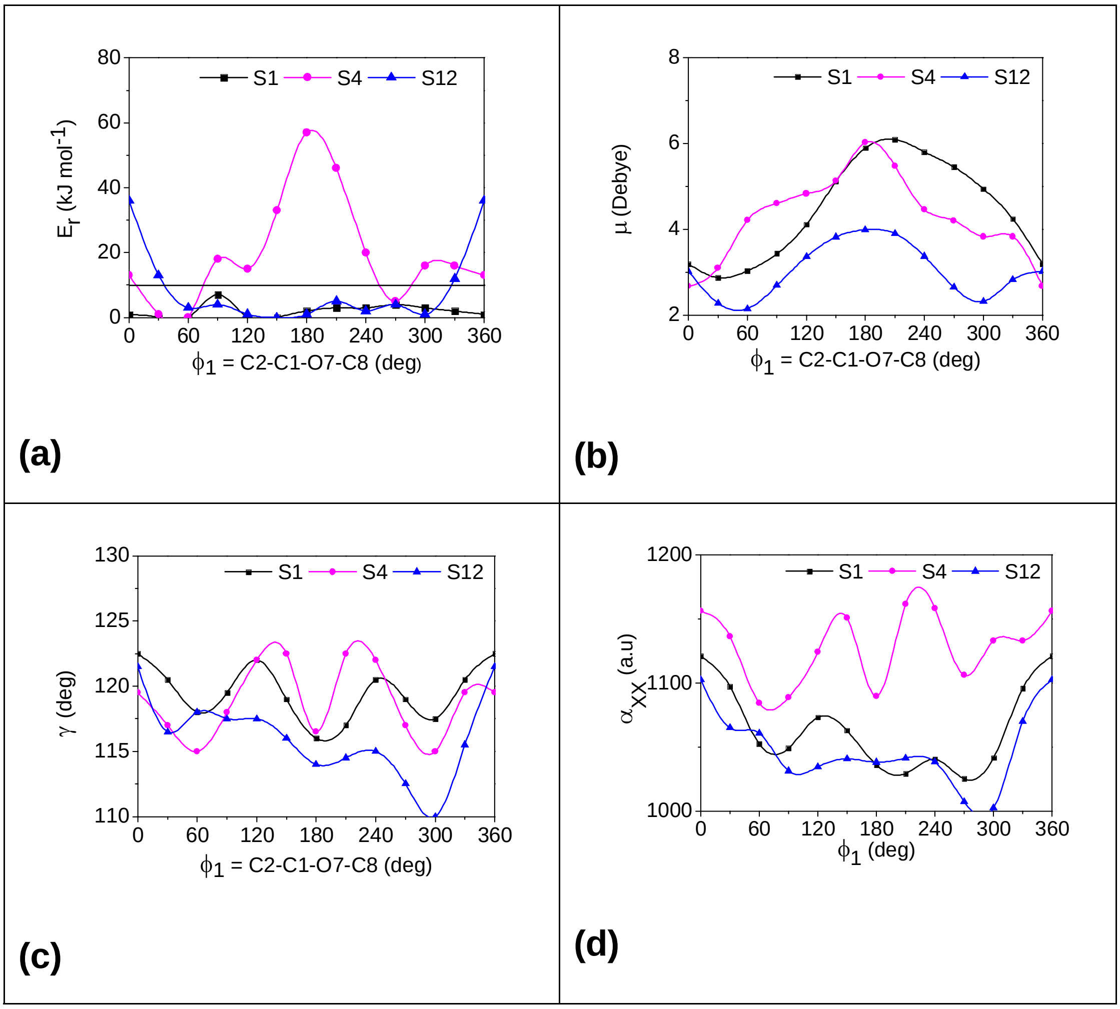

Fig. 8 One-fold scans (DFT) related to the torsion angle ϕ_l. [(a): relative energy E_r, (b): dipole moment μ, (c): bending angle γ, (d): polarizability α_{xx} (diagonal component)]

It results that a significant effect of the substitutions on the flexibility of the legs related to the type and position of the substituents. For the molecules **S1** and **S9**, the barriers are generally lower than 10 kJ mol^{-1} over the whole range of ϕ_1 (Fig. 7a). In the molecules **S4** and **S12** the rotational barriers are remarkably increased up to 60 kJ mol^{-1}(HF) and 40 kJ mol^{-1}(DFT). This is caused by a strong repulsion between the substituents on the central phenyl ring and the adjacent carbonyl group, especially in conformations with $\phi_1 = 180^o$ (**S4**) and $\phi_1 = 0^o$ (**S12**). In all cases the preferred conformers are found in ranges of ϕ_1 from 60^o-120^o and 240^o-300^o which is in agreement with the X-ray structure of **S4** [88].

3.3.1.3 Two-fold potential energy surface scans

The strong effect of the nitro group and chlorine, fluorine substitutions on the conformational flexibility of the bent-core legs can be also illustrated by two-fold scans (Ramachandran-like plots) with respect to the torsion angles ϕ_1 and ϕ_1'(Fig. 9). The two-fold scan of system **S3** significantly differs from **S4** and **S1** in global maxima, minima and relative energy values. In summary a higher conformational flexibility of the bent-core legs was observed in **S3** than **S4** except ϕ_1' = 120° to 240°. In the case of system **S9**, a small effect was observed in the relative energy value which was not observed in one-fold scan. In system **S12**, a remarkable effect was observed in the relative energy values which are about 10 times higher (E_r max = 354 kJ mol^{-1}; please see Fig. 9) than the values of one-fold scans (E_r max = 34 kJ mol^{-1}; please see Fig. 7a).

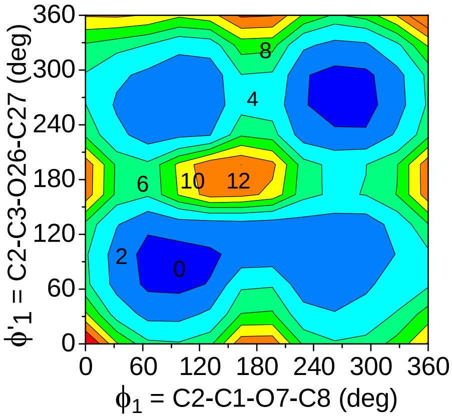

(S1)

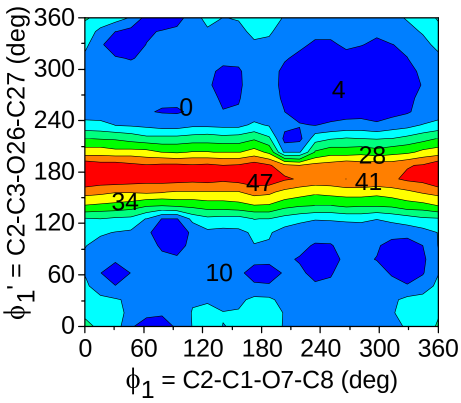

(S3)

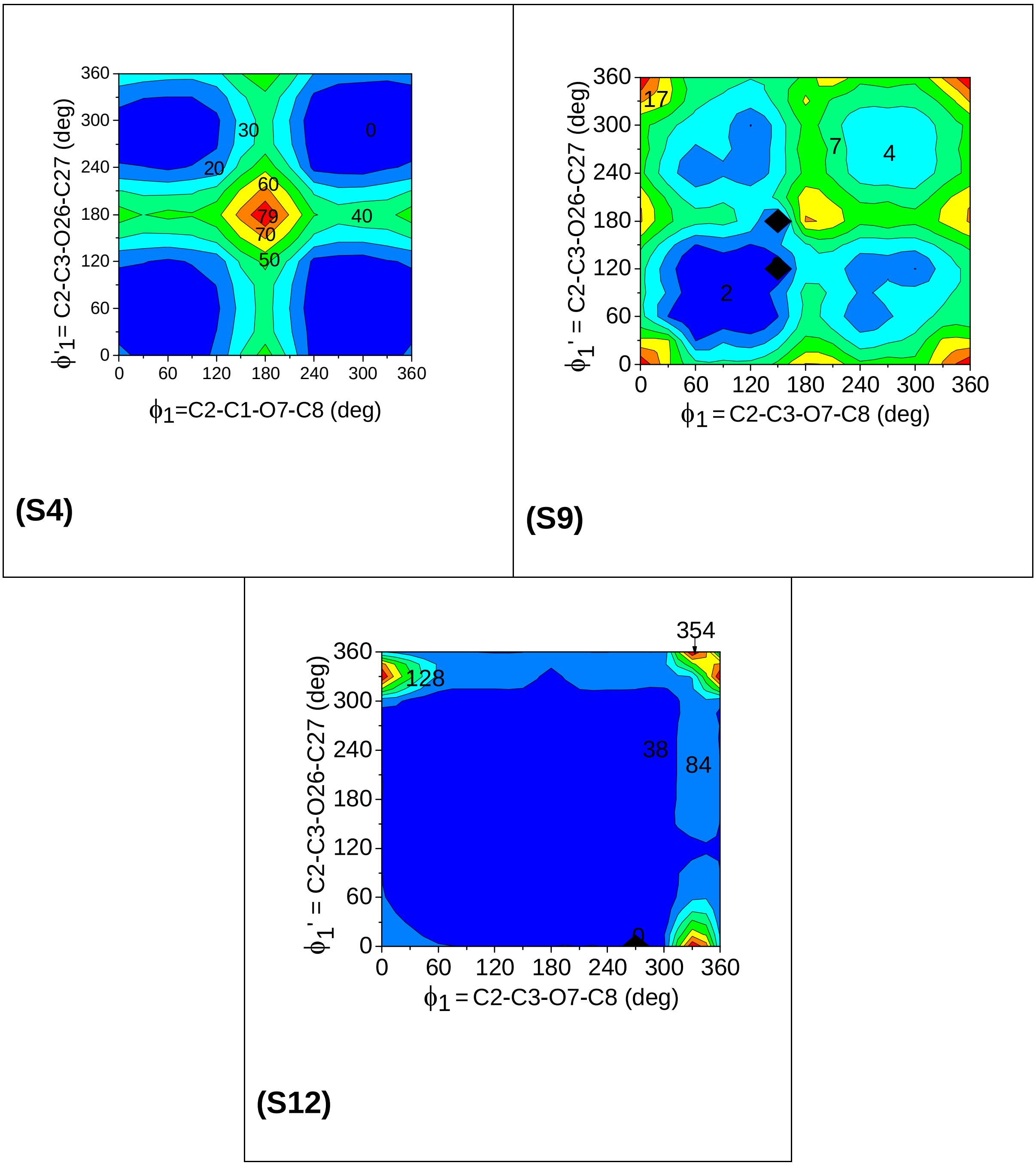

(S4)

(S9)

(S12)

Fig. 9 Two-fold potential energy surface scans (HF) related to the torsion angle ϕ_1 and ϕ_1' for five different systems.

This follows from the significant higher values of the relative energy for the global and local maxima in the two-fold relaxed PES scan of **S3**, **S4** and **S12**. In some way it could be a reason for the loss of B-phases in **S4** in comparison to **S1**.

3.3.1.4 Dipole moments, ESP group charges and polarizabilities

The dependency of the dipole moment (μ) on conformers with constraints to the torsion angle ϕ_1 is shown in Fig. 7b (HF) and in Fig. 8b (DFT). Within a considered bent-core molecule the magnitude of the dipole moment varies of about 1-3 Debye related to the torsion angle ϕ_1. The curves show the common trend in the dipole moment μ: **S12** < **S1** < **S9** < **S4** (Fig. 7b). The sequence is also supported by the energy weighted simple mean values of the dipole moment and its components (Table 3), where conformations with a relative energy less than 10 kJ mol^{-1} are considered. The main contribution to the dipole moment comes from the μ_y component oriented perpendicular to the long axis of the molecule and parallel to the plane of the central ring (Fig. 4). The negative sign indicates the direction of μ_y from C5 to C2 in this type of bent-core molecules. The large differences in the dipole moments, especially in **S12** and **S4**, can be seen as hints for their different phase behaviour and mesophase stability [3] caused by their diverse global polarity. The results show a relative large effect on the values of the μ_y component of the dipole moment in the considered bent-core molecules. Obviously, the μ_y component is more important in banana-shaped than in calamitic mesogens with respect to the formation of smectic layers.

The results of the ESP group charges (HF method) for the most stable conformers of the 1,3-phenylene systems with substitutions on the central ring are illustrated in Fig. 10.

The ESP group charges show that the electron density is significantly decreased on the central ring in the sequence of the molecules **S1** > **S12** > **S9** > **S4**. A similar trend was found for the ESP group charges on the ester groups and the external phenyl rings. But the effect is weaker. Where as the charges at the intermediate rings are nearly the same for the considered molecules. It is remarkable that the ESP group charges show alternating values on the rings along the bent-core arms in all cases. The ESP group charges obtained by the DFT method give an analogue tendency but the values are generally smaller. The findings are in agreement with the maximum values of the calculated electrostatic potential on the rings in similar molecules by J. P. Bedel *et al*. [89].

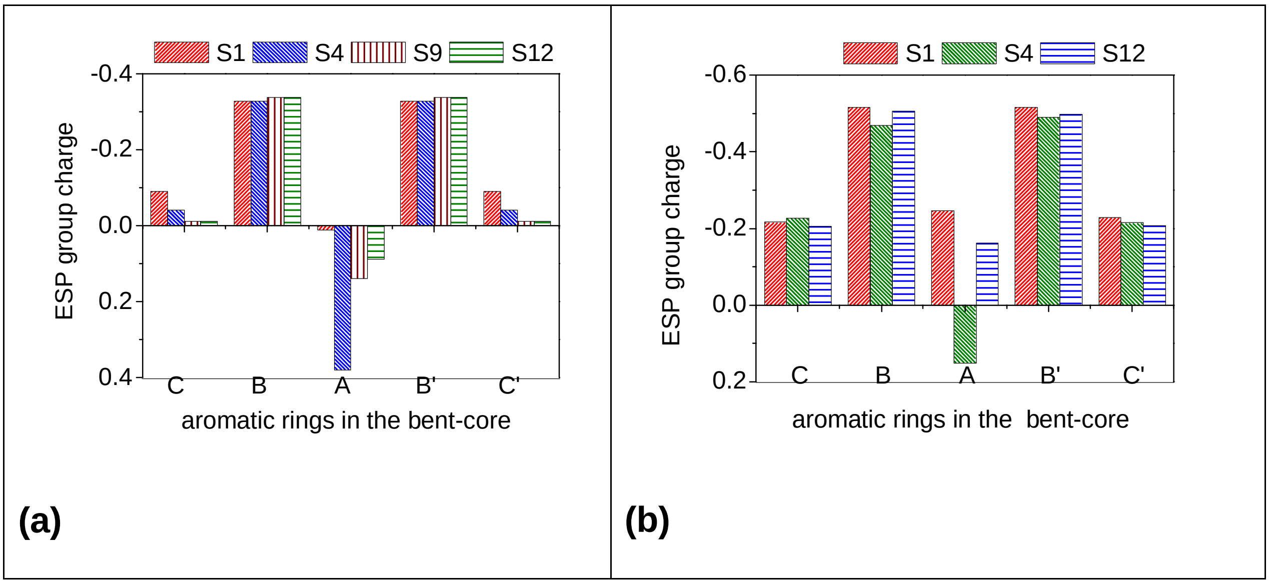

Fig. 10 Electrostatic potential group charges along a leg of bent-core mesogens with substituents on the central phenyl ring (a: HF, b: DFT).

Table 3 HF energy weighted simple mean values of dipole moment and its components for banana-shaped molecules with substituents on the central phenyl ring [a].

System	$\bar{\mu}_x$	$\bar{\mu}_y$	$\bar{\mu}_z$	$\bar{\mu}$	ϕ_1	ϕ'_1
S1	**0.0(0.0)**	**-3.13(-3.67)**	**0.0(0.0)**	**3.13(3.67)**	**239**	**239**
S4	**-0.07(0.0)**	**-5.17(-6.26)**	**-0.13(0.0)**	**5.18(5.98)**	**59**	**59**
S9	**-0.06(0.0)**	**-4.10(-4.75)**	**-0.09(0.0)**	**4.12(4.75)**	**125**	**125**
S12	**-0.33(0.0)**	**-0.07(-0.68)**	**-0.35(0.0)**	**0.54(0.68)**	**132**	**132**

[a] the μ values of the most stable conformers in parentheses (μ–Debye,ϕ_1,ϕ'_1 – degree)

Moreover, the conformers of the substituted banana-shaped molecules (HF, DFT) show remarkable changes of the bending angle (γ) with respect to the torsion angle ϕ_1 (Fig. 7c and 8c).

Table 4 Dipole moments μ and their components, diagonal elements α_{xx} of the polarizability, bending angle (γ), and values for the molecular lengths (L_C core length and L_T total length) of the most stable conformations of three systems (DFT results).

System	μ_x	μ_y	μ_z	μ	α_{XX}	α_{YY}	α_{ZZ}	γ	L_C	L_T
S1	**- 0.05**	**- 4.75**	**- 0.09**	**4.76**	**1064**	**606**	**305**	**120**	**26.12**	**40.06**
S4	**0.46**	**- 4.07**	**-0.60**	**4.14**	**1085**	**623**	**361**	**115**	**26.77**	**38.45**
S12	**- 0.09**	**- 3.77**	**0.03**	**3.77**	**1029**	**670**	**345**	**116**	**25.37**	**37.64**

Dipole moments in Debye, polarizability in atomic units (1 a.u. is approximately 1.649 10^{-41} C^2 m^2 J^{-1}), bending angle in degree, lengths in Å.

The highest values are found for **S4** and the lowest ones for **S12**. This tendency is also indicated by the range of the minimum and maximum values of the bending angle γ with 115^o-126^o (**S12**), 119^o-128^o (**S9**), 119^o-129^o (**S1**) and 119^o-135^o (**S4**) including conformers with a relative energy less than 10 kJ mol^{-1}. The increased bending angle of **S4** is in agreement with liquid crystalline state NMR findings [3] and solid state X-ray data [88]. The calculated bending angle (γ) for **S1** and **S9** are comparable which is supported by the NMR findings 122^o and 116^o-118^o respectively [3,18].

From the diagonal elements of the polarizability (see Table 4) it follows that α_{XX} is the essential component which is oriented to the long axis of the molecule. The dependence of α_{XX} related to ϕ_1 is illustrated in Fig. 8d. The trends in the curves confirm the sequence of α_{XX} for the most stable conformers α_{XX} : **S3** < **S1** < **S12** (Table 4). These findings are supported by the energy weighted values α_{XX} including conformations lower than 10 kJ mol^{-1} α_{XX}: **S3** (1036) < **S1** (1059) < **S12** (1108) (the values are in atomic units).

The relaxed rotational barriers with respect to the torsion angle ϕ_2 = C1-O7-C8-C10 were illustrated in Fig. 11 for the bent-core molecules. In contrast to ϕ_1 the conformational degree of freedom for ϕ_2 is rather limited. It results a relatively large rotational barrier of about 40 kJ mol^{-1} for $\phi_2 = 0^{o}$ which is independent of the substituents on the central unit. For this constraint the energetically preferred coplanar arrangement of the carbonyl group and the adjacent phenyl ring is sterically hindered by a repulsion of the rings A and B and it results a less stable conformer.

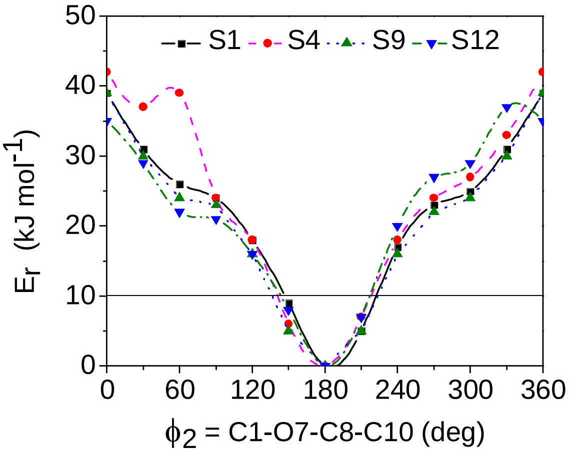

Fig. 11 Relaxed rotational barriers (HF) related to the torsion angle ϕ_2.

3.3.2 Polar substituents on the external phenyl rings

3.3.2.1 Relaxed rotational barriers - ϕ_7

In order to investigate the influence of substituents in different positions of the external phenyl rings on the conformational behaviour of the terminal chains the relaxed rotational barriers were calculated with respect to the angle ϕ_7. The results for the fluorine and chlorine substituted systems are presented in Fig. 12. The applicability of HF results (Fig. 12a) was shown by corresponding DFT results (Fig. 12b). A fluorine substitution in the positions 19 and 38 (see Fig. 3) of the external phenyl rings **S7** has a minor effect on the conformational behaviour of the terminal hexyloxy chains. The relaxed rotational barrier of **S7** corresponds mostly to that **S4** (not shown in Fig. 12). Whereas a fluorine substitution in the positions 20 and 39 (**S5**) increase the conformational flexibility of the hexyloxy groups.

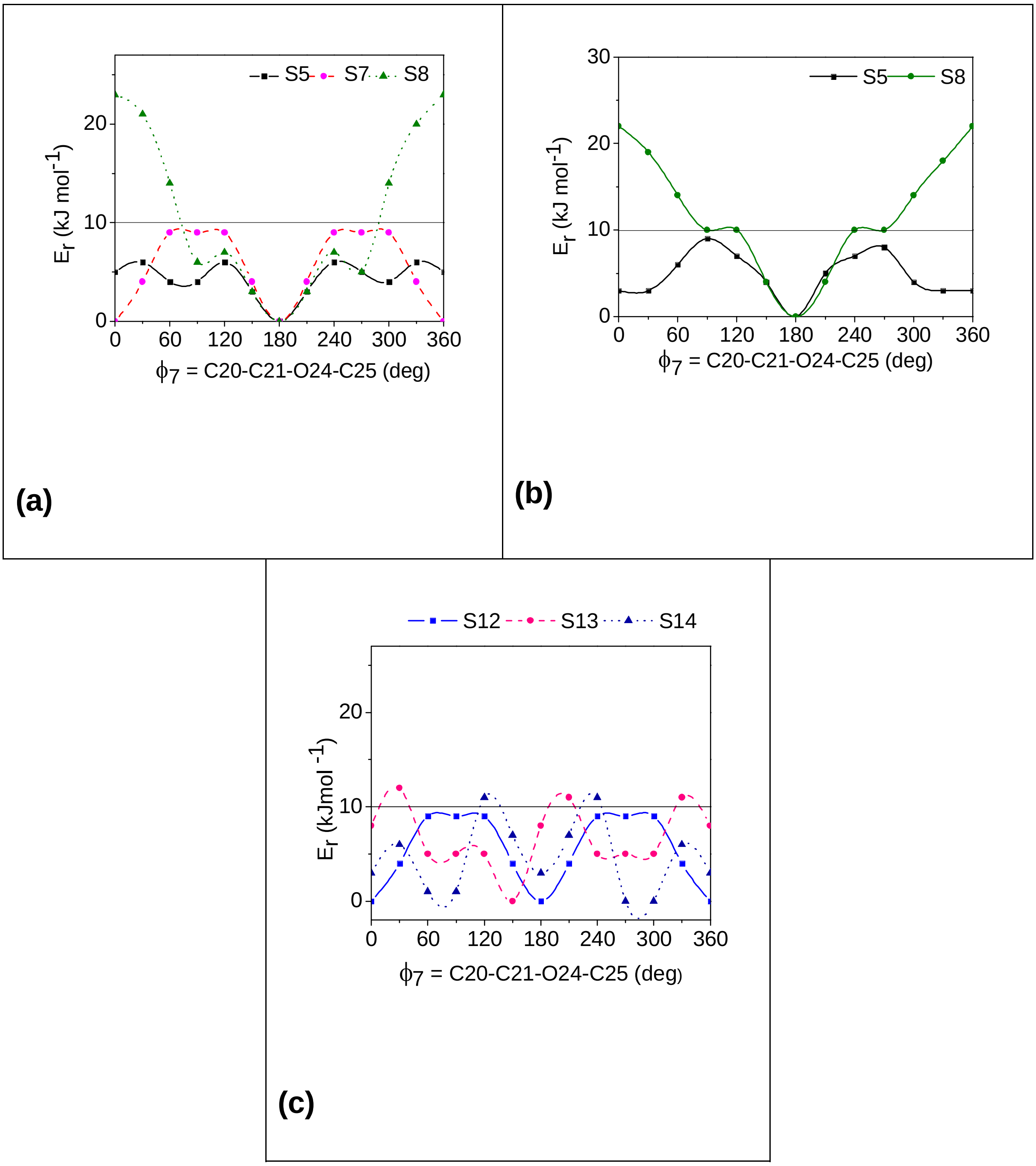

Fig. 12 Relaxed rotational barriers related to the torsion angle ϕ_7:
(a,c): HF b: DFT.

Otherwise, the larger chlorine atoms in these positions (**S8**) cause a remarkable increasing of the relaxed rotational barrier for the side chains. This can be explained by the larger repulsion between the hexyloxy group and the adjacent chlorine atom, especially for the constraint $\phi_7 = 0^o$. Similar results were found in the systems **S10** and **S11**. Obviously, substitutions on the central phenyl ring have less influence on the conformational behaviour of terminal chains. The substitution of methyl and trifluoromethyl groups in the positions 19 and 38 of **S12** has only a low effect on the relaxed rotational barrier of ϕ_7 (Fig. 12c). The curves for **S13** and **S14** are more structured in comparison to that one for **S12** but the high of the barriers is comparable.

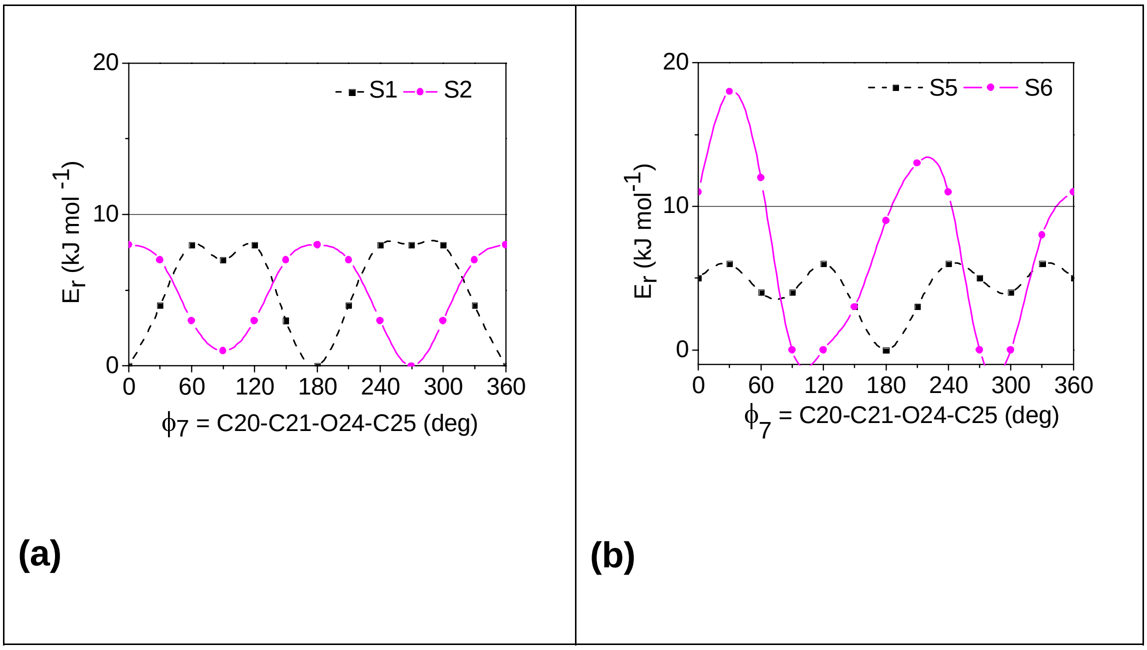

Fig. 13 Relaxed rotational barriers (HF) related to the torsion angle ϕ_7 for systems with terminal hexyloxy and hexyl chains (a: unsubstituted, b: substituted)

For comparison the calculations on the 1,3-phenylene bent-core molecules with hexyl groups as terminal chains were performed to study their conformational and electronic effect. The results are shown in Fig. 13 for the corresponding hexyloxy **S1** and **S5** and hexyl **S2** and **S6** systems. In the system **S1,** the replacement of the terminal hexyloxy groups by hexyl ones **S2** leads to a shift of the positions of the minima and maxima but the rotational barriers have comparable values (Fig. 13a). Whereas the **S5** and **S6** molecules show a significant difference in the relaxed rotational barrier related to the C21-O24 and C21-C24 bonds, respectively (Fig. 13b). In the hexyl compound **S6** the barrier is increased by about 20 kJ mol^{-1} in comparison to that one with terminal hexyloxy chains **S5**. Obviously, the rotation of the hexyl chains are more hindered by the adjacent fluorine atoms in the positions 20 and 39 than in the case of the hexyloxy chains.

3.3.2.2 Dipole moments and ESP group charges

The energy weighted simple mean values for the dipole moments and its components were summarized in Table 5 for the bent-core molecules with substituents on the external phenyl rings. Generally, the polar effect of small substituents on the external phenyl rings of the bent-core molecules is less distinct compared to a corresponding substitution on the central phenyl ring. Remarkable changes on the largest component μ_y were found especially in the chlorine **S8** and trifluoromethyl **S14** substituted molecules.

The ESP group charges of **S5, S7** and **S8** systems with different substituents on the external rings are shown in Fig. 14. The polar substituents cause a decrease of the electron density on the external rings in comparison to the externally unsubstituted system (**S4**), especially in the **S8** molecule. The ESP group charges on the azomethine fragments are changed only when the fluorine substituents are in adjacent positions (19 and 38) to the C=N group. Generally, the alternating behaviour of the ESP group charges on the rings along the legs is retained with a low electron density on the central and external rings but a high electron density on the intermediate rings.

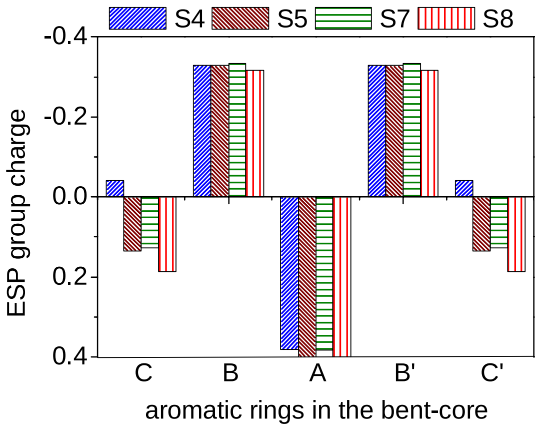

Fig. 14 Electrostatic potential group charges along a leg of bent-core mesogens with substituents on the external phenyl rings (HF).

Table 5 HF energy weighted simple mean values of dipole moment and its components for banana-shaped molecules with substituents on the external phenyl rings[a].

System	$\bar{\mu}_x$	$\bar{\mu}_y$	$\bar{\mu}_z$	$\bar{\mu}$
S5	**-0.12 (0.0)**	**-5.5 (-6.26)**	**-0.16 (0.0)**	**5.5 (6.26)**
S7	**-0.02 (0.0)**	**-4.92 (-7.11)**	**-1.13 (0.0)**	**5.04 (7.11)**
S8	**-1.37 (-1.75)**	**-4.28 (-3.67)**	**-0.25 (+0.65)**	**4.51 (4.12)**
S10	**-0.11 (0.0)**	**-3.81 (-4.49)**	**-0.48 (-0.02)**	**3.85 (4.49)**
S11	**-0.04 (0.0)**	**-4.94 (-5.39)**	**-0.21 (0.0)**	**4.94 (5.39)**
S13	**-0.01 (0.0)**	**-0.84 (-1.05)**	**-1.34 (0.0)**	**1.58 (1.05)**
S14	**-0.10 (-0.53)**	**-2.89 (-3.24)**	**-0.82 (+0.52)**	**3.01 (3.35)**

[a] μ (Debye) values of the most stable conformers in parentheses.

Moreover, the substitution of the terminal hexyloxy chains by hexyl groups results in a lower value of the dipole moment for **S5** (6.26 D) and **S6** (4.87 D). Therefore, different types of terminal chains can influence the phase behaviour especially in lateral substituted bent-core mesogens.

3.4 MM results - dimers

In order to estimate the interaction between bent-core molecules, we have considered two different arrangements, namely stacking and inplane. The illustration of the two different arrangements was given in Fig. 15.

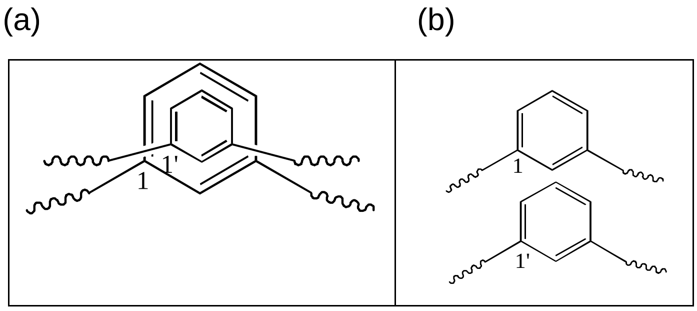

Fig. 15 (a). Stacking, (b) Inplane arrangements of bent-core molecules

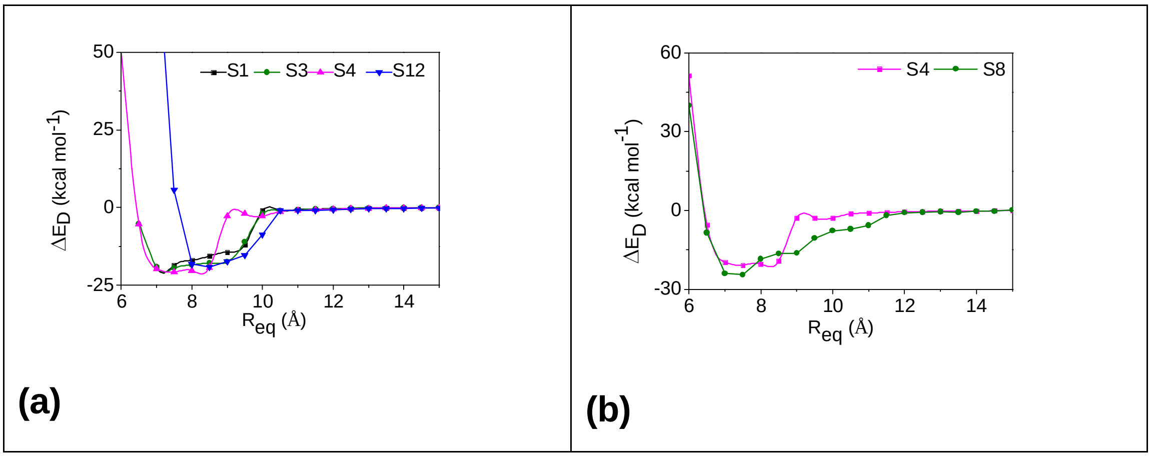

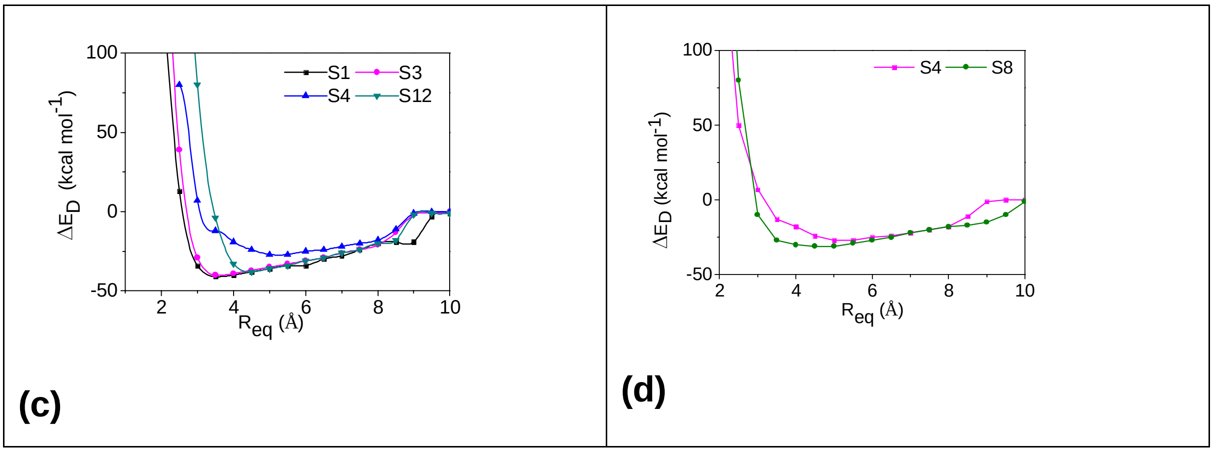

Fig. 16 Dependency of dimerisation energy curves for the systems **S1**, **S3**, **S4**, **S8** and **S12**: a, b: Inplane arrangements; c, d: stacking arrangements.

For this we have considered the unsubstituted system **S1**, substitution on the central ring **S3**, **S4**, **S12** and substitution on the outer phenyl rings **S8**. The distances between the two molecules are considered from the atoms 1 and 1' (please see Fig. 15). The R_{eq} (Figs. 16c and 16d) in stacking arrangement is in the following order in the considered systems: **S1**, **S3**: 3.5Å < **S8**, **S12**: 4.5Å and **S4**: 5 - 5.5Å. In the inplane arrangement (Figs. 16a and 16b) the R_{eq} is following in this order: **S1**, **S3**: 7 - 9Å, **S4**: 7 - 8.5Å and **S8**: 7.5Å. Generally, the results indicate that 2-nitro substitution in the central unit (**S4**) significantly increases the R_{eq} distances in both stacking and inplane arrangements. Moreover, introduction of lateral Cl substitution (**S8**) slightly increases the energy values than the corresponding laterally unsubstituted system (**S4**).

3.5 MD results - monomers

3.5.1 Trajectories of torsion angles - ϕ_1

MD simulations were performed on the isolated molecules in vacuum at 300K and at the clearing temperatures of the compounds. The trajectories of the torsion angle ϕ_1

were shown for the three systems at 300 K in Fig. 17. The MD results on the isolated molecules support the conformational findings from the relaxed rotational barriers within the DFT method (Figs. 7a and 8a). From the trajectories of the torsion angle ϕ_1 the sequence for the flexibility of the legs **S1** > **S12** > **S4** can be concluded. The corresponding trajectories at the clearing temperature of the compounds which are not shown indicate a similar trend. The flexibility of the legs is increased in all cases by the higher temperature but the main differences in the conformational behavior of the molecules are retained.

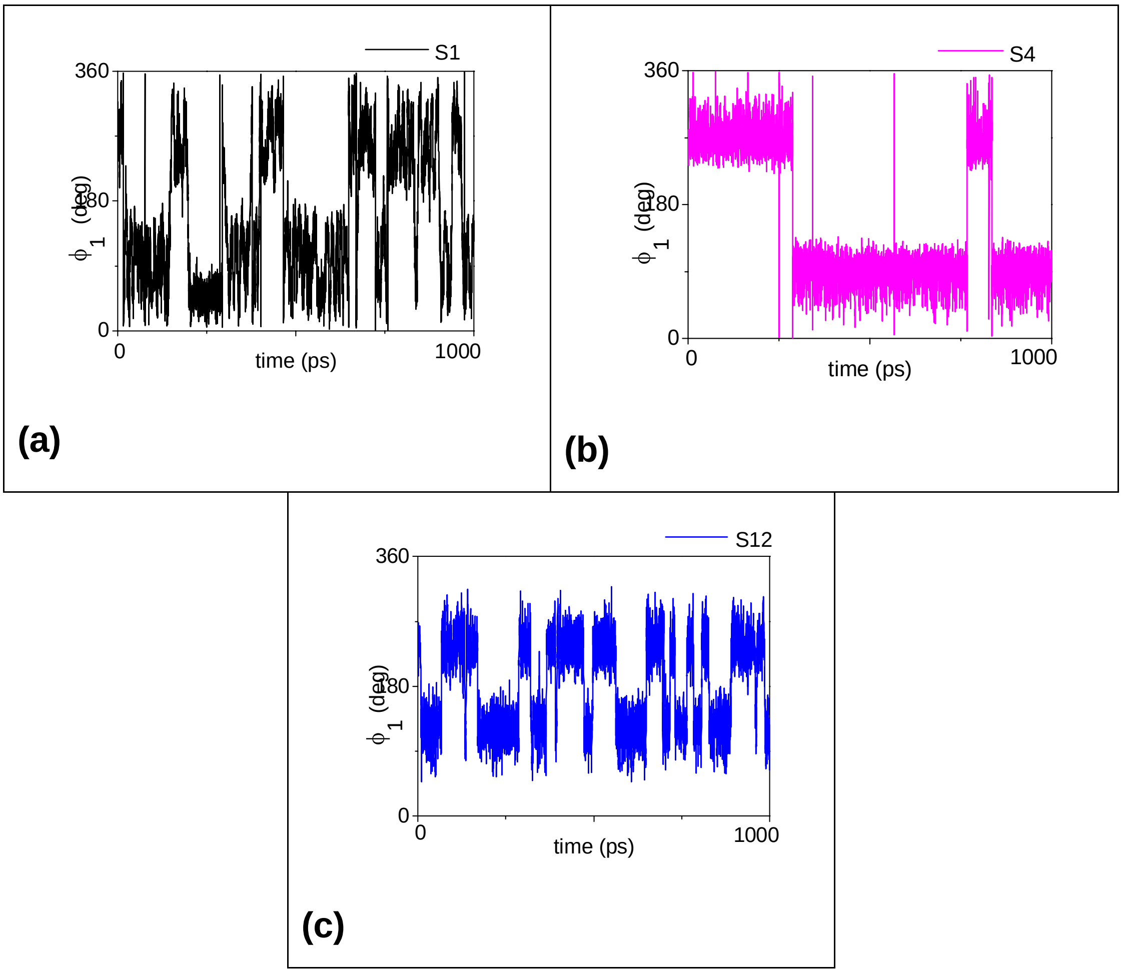

Fig. 17 Trajectories of the torsion angles ϕ_1 for the isolated molecules of the systems at 300K.

In order to investigate the flexibility of the legs in the banana-shaped molecules in the aggregate state MD simulations on clusters with 64 monomers were performed.

From the MD results on clusters similar trajectories of ϕ_1 for a molecule in the environment of the other molecules were generated at 300 K and at the clearing temperature of the compounds. The trajectories of single molecules from the MD results of the clusters at 300K temperature are shown in Fig. 18. It is remarkable that the conformational degree of freedom for the arms of the bent-core molecules in the clusters is significantly reduced in all systems. The reduced flexibility of the bent-cores is in agreement with samulski's "cage effect" [90].

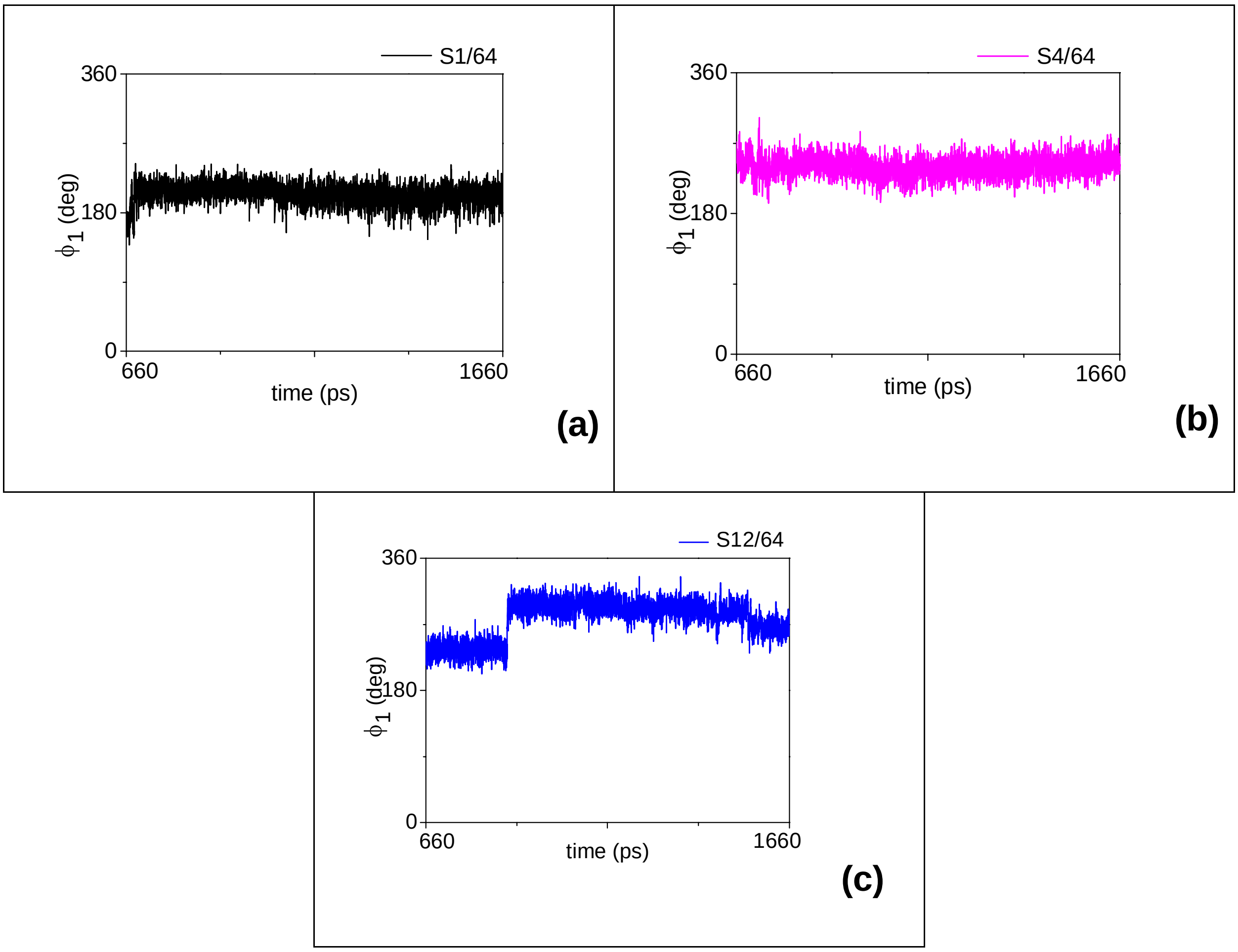

Fig. 18 Trajectories of the torsion angle ϕ_1 for a molecule in the cluster environment of the systems at 300K.

Obviously, the environment of the other molecules leads in all cases to the effect that only small areas of ϕ_1 are preferred but the values are different for the systems. The results are in agreement with the findings of Samulski on the reduced conformational flexibility of aliphatic chains in the condensed state which is known as “cage effect” [90]. This means that the substitution of the molecules leads also in the clusters to essentially different preferred arrangements of the cores. The corresponding trajectories at the clearing temperature of the compounds are not illustrated but

show the same trends. The temperature effect causes a certain broadening of the areas of ϕ_1. A comparison of the trajectories of the isolated molecules (Fig. 17) and the corresponding ones of a molecule in the cluster environment (Fig. 18) indicates a large aggregation effect regarding the conformational behavior of the banana-shaped mesogens.

3.5.2 Average structure from MD - superposition with X-ray structure

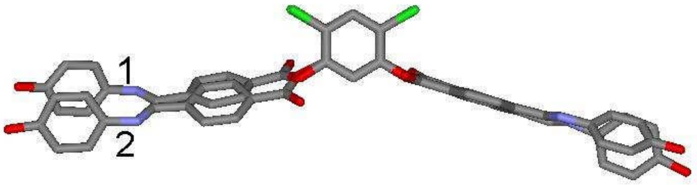

Fig. 19 Superposition of X-ray structure **1** with the average structure **2** obtained from MD for the system **S4**.

The average structure of the single molecule was calculated from the trajectories of single molecule from the MD run of 64 molecules at clearing temperature for the system **S4**. The first 500 frames of the MD run at clearing temperature were considered for the calculation of average structure which was compared with solid state X-ray structure of system **S4**. The average structure obtained from MD results matches very well with the solid state X-ray structure than the conformations obtained from DFT and HF calculations in terms of bending angle. The calculated bending angle γ value for the average structure from MD is 144° and γ for the corresponding X-ray structure is 140°. The higher bending angle of the average structure can be result from the higher temperature. Moreover, the found large bending angle for the system **S4** is in agreement with the bending angle from the NMR experiments in the liquid crystalline states [3].

3.5.3 B-factors

B-factors can be used as a measure to describe the mobility of groups or atoms during the MD run. In the investigated systems the B-factors ($8/3\ \pi^2 <\Delta r^2>$) of the carbonyl oxygen atoms of the ester linkage groups can serve as an indicator for the mobility of the legs of the banana-shaped systems.

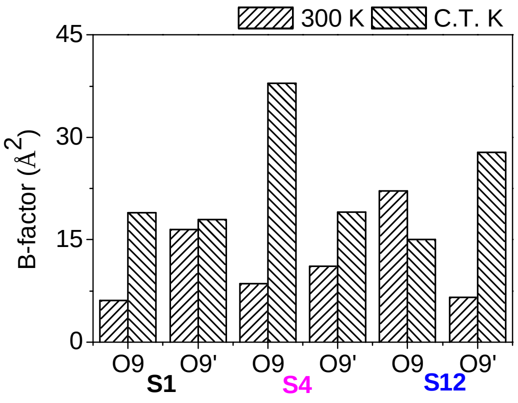

Fig. 20 B-factor values for the carbonyl oxygen atoms of a molecule in the cluster environment of the systems at 300 K and at the clearing temperature (for numbering of the atoms please see Fig. 3).

Therefore, the B-factors are calculated for a molecule in vacuum and in the cluster environment both at 300 K and the clearing temperature. The values for a molecule in the cluster environment at 300K are illustrated in Fig. 20. A considerable temperature effect on the B-factors was found. In the cluster environment the B-factors are higher at the clearing temperature than at 300 K. The largest effect was obtained for system **S4**. For the isolated molecules in vacuum the corresponding

B-factors are generally higher up to 60 Å^2 but there is no remarkable temperature effect in the values (which is not shown in the above Fig. 20). In vacuum the B-factor values for all the systems are comparable at 300K and the clearing temperature therefore not drawn.

3.5.4 Bending angles and molecular lengths

The bending angle (γ) is a key factor in banana-shaped compounds. Therefore γ was calculated for single molecules in vacuum and in the environment of the other molecules in clusters with 64 monomers both at 300 K and at the clearing temperature to study aggregation and temperature effects. Within the MD procedure the full width half maximum (FWHM) values and the maximal frequency (γ_{max}) of bending angle were calculated. The results are summarized in Table 6.

Table 6 Full width at half maximum (FWHM) values and bending angles of maximal frequency (γ_{max}) for systems **S1**, **S4** and **S12**.

System	**Single molecule in vacuum**				**Single molecule in cluster environment**			
	300 K		**C.T.**		**300 K**		**C.T.**	
	FWHM	γ_{max}	**FWHM**	γ_{max}	**FWHM**	γ_{max}	**FWHM**	γ_{max}
S1	**35**	**116**	**30**	**118**	**9**	**120**	**13**	**125**
S4	**25**	**121**	**31**	**120**	**9**	**127**	**17**	**140**
S12	**22**	**119**	**26**	**119**	**6**	**140**	**12**	**124**

FWHM and γ_{max} values in degree.

In vacuum the bending angles of the systems show the sequence γ_{max} : **S4** > **S12** > **S1** both at 300 K and at the clearing temperatures. The γ_{max} values show a different trend than the bending angles γ in the most stable structures of the DFT calculation (Table 4). In the case of the MD studies contributions of less favored conformers are included. In the cluster environment the γ_{max} values differ remarkably between at 300 K and the clearing temperature. Generally, the γ_{max} values of the molecules in the clusters are larger than in vacuum. This can be explained by the larger conformational degree of freedom of an isolated molecule in the gas phase which causes that conformers with small bending angles are also realized. In the cluster environment the substituted compounds show a different trend in the γ_{max} values at 300 K (γ_{max}:**S12** > **S4**) and at the clearing temperature (γ_{max}:**S4** > **S12**). Especially for the dichloro- substituted compound **S4** shows a clear increase of the bending angle γ_{max} from the single molecule in vacuum to the single molecules in the cluster environment. This tendency is in agreement with experimentally results. The NMR studies performed in the liquid crystalline state of several bent-core mesogens have proved that the attachment of chlorine atoms at the positions 4 and 6 of the central phenyl ring increases the real bending angle up to 165° [3].

Table 7 Molecular lengths of the systems in Å at 300K and at the clearing temperatures in Kelvin.

System	Core length (L_C)				Total length (L_T)			
	Single molecule in vacuum		Single molecule in cluster		Single molecule in vacuum		Single molecule in cluster	
	300K	C.T. K	300K	C.T. K	300K	C.T. K	300 K	C.T.K
S1	18.0	22.4	26.7	27.5	18.2	26.4	35.1	36.4
S4	26.8	26.5	27.8	29.0	35.1	33.6	37.8	38.0
S12	26.0	25.8	29.3	25.9	33.1	32.7	39.2	34.7

The core (L_C) and total (L_T) length of the molecules were calculated as mean values from their trajectories within the MD run. The results are given in Table 7. The core length (L_C) was defined as the distance between oxygen atoms of the hexyloxy chains. The L_C values show that there is no significant effect related neither to the temperature nor to the aggregation state. The data of the total length (L_T) – distance between the terminal carbon atoms of the hexyloxy chains – indicate an aggregation effect. Molecules in cluster environment have larger L_T values than those ones in vacuum. This can be attributed to a smaller rate of conformations with folded hexyloxy chains in the aggregated state. The substituted compounds **S4** and **S12** indicate a different temperature dependence of the L_C and L_T values of the molecules in clusters. This behavior is in agreement with the tendency found in the bending angle γ_{max} for the molecules in clusters at 300 K and at the clearing temperature (Table 6). The findings of the substituted systems both in the molecular length and the bending angle of the molecules in the clusters are hints for their different mesogenic properties.

3.6 MD results - clusters

3.6.1 Radial atom pair distribution function and orientational correlation function

The structure formation of the molecules in the clusters can be analyzed by the calculation of the radial atom pair distribution function g(r). The g(r) values were related to the reference atom C2 which describes the position of the central unit of the banana-shaped molecules. The results for the clusters at two different temperatures are illustrated in the Fig. 21. The systems show nearly the same tendency in the structure formation both at 300 K and the clearing temperature with the sequence of **S12** > **S1** > **S4**. Especially in the case of the nitro substituted compound **S12** a certain long-range order of the molecules was observed in both temperatures. The unsubstituted compound **S1** shows a short range order at 300 K which is decreased at clearing temperature. The g(r) curves are comparable for system **S4** at both temperatures and indicate a lower order.

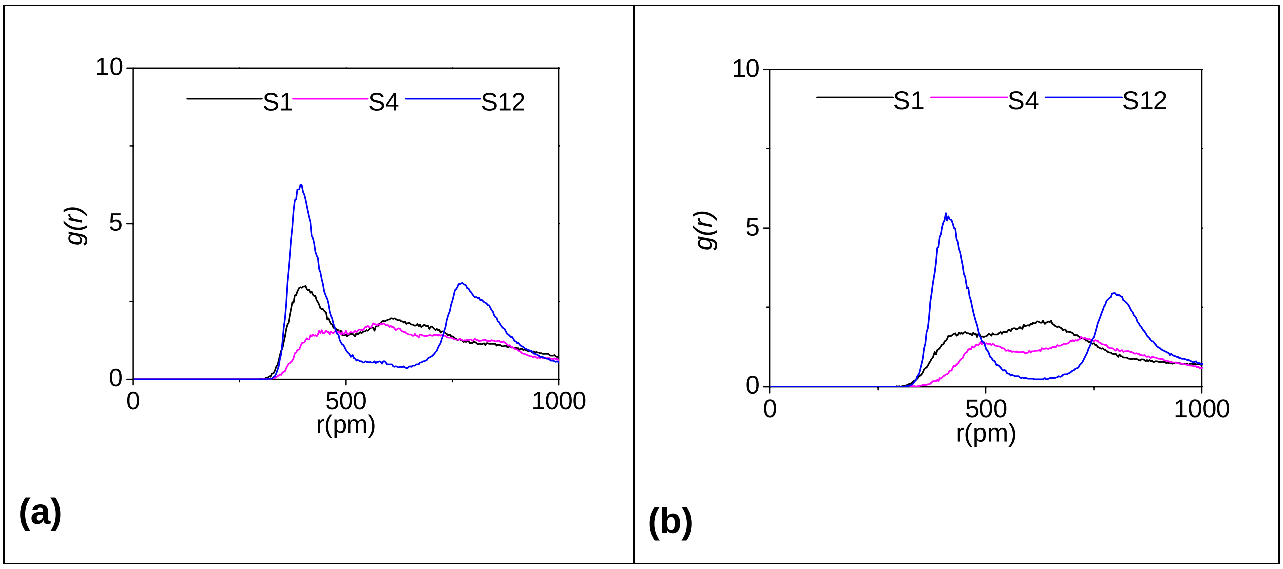

Fig. 21 Radial atom pair distribution function g(r) for the systems [(a): 300 K (b): clearing temperature)].

Further information on the orientation of the molecules results from the calculation of the orientational correlation function g(o). The g(o) data are obtained by the calculation of the radial dependence of the cosines between the vectors related to the C2 and C5 atoms of the central unit.

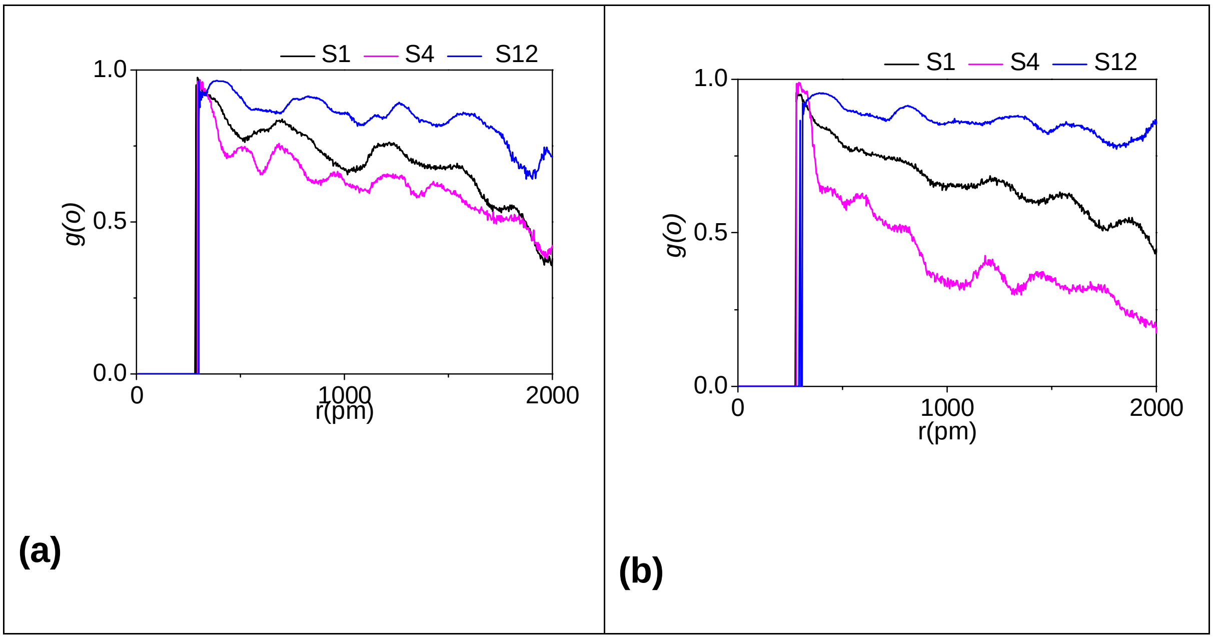

Fig. 22 Orientational correlation function g(o) for the systems (a: 300 K, b: clearing temperature).

The averaging procedure is carried out via the numbers of the monomers and the time steps during the MD run. The results are presented in Fig. 22. The g(o) curves support the trends found in g(r*)* results. The long-range order is increased in system **S12** and reduced in system **S4**. The effect is more distinct in the curves at clearing temperature. This is a good evidence that the chlorination in the 4,6 positions of the central 1,3-phenylene unit (**S4**) can induce significant perturbations in the bent conformations of the monomers and therefore essentially influence the aggregation of the banana-shaped molecules.

3.6.2 Diffusion coefficients and root mean square deviations

The mobility of the molecules in the clusters has been investigated by diffusion coefficients which were calculated using the Einstein model within the molecular dynamics run [87, 88]. The D values for the systems were calculated form the MD runs at 300 K and at the clearing temperature. For both temperatures the last 500 ps of the equilibration step were considered for comparison which corresponds to total simulation periods of 1160-1660 ps (300K) and 2220-2720 ps (clearing temperature), respectively. The D values are summarized in Table 8.

Table 8 Diffusion coefficients D of the clusters at 300 K and at the clearing temperatures (D values in 10^{-12} m^2 s^{-1})

System	D (300K)	D (C.T.K)
S1	17.13	51.48
S4	10.38	23.95
S12	6.35	173.88

As expected the diffusion coefficients are generally larger at higher temperature. Nevertheless, it is remarkable that the D values show different sequences at 300 K (**S1** > **S4** > **S12**) and at the clearing temperature (**S12** > **S1** > **S4**). This effect can not be explained by the small differences in their clearing temperatures. (please see

Table 1). Obviously, the chlorine and the nitro substituted compounds show a contrary temperature dependence of D related to the unsubstituted species which are hints for their different aggregation behavior. The flexibility of molecules or parts of them in clusters can be indicated by the calculation of the root mean square deviations (RMSD) of the corresponding atoms within the MD simulation. The RMSD values of the core and a terminal hexyloxy chains were calculated for the three systems to investigate the flexibility of the different segments of the banana-shaped molecules in the aggregated state. In both cases the heavy atoms of the segments were considered, only.

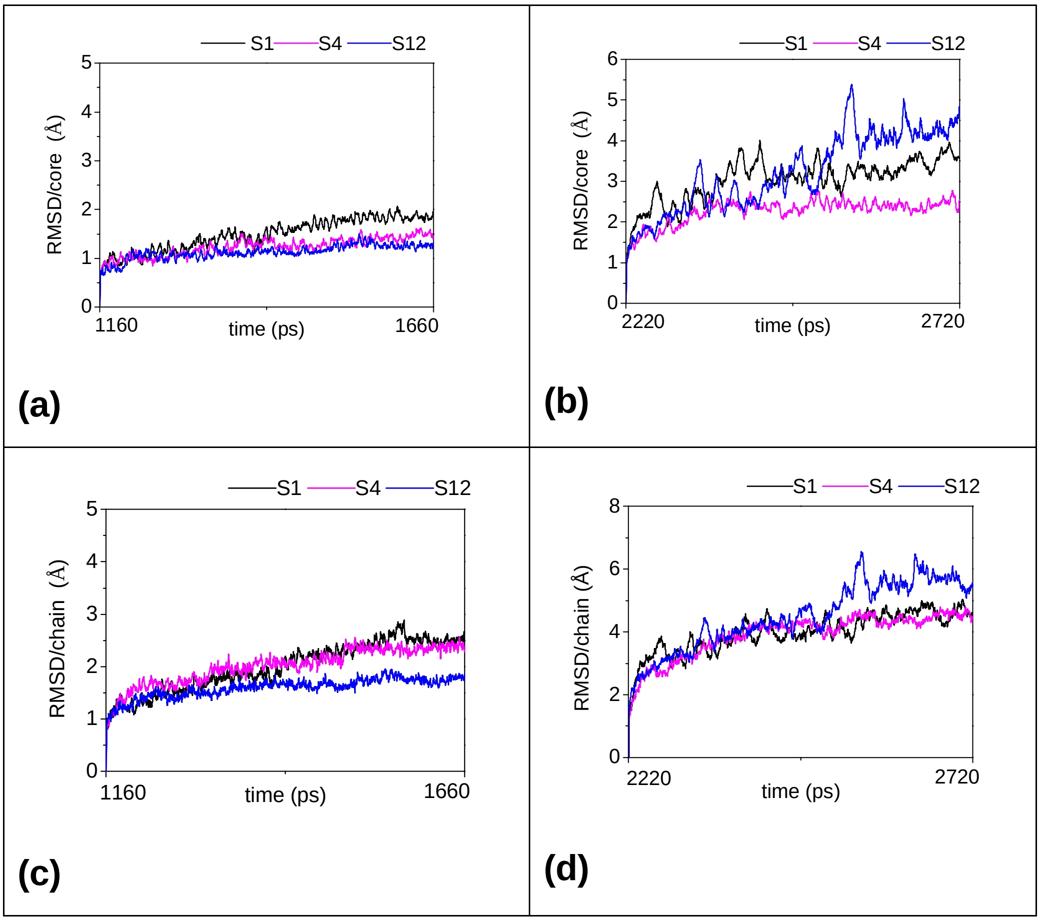

Fig. 23 RMSD values of the core and the terminal hexyloxy chain for the systems [(a). core/300 K, (b). core/clearing temperature, (c). chain/300K d: chain/clearing temperature].

The results of RMSD values at 300 K and at the clearing temperature are illustrated in Fig. 23. Similar to the calculation of the diffusion coefficients the last 500 ps of the MD run were used as scoring period for the RMSD data. The curves indicate a significant temperature effect concerning the flexibility of the core and the terminal hexyloxy chain. Generally, the RMSD values are larger at higher temperature. It is remarkable that the nitro substituted system **S12** shows a higher flexibility at the clearing temperature both in the core and the terminal chains in comparison to the chlorinated compound **S4**. These findings support the trend found in the calculated diffusion coefficients and are further hints for the different aggregation and mesophase behavior of the substituted banana-shaped compounds.

Chapter 4 Influence of the orientation of ester linkage groups on bent-core compounds

The influence of the orientation of ester linkage groups on the structural and electronic properties of five-ring bent-core molecules with a central 1,3-phenylene unit has been investigated including hexyloxy and dodecyloxy terminal chains. The conformational behavior of the ten isomers was studied in a systematic way. The one- and two-fold potential energy scans were calculated to show the influence of the orientation of carboxyl linkage groups on the flexibility of the wings. MD simulations were carried out on the monomers and clusters with 64 and 128 molecules. The aggregation behavior of the molecules was analyzed. Moreover, we have studied the effect of pressure on the structural changes by MD simulations on the clusters of such molecules at 300 K. The size and cage effects were also investigated on such compounds.

4.1 Systems and definitions

Figs. 24, 25 and Table 9 illustrate the considered ten isomeric bent-core molecules with different orientation of ester connecting groups. The conformational properties of single molecules were studied by *ab initio* and DFT methods. The DFT conformational findings on isolated molecules were compared with the results of MD simulations on single molecules.

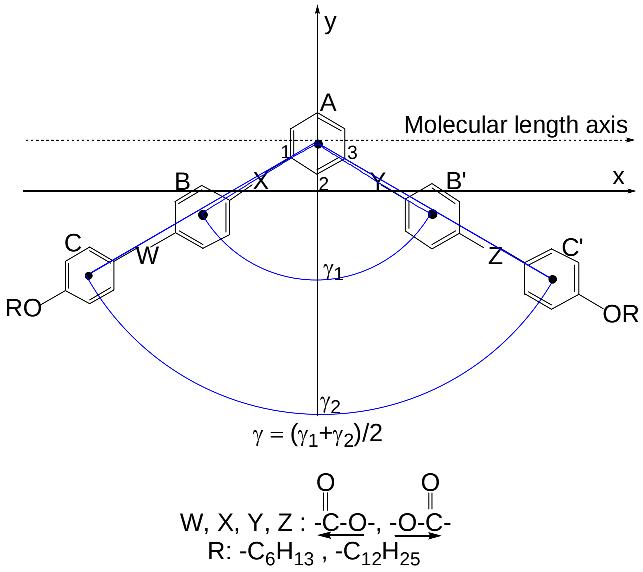
y
A
Molecular length axis
1
3
B
X
2
Y
B'
x
C
W
C'
Z
RO
OR
γ1
γ2
γ = (γ1+γ2)/2
W, X, Y, Z : -C(=O)-O-, -O-C(=O)-
R: -C6H13 , -C12H25

Fig. 24 The general structure of ten isomers with the definition of coordinate systems

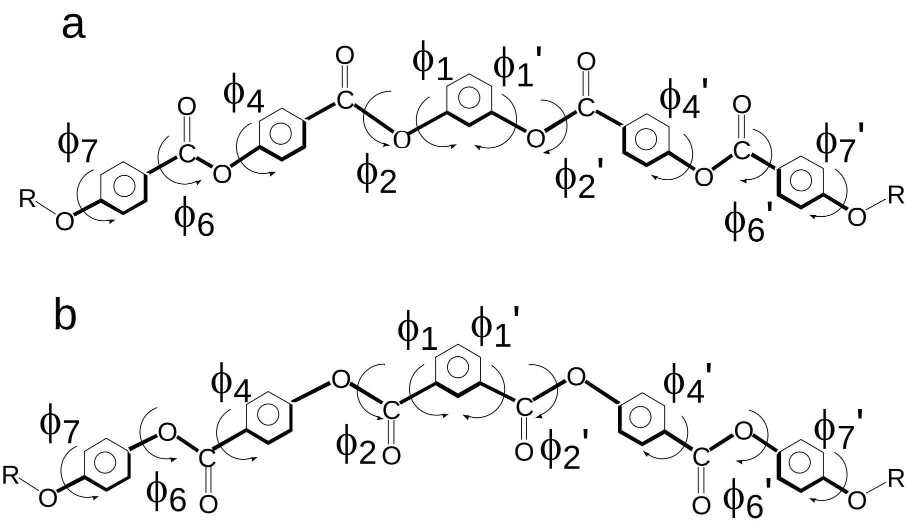
a
ϕ7
ϕ4
ϕ6
ϕ1
ϕ1'
ϕ2
ϕ2'
ϕ4'
ϕ7'
ϕ6'
R
O
C
b
ϕ7
ϕ4
ϕ6
ϕ1
ϕ1'
ϕ2
ϕ2'
ϕ4'
ϕ7'
ϕ6'

Fig. 25 Definition of significant torsion angles by the corresponding atoms of the bold chains; a: system **E1**; b: system **E4**.

Table 9 Illustration of the direction of the carboxyl connecting groups in the banana-shaped isomers (see also Fig. 21).

System	**W**	**X**	**Y**	**Z**	Orientation of the dipole of the C-O bond in the ester groups	**E_r[a] DFT**	**T [b]** [91]
E1	**-COO-**	**-COO-**	**-OOC-**	**-OOC-**	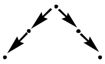	**0**	**SmCP$_A$ 119 I**
E2	**-COO-**	**-OOC-**	**-COO-**	**-OOC-**	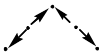	**7**	**Cr 157 I**
E3	**-OOC-**	**-COO-**	**-OOC-**	**-COO-**	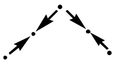	**29**	**SmCP$_A$ [c] 162 I**
E4	**-OOC-**	**-OOC-**	**-COO-**	**-COO-**	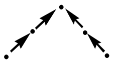	**22**	**Col 189 I**
E5	**-COO-**	**-COO-**	**-COO-**	**-COO-**	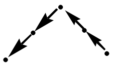	**10**	**Col 140 I**
E6	**-COO-**	**-COO-**	**-COO-**	**-OOC-**	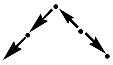	**4**	**SmCP$_A$ 112 I**
E7	**-COO-**	**-COO-**	**-OOC-**	**-COO-**	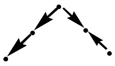	**14**	**SmCP$_A$ 133 I**
E8	**-COO-**	**-OOC-**	**-COO-**	**-COO-**	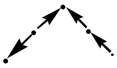	**14**	**Col 168 I** **SmCP$_A$ 158**
E9	**-COO-**	**-OOC-**	**-OOC-**	**-COO-**	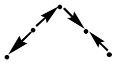	**18**	**Col 144 I**
E10	**-OOC-**	**-COO-**	**-COO-**	**-COO-**	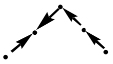	**25**	**Col 168 I**

a: Relative energy of the most stable conformer in kJ mol^{-1}; [b] Clearing temperature for systems with dodecyloxy terminal chains in ℃; [c] Undulated SmCP phase which is also considered as a columnar phase [91].

4.2 Computational details

As described in the chapter 3, the *ab initio* - HF/STO-3G and DFT-B3LYP/6-31G(d) calculations were carried out using the program package Gaussian98 [64] and the molecular dynamics (MD) simulations have been carried out with implemented AMBER program using gaff force field. MD studies were performed on the isolated molecules in vacuum at 300 K and at their clearing temperatures including the simulated annealing procedure by increasing the temperature up to 1000 K and a simulation time of 1 ns. A time step of 1 fs was used in all simulations. The non-bonded interactions were calculated with a cut-off radius of 10000 pm. The results of the molecular dynamics calculations have been analyzed by trajectories of significant structural parameters. The MD simulations on the clusters were performed with 64 and 128 monomers using an antiferroelectric starting structure model [3] for all systems. The size effect is analyzed by comparative MD simulations on the system **E3** including studies on clusters with 64 and 128 monomers, respectively. For the treatment of the clusters a total simulation time of 1.5 ns and a time step of 2fs were used at 300 K including heating phases. For the analysis of the MD data at 300 K the last 200 ps of the equilibration phases were taken into account. The MD simulations were carried out within the n, p, T ensemble. Moreover, the effect of pressure on the properties of bent-core mesogens is investigated by MD simulations at 300 K with pressure values of 1, 100 and 500 bar. The SHAKE algorithm was used for all the atoms. The non-bonded interactions in the clusters were calculated with a cut-off radius of 1000 pm. The analysis of the MD results was carried out in a similar manner as already described in chapter 3.

4.3 DFT and HF results

4.3.1 Relaxed rotational barriers – ϕ_1 and ϕ_7

A systematic investigation of the relaxed rotational barriers of significant torsion angles indicates that the conformational flexibility of the wings of bent-core molecules is essentially determined by the direction of the carboxyl connecting groups in the isomers. First, this is illustrated for relaxed rotational barriers related to the torsion angle ϕ_1. The ten isomers essentially show two different types of barriers for ϕ_1 indicated by the systems **E1** and **E4** in Fig. 26.

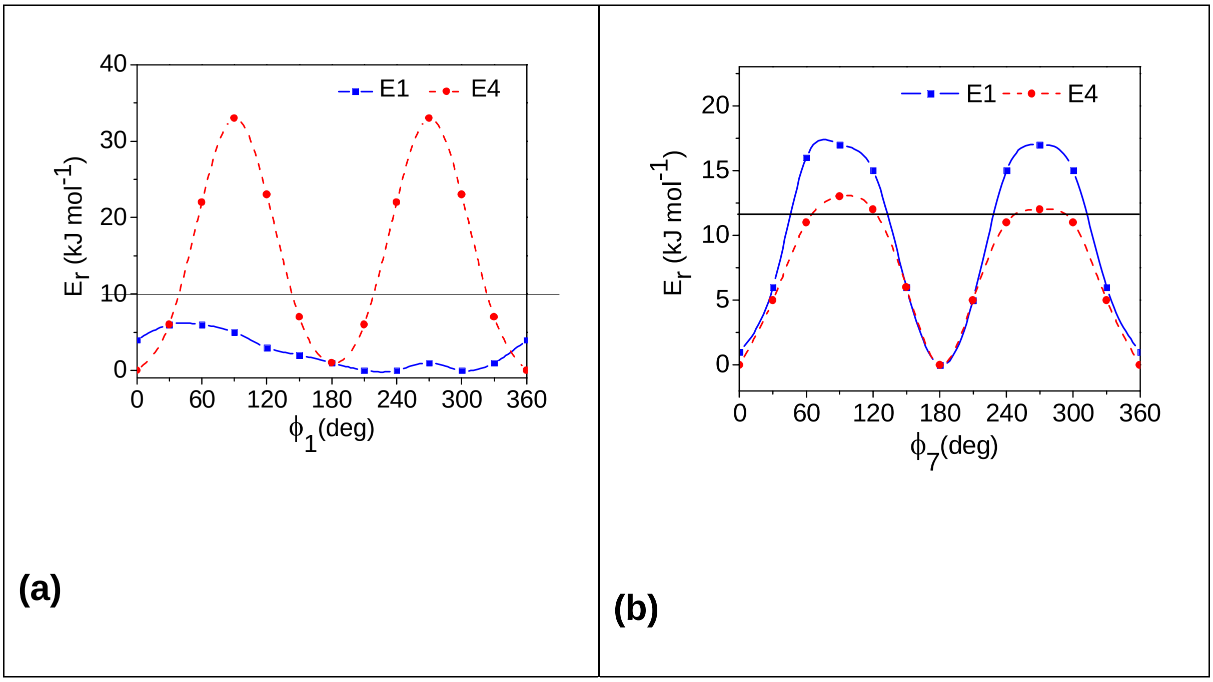

Fig. 26 Relaxed rotational barriers (DFT) related to the torsion angles ϕ_1 and ϕ_7 for the systems **E1** and **E4**.

If the linkage group is connected by an oxygen atom to the central 1,3-phenylene unit (O-C bond) it results a barrier lower than 10 kJ mol^{-1} like in system **E1** which corresponds to a high flexibility for this segment of the molecule. Similar trends are also obtained for the curves of the systems **E3**, **E5**, **E6**, **E7** and **E10**. This indicates that there is only a small influence of the direction of other connecting groups on the barriers. Otherwise, if the linkage group is connected by a carbon atom to the central ring A (C-C bond) like in system **E4** it arises a rather high barrier of about 30 kJ mol^{-1} and the conformational degree of freedom is decreased for the corresponding leg of the compound (Fig. 26a). The same conformational behaviour was found for this bond in the systems **E5**, **E8** and **E9**. It indicates that there is no coupling effect by the orientation of the other connecting groups on the relaxed rotational barriers for these isomers.

The relaxed rotational barriers with respect to the torsion angle ϕ_2 show a rather limited conformational degree of freedom with a barrier of about 40 kJ mol^{-1} for all isomers. The preferred conformers are characterized by a coplanar arrangement of the carbonyl group and the adjacent phenyl ring (ϕ_2 = 180°). This is in agreement with conformational studies on other bent-core systems including ester and azomethine connecting groups [81].

The one-fold PES scans related to torsion angle ϕ_4 of the second connecting group (W) are comparable with the corresponding results for the torsion angle ϕ_1 of the first linkage group (X). We have found two types of relaxed rotational barriers depending on the connecting atom of W to the ring B. In the case of an O-C bond it results a low barrier and high flexibility for the wing. For a C-C bond the opposite effect was obtained. This supports the findings that there is no or only a small influence of the rotation about the O-C (C-C) bonds by the direction of the other connecting groups. Moreover, the conformational studies show that the flexibility and the bending of the ten isomers are mainly determined by the type of the bond related to the angles ϕ_1, ϕ_4, ϕ_1' and ϕ_4'. In some way isomers with higher flexibility of the wings can be related to lower clearing temperatures and to the preferred formation of smectic phases, e.g. **E1**, **E6** and **E7** excepting **E3**. On the other hand, compounds with lower conformational degree of freedom show mostly higher phase stability and form columnar phases, e.g. **E4**, **E8** and **E9** (see Table 9). The degree of conformational flexibility can be estimated for such banana-shaped compounds by the numbers of oxygen atoms of the linkage groups which are directly connected to the rings A (X, Y) as well as B and B’ (W, Z). Such a connection to the three rings by four or three oxygen atoms gives compounds with high, by two oxygen atoms intermediate and by one or zero oxygen atoms low flexibility.

The conformational degree of freedom of the terminal chains exerts influence on the aggregation of the bent-core compounds. Therefore, we have carried out one-fold PES scans related to the torsion angle ϕ_7 to investigate the effect of the direction of the linkage groups. The results are illustrated in Fig. 26b for the systems **E1** and **E4**. There is a small coupling effect on the one-fold PES scan with respect to ϕ_7 by the orientation of the neighboured linkage group W, only. It results a barrier of about 18 kJ mol^{-1} if W is connected by a carbon atom to the ring C like in the systems **E1**, **E2**,

E5 - **E9**. The barrier is decreased to 12 kJ mol^{-1} in the isomers **E3**, **E4** and **E10** where the neighboured connecting group W is bound by an oxygen atom in the para position to the chain. The small energetic effect on the rotational behaviour of the terminal chains by the orientation of the neighboured linkage group can have a limited contribution in the aggregation of such compounds.

4.3.2 Effect of external electric field on the rotational barrier

The behavior of bent-core molecules in electric fields is of interest with respect to neighboring effects in such compounds. Therefore, we have calculated one-fold PES scans related to the angle ϕ_1 in the presence of an electric dipole field in the y direction of 0.006 atomic units. The results for the systems **E1** and **E4** are shown in Fig. 27

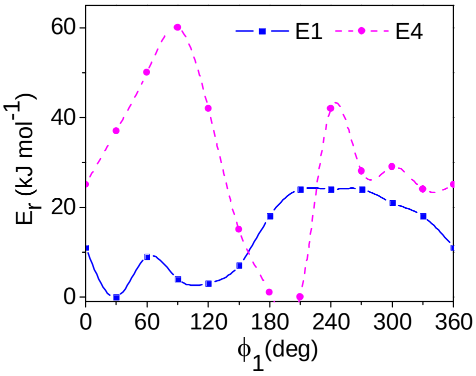

Fig. 27 Influence of an external electric field on the relaxed rotational barriers (DFT) for the systems **E1** and **E4** (dipole field in the y direction with an amount of 0.006 a.u.)

A comparison of the results in Figs. 26a and 27 indicates that an external dipole field increases the rotational barrier both in systems **E1** and **E4** by about 10 and 20 kJ mol^{-1} respectively. The positions of minima and maxima are different which causes another trend in the curves for the systems with and without an external field. Obviously, the conformational flexibility of the banana-shaped systems is significantly decreased by the influence of an external electric field in the direction of the polar axis.

4.3.3 Two-fold potential energy surface scans

The investigations on the effect of the direction of the linkage group on the conformational behaviour of the isomers are completed by Ramachandran-like plots with respect to the torsion angles ϕ_1 and $\phi_{1'}$ including 30° steps. The results are illustrated in Fig. 28 for the systems **E1**, **E3** and **E7** which represent isomers with two O-C bonds and two C-C bonds as well with one O-C and one C-C bond, respectively, for the legs connected to the central unit A. The findings from the Ramachandran-like plots support the results on the conformational flexibility of the isomers obtained by one-fold PES scans related to the angle ϕ_1. Isomers with a linkage of the two wings to the central unit A by O (C) atoms show low (high) energy maps of the type Fig. 28 **E1** (**E3**). If the central unit A is connected with the wings by a C and O atom like in system **E7** it results an intermediate energy map of the type Fig. 28 (**E7**).

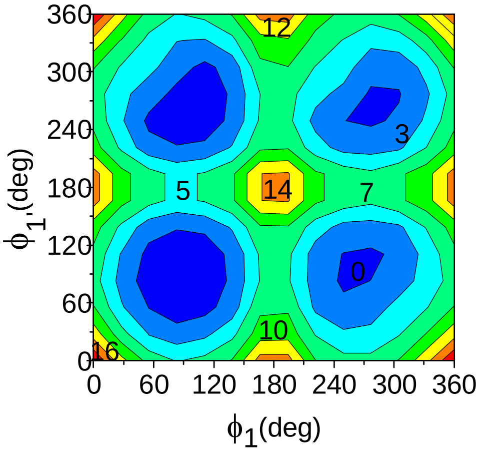

(E1)

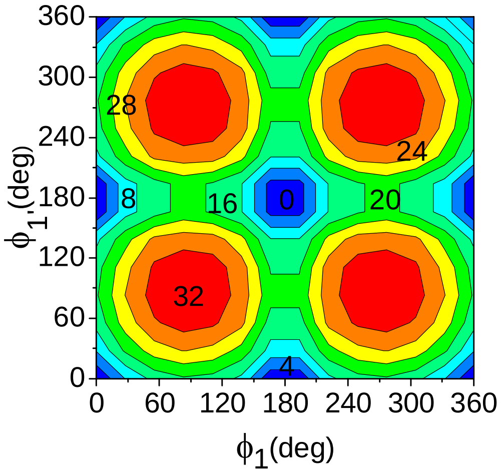

(E3)

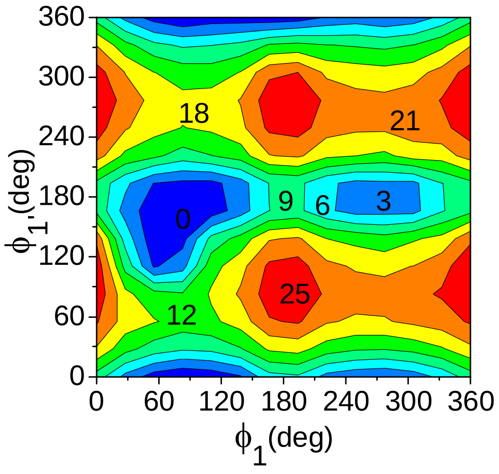

(E7)

Fig. 28 Two-fold potential energy surface scans (HF) related to the torsion angles ϕ_1 and ϕ_1' (energy values in kJ mol^{-1}).

Moreover, the Ramachandran-like plots illustrate that the stationary points (minima, maxima and saddle points) result in different areas of the maps for the systems **E1**, **E3** and **E7**.

4.3.4 Dipole moments, bending angles and ESP group charges

The polarity and the bent character are important properties of bent-core mesogenic compounds. Therefore, we have calculated the dependency of the dipole moment μ and the bent-core angle γ with constraints to the torsion angle ϕ_1 for the isomers. The results for the systems **E1** and **E4** are summarized in Fig. 29.

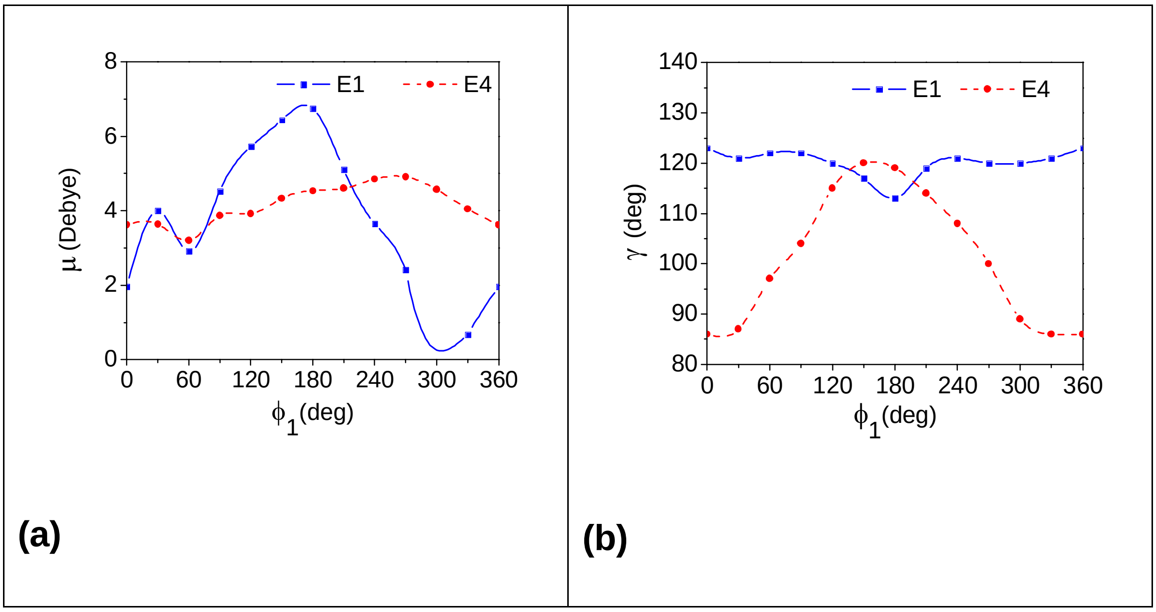

Fig. 29 One-fold scans (DFT) related to the torsion angle ϕ_1 [(a). dipole moment μ, (b). bending angle (γ)].

Table 10 Dipole moments and its components for the ten banana-shaped isomers in Debye.

Isomer	DFT– B3LYP/6-31G(d)							
	without an external electric field				with an external electric field [a]			
	μ_x	μ_y	μ_z	μ	μ_x	μ_y	μ_z	μ
E1	0.00	-0.77	0.00	0.77	-0.04	-4.61	1.45	4.83
E2	-1.37	-2.64	-2.69	4.02	-2.83	-7.99	-0.03	8.48
E3	0.00	-2.18	0.00	2.18	-2.09	6.04	-0.72	6.44
E4	-1.04	-3.70	0.20	3.61	-3.05	3.93	-0.98	5.07
E5	-7.82	-3.70	-0.20	8.65	-6.59	-5.76	-4.99	10.07
E6	-3.94	-4.97	-1.14	6.45	-6.33	-7.65	-2.19	10.17
E7	-1.54	-4.30	-1.22	4.73	-4.45	6.58	-1.31	8.06
E8	-3.13	-4.64	-2.59	6.17	5.81	9.08	-1.16	10.84
E9	1.39	-3.19	-2.92	4.55	-1.19	-8.57	2.58	9.03
E10	-3.95	-3.13	0.89	5.15	4.69	6.86	-2.73	8.75

([a] The amount of electric dipole field in y direction is 0.006 atomic units).

The curves for the dependency of μ with variation of ϕ_1 show a significant different trend for both systems. For system **E1** the values of μ vary in a rather large range of about 1-7 Debye (Fig. 29a). System **E4** shows a relatively small angle dependency of μ with values of about 4 Debye. The dipole moments and its components for the most stable conformations of the isomers are given in Table 10. It is remarkable that the values differ from about 1 Debye **E1** up to about 9 Debye **E5** which is caused only by a different direction of the connecting groups. The main contribution to the dipole moment results from the μ_y component excluding system **E4**. The y-axis represents the polar axis of the bent-core molecules (Fig. 24). For comparison the corresponding values of the μ as well as μ_x, μ_y and μ_z of the isomers are added by data which were obtained from calculations with an external electric dipole field in the y direction of 0.006 a.u. Generally, in the presence of an external field the values of the total dipole moments are increased by about 4 Debye (Table 10). From the values of the dipole moments in the absence of an external electric field a certain trend is found to the phase properties within the ten isomers. If the total dipole moment of an isomer is relative small and the component of the polar axis (μ_y) yields the major contribution to μ then the formation of smectic phases is preferred **E1**, **E3** and **E7**, excepting **E6**, otherwise columnar phases are favored **E5**, **E8**, **E9** and **E10**, excepting **E4**. The one-fold scans of the bending angle (γ) related to the torsion angle ϕ_1 show a remarkable difference for the isomers which is illustrated for the systems **E1** and **E4** in Fig. 29b. In the system **E1** there was a small torsion angle dependency of γ and over the whole range and a high value of about 120° was obtained. Similar trends were observed for the systems **E3**, **E6** and **E7** not shown in Fig. 29b. System **E4** shows a significant dependency of γ related to the angle ϕ_1 (Fig. 29b). A similar torsion angle dependency of γ was observed in the systems **E4**, **E8**, **E9** and **E10**. From the behaviour of the γ/ϕ_1 curves a correlation was found in some way with phase properties of the ten isomers. Large γ values and a small dependency related to ϕ_1 are obtained for smectic mesogens like systems **E1**, **E3**,

E7 and **E8**. Otherwise, a strong dependency of γ related to ϕ_1 including small γ values was found for the systems **E3**, **E4**, **E8**, **E9** and **E10** and can be seen as a hint for the formation of columnar phases.

Moreover, from electrostatic potential group charges (q/ESP) a global pattern of the charge distribution on the rings and connecting groups can be obtained. The q/ESP values for the isomers at the centres on the aromatic rings are illustrated in Fig. 30. The charges at the connecting groups show no significant changes for the systems and are therefore not drawn in Fig. 30 due to clarity The electron density ρ (ρ corresponds to –q/ESP) on the central ring A and on the external rings C, C' of the isomers correlates with the mesophase properties of the banana-shaped compounds. In such cases where the electron density on the central ring is smaller than that one of the external rings $\rho(A) < \rho(C, C')$ there is a tendency to form smectic phases, e.g. systems **E1**, **E3**, **E6** and **E7**. The opposite case $\rho(A) > \rho(C, C')$ can be seen as a hint for the favored formation of columnar phases by these compounds, e.g. systems **E4**, **E5**, **E8**, **E9** and **E10**. The findings for the electron density are in agreement with the maximum values of the calculated electrostatic potential on the rings in other bent-core molecules by J. P. Bedel *et al*. [89].

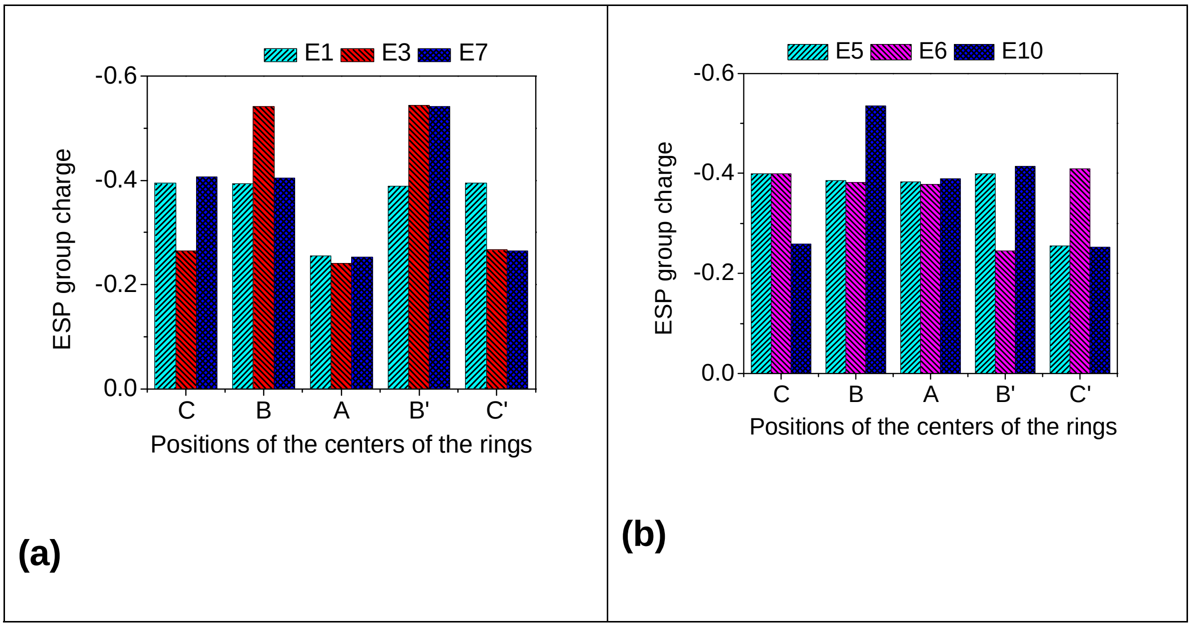

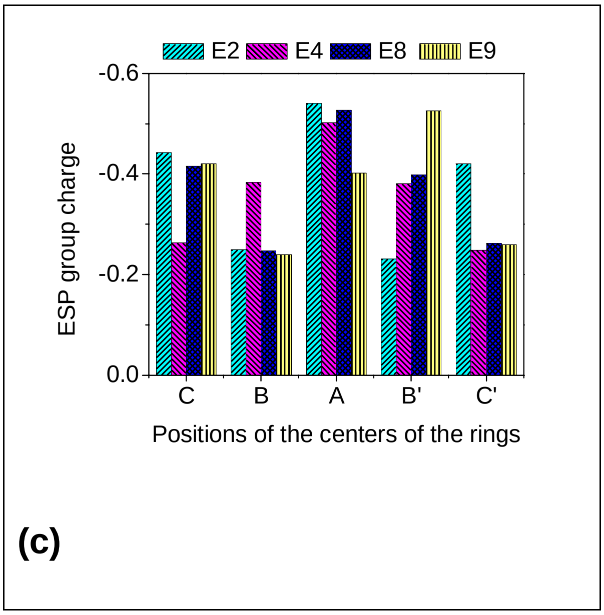

Fig. 30 Electrostatic potential group charges on the centers of the rings for the ten banana-shaped isomers (DFT results).

4.3.5 Correlation between dipole moments and dielectric constants

Assuming that the static dielectric constant ε_0 is a measure for the sum of the effective dipole moment μ and applying the model of Kirkwood [92] one should expect a linear relation between the left side of the equation (4.1) and the calculated squared dipole moments for the optimal conformation.

$$\frac{(\varepsilon_0 - 1)(2\varepsilon_0 + 1)}{9\varepsilon_0} \approx \alpha + \frac{\mu^2}{3kT} \qquad \text{..........(4.1)}$$

Thereby, the polarisability α is constant in first approximation for the investigated isomers with the same number of atoms and bond types. In some way this is supported by the calculation of the polarisabilities of the most stable structures for the ten isomers in standard orientation (Fig. 24) within the DFT method. For the diagonal elements of the polarisability in atomic units (1 a.u. of polarisability is approximately 1.649 10^{-41} C^2 m^2 J^{-1}) it results α_{xx}=916, α_{yy}=514, α_{zz}=294 (**E1**) and α_{xx}=638, α_{yy}=687, α_{zz}=345 (**E4**). These two systems show the most significant deviations in the orientation of the ester linkage groups (Table 9) and the highest differences of the calculated polarisability, respectively, especially in the component with the main contribution of α_{xx}. The components of the other isomers are mostly between the corresponding values of the systems **E1** and **E4** and therefore not given in detail. The dielectric constants were measured for the isomers with dodecyloxy terminal chains in a metal cell by the aid of a Solartron Schlumberger equipment in the frequency range from 10Hz to 10 MHz. In order to separate the static dielectric constant from the effect of the electrical double layer a fitting program was used [93]. Thus, the error of the static dielectric constant is reduced to 2%. Due to the different phase transition temperatures all data were interpolated or extrapolated to the common temperature of 430 K. The measured eight ε_o values and the calculated dipole moments for the most stable conformations within the DFT method are correlated in Fig. 31 according to the relation of equation (4.1).

In some way, a linear correlation was found for the considered isomers excluding system **E1**. This system has a very small dipole moment and a low clearing point temperature which could be a reason for the deviation of the **E1** from the common trend. The findings of the dielectric measurements support that the calculated dipole moments of the most stable conformations reproduce the common trend of the global polarity of the banana-shaped compounds.

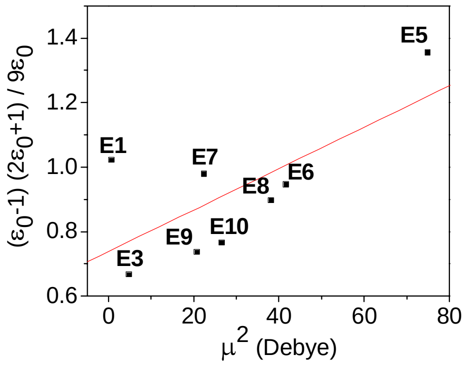

Fig. 31 Correlation between the static dielectric constants ε_0 and the dipole moment μ (Debye) according the Kirkwood model equation (**4.1**).

4.4. MM results - dimers

In order to estimate the interaction between bent-core isomers, we have considered two different arrangements, namely stacking and inplane. The illustration of the two different arrangements was given in Fig. 32.

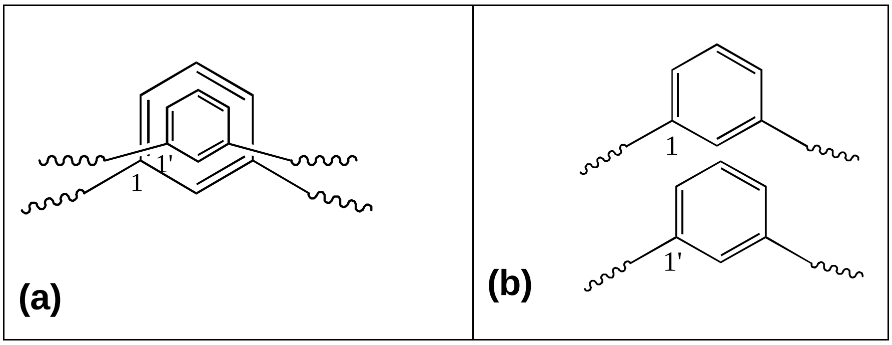

Fig. 32 Stacking (a) and Inplane (b) arrangements of bent-core molecules

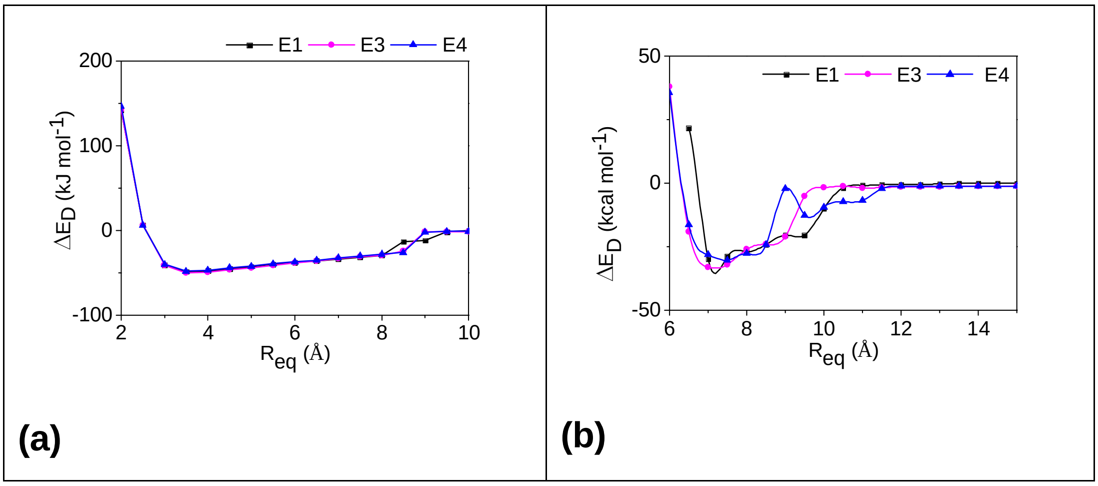

Fig. 33 Dependency of dimerisation energy (ΔE_D) curves for the dimers of the systems **E1**, **E3** and **E4** a: stacking, b: Inplane arrangements (MM).

For the calculation of dimerisation energy, we have considered systems **E1**, **E3** and **E4**. The distance between the atoms was considered from the atoms 1 and 1' (see

Fig. 32). From the Fig. 33a, the R_{eq} (1→1') distance in the stacking arrangement is 3.5 Å. The similar R_{eq} (1→1') distance was obtained for the considered three systems in the stacking arrangement. This indicates that different orientation of ester connecting groups does not have the influence in the stacking arrangement of the molecules. From the Fig. 33b, the R_{eq} (1→1') distance in the inplane arrangement is about 7.0 Å for all the systems. Only a small difference was observed in the pattern of the curves.

4.5. MD results - monomers

4.5.1 Trajectories of torsion angles – ϕ_1

MD simulations were performed on the isolated molecules in vacuum at 300 K and at the clearing temperature of the compounds. The trajectories for the significant torsion angle ϕ_1 of the systems **E1** and **E4** at clearing temperatures are shown in Fig. 34. The trajectory of the torsion angle ϕ_1 for system **E1** indicates a high conformational flexibility. Conformations including the whole range of ϕ_1 are realized during the MD run. Similar results are obtained for the systems **E3**, **E5**, **E6**, **E7** and **E10**. The trajectory of ϕ_1 for system **E4** shows a total other behavior. The conformational degree of freedom with respect to this torsion angle is very limited (ϕ_1 near 0^o) for the system **E4**. Conformers with ϕ_1 about 180^o are found for very few time steps, only. A similar trend was found for the trajectories of ϕ_1 in the systems **E2**, **E8** and **E9**. The MD simulations on the isolated molecules are in agreement with the conformational findings of DFT calculations with respect to the relaxed rotational barriers of the torsion angle ϕ_1 in these systems (Fig. 26).

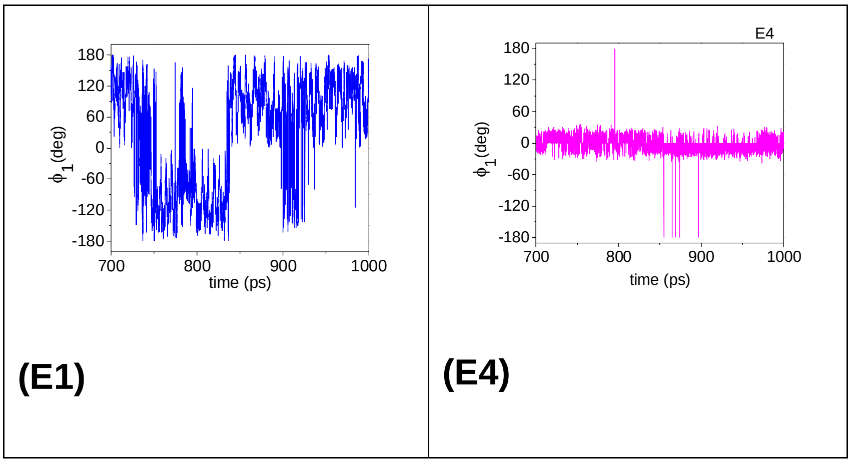

Fig. 34 Trajectories of the torsion angle ϕ_1 for the systems **E1** and **E4** at clearing temperatures.

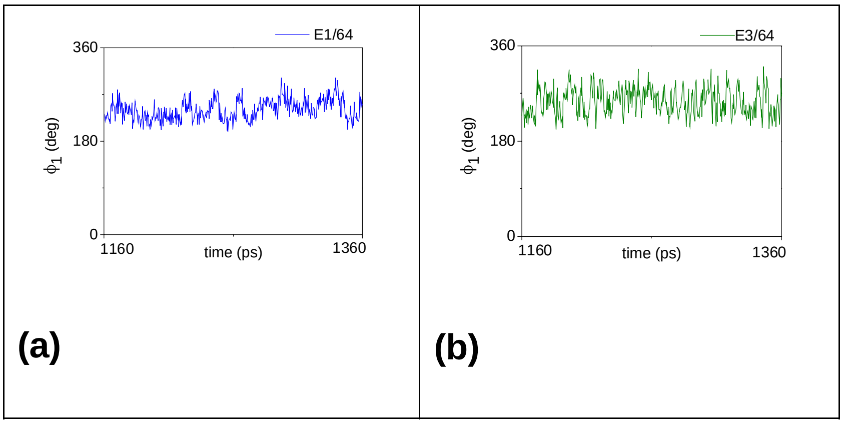

Fig. 35 Trajectories of the torsion angle ϕ_1 for a molecule in the cluster environment of the systems **E1** and **E3** at 300K.

In order to investigate the flexibility of the wings of the bent-core molecules in the aggregate state, MD simulations on clusters with 64 monomers were performed for the systems **E1** and **E3**. From the MD results on clusters similar trajectories of ϕ_1 for a molecule in the environment of the other molecules were generated at 300 K (Fig. 35). It is remarkable that the conformational degree of freedom for the legs of the bent-core molecules in the clusters is significantly reduced in all systems. Obviously, the environment of the other molecules leads in all cases to the effect that only small areas of ϕ_1 are preferred but the values are different for the systems.

4.5.2 Bending angles and molecular lengths

The bending angle (γ) was calculated for single molecules in vacuum and in the environment of the other molecules in clusters with 64 monomers at 300 K. Within the MD procedure the full width at half maximum (FWHM) values and maximal frequency (γ_{max}) of bending angle were calculated. The results are summarized in Table 11. In vacuum the bending angle of the systems shows the sequence γ_{max} : **E3** > **E1** at 300 K. The γ_{max} values show a different trend than the bending angles γ in the most stable structures of the DFT calculation [γ: **E1** (120°) > **E3** (116°)]. In the case of the MD studies contributions of less favored conformers are included. In the cluster environment the γ_{max} values differ considerably from the results at 300 K in vacuum. Generally, the bending angle γ_{max} of the molecules in the clusters are larger than in vacuum. This can be explained by the larger conformational degree of freedom of an isolated molecule in the gas phase which causes that conformers with small bending angles are also realized.

The molecular length can be considered as a relevant parameter which characterizes the bent character and determines the layer distance in mesogenic phases of the banana-shaped compounds. Within the DFT and MD simulations we have calculated the molecular length of the molecules from the distance of the terminal carbon atoms of the two alkyloxy chains. In the DFT and molecular mechanics (MM) calculations the most stable conformations of the isomers were considered to obtain the values for the molecular length L_{DFT} and L_{MM}. Within the MD simulations the mean value of the molecular length ($\overline{L}_{MD}$) was regarded.

Table 11 Full width at half maximum (FWHM) values and bending angles of maximal frequency (γ_{max}) for the systems.

System	Single molecule in vacuum		Single molecule from cluster at 1 atm	
	FWHM	γ_{max}	FWHM	γ_{max}
E1	**23.4**	**117**	**6.3**	**120**
E3	**22.8**	**119**	**9.0**	**123**

FWHM and γ_{max} values in degree

$\overline{L}_{MD}$ was calculated from the trajectory of the corresponding distance at the clearing point temperature of the compound (Table 12). A simulated annealing procedure by increasing the temperature up to 1000 K was used to include all relevant conformers. From X-ray investigations of banana-shaped mesogens the layer distance d in the liquid crystal state was reported. The L values for the isomers with dodecyloxy terminal chains were calculated from the layer distance [91].

No correlation was found between the L_{DFT}, L_{MM} and $\overline{L}_{MD}$ values of the isolated isomers with dodecyloxy terminal chains with the corresponding X-ray layer distances d. Generally, the L_{DFT} and L_{MM} values (45-55 Å) are larger than the d ones (36-50 Å). These are hints for a partial intercalation of the long terminal chains in the liquid crystal state. The $\overline{L}_{MD}$ results (30-40 Å) are too small because overestimated folded conformations of the isolated molecule are also included.

Table 12 Molecular lengths of the systems in Å at 300K in vacuum and in the clusters.

System	**In vacuum single molecule**		**Single molecule from cluster at 1 atm**	
	L_C	**L_T**	**L_C**	**L_T**
E1	**25.6**	**28.3**	**25.4**	**44.4**
E3	**26.0**	**25.3**	**27.2**	**50.9**

The core (L_C) and total (L_T) length of the molecules were calculated as mean values from their trajectories within the MD run. The results are given in Table 12. From Table 12 follows that molecules in cluster environment have larger L_T values than those ones in vacuum. This can be attributed to a smaller rate of conformations with folded dodecyloxy chains in the aggregated state than in vacuum. The orientation of the ester connecting groups has significant effects on the core and total length of the molecules. This can be seen from the core and total length values of system **E1** and **E3**. These results are in agreement with tendency found in the bending angle γ_{max} for the molecules in clusters at 300 K (see Table 11). The reduced length of the alkoxy side chains was obtained for the system **E1** in comparison with DFT results (all trans orientation of carbon atoms in the terminal). By changing the direction of the ester connecting groups in the bent-core part, this effect was reduced in system **E3**. This indicates that different orientation of the ester connecting groups of the molecules leads also in the clusters to essentially different preferred arrangements of the alkoxy side chains. The findings of the molecular length and the bending angle of the molecules in the clusters are hints for their mesogenic properties.

4.6 MD results - clusters

4.6.1 Radial atom pair distribution function

The structure formation of the molecules in the clusters can be analyzed by the calculation of the radial atom pair distribution function g(r). The g(r) values were related to the reference atom C2 located in the central aromatic ring of the bent-core molecules. The results for the clusters at 300 K were illustrated in the Fig. 36 for two different systems. From the results, the order of structure formation in the cluster as follows **E1** > **E3**. The g(r) peaks confirm that different orientation of the ester connecting groups have a significant effect on the organization of bent-core molecules in their clusters.

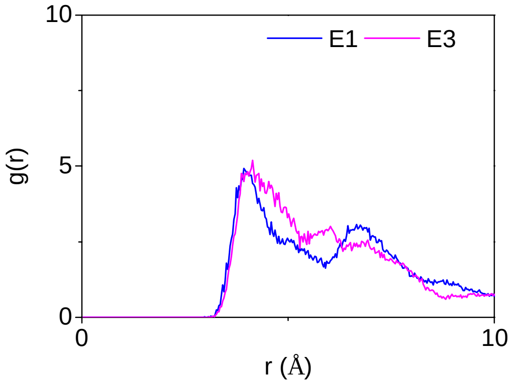

Fig. 36 Radial atom pair distribution functions g(r) for systems at 300K

4.6.2 Pressure effect on g(r)

By increasing the pressure values from 1 bar to 500 bar values, a considerable change was observed in the first neighbor C2-C2' distances and the organization of the clusters. At higher pressure values, a significant decrease in the first peaks was observed in **E1** which is not much in **E3**. The nearest neighbor distance is smaller in system **E1** and higher in **E3** at higher pressure conditions. Generally, at higher pressure conditions (100 bars and 500 bars) a significant difference was observed in the behavior of the g(r) curves. These results suggest that the moderate high pressure conditions can significantly change the arrangement of the bent-core molecules in cluster environment.

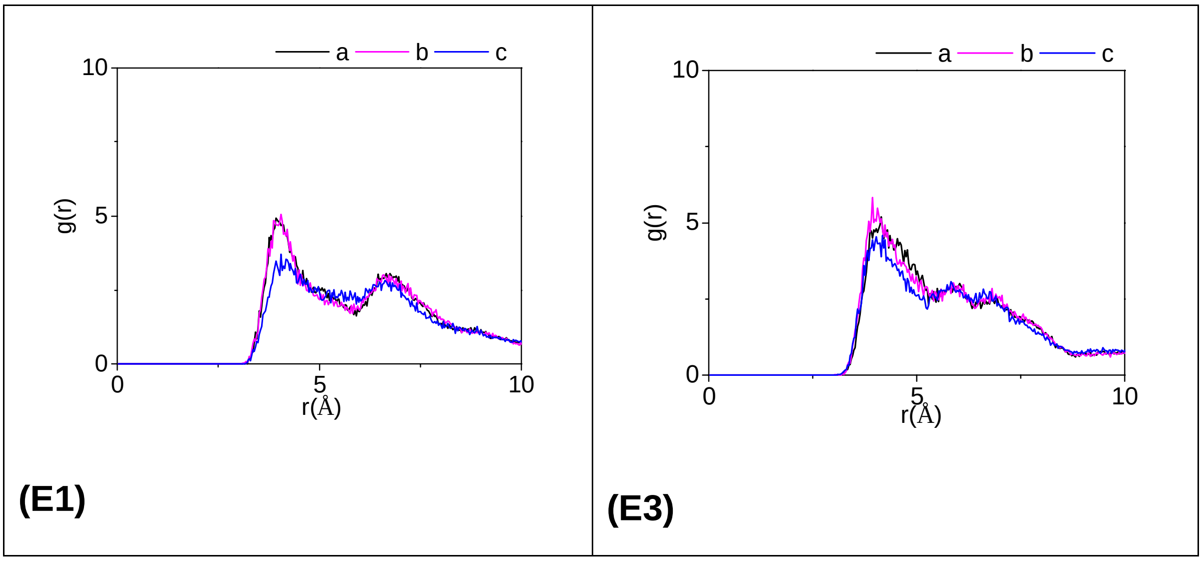

Fig. 37 Radial atom pair distribution functions g(r) for systems at 300K

a: 1 bar, b: 100bar, c: 500bar.

4.6.3 Size effect on g(r)

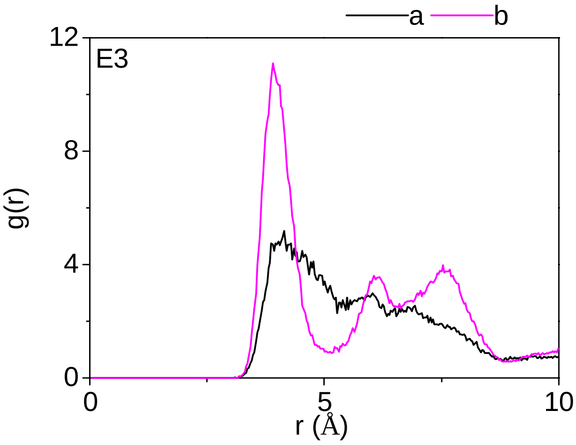

Fig. 38 Radial atom pair distribution functions g(r) for systems at 300K

a: 64 cluster - **E3**, b: 128 cluster - **E3**.

To study the size effect on g(r) curves, MD simulations were made on two different sizes of clusters with 64 and 128 monomers. The results for the system **E3** were given in Fig. 38. The increased density on the 128 cluster was shown by sharp g(r) values. Moreover, increasing the size of the clusters leads to certain order in the system (128 cluster).

4.6.4 Orientational correlation function

Information on the arrangement of such molecules in clusters can be obtained from the calculation of the orientational correlation function g(o). The g(o) data are obtained by calculation of the radial dependence of the cosines between the vectors related to the C2 and C5 atoms of the central aromatic ring of the bent-shaped system. The averaging procedure is carried out via the numbers of the monomers and the time steps during the MD run. The results are presented for the two systems in Fig. 39. The g(o) curves suggest that both systems have nearly a similar arrangement of the central units of the bent-core molecules.

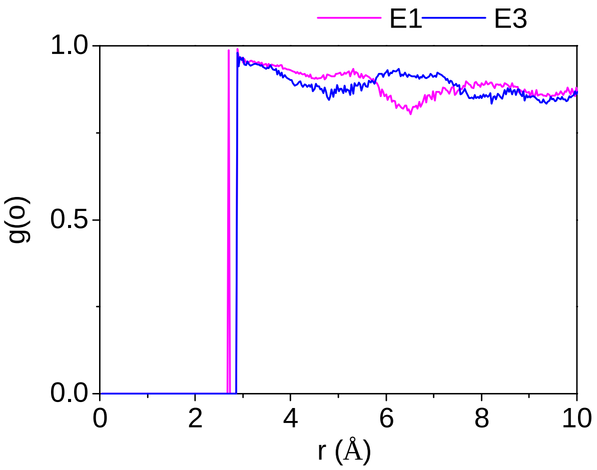

Fig. 39 Orientational correlation function g(o) for systems at 300 K.

The g(o) curves support the trends found in g(r*)* results. Different orientations of the ester connecting groups like in the systems **E1** and **E3** have a considerable influence on the arrangement of such molecules.

4.6.5 Diffusion coefficients

The mobility of the molecules in the clusters has been investigated by diffusion coefficients D which were calculated using the Einstein model within the molecular dynamics run. Calculated D values for the system **E1** and **E3** at 300 K are as follows, **E1**: 38 and **E3**: 37 (values are in 10^{-10} m^2 s^{-1}). The results suggest a similar mobility of both systems. Also the value of the diffusion coefficient for the system **E3** with 128 monomers is 16.5 (D in 10^{-10} m^2 s^{-1}). It shows that by increasing the number of atoms in the cluster slightly decrease in the diffusion coefficient. The diffusion coefficients values were not significantly altered by different orientation of the ester connecting groups.

Chapter 5 Bent-core vs. linear mesogens

We have investigated two different shapes of isomeric mesogenic molecules (bent-core and linear isomers). The comparative DFT calculations and MD simulations were made on a bent-core molecule and its corresponding linear isomer. The investigations were performed to study the influence of the shape on the conformational and aggregation behavior of such compounds. Moreover, we have analyzed the influence of applying external high pressure conditions on properties such as molecular length, radial distribution function, density and diffusion coefficients in clusters by molecular dynamics simulation studies.

5.1 Systems and explanations

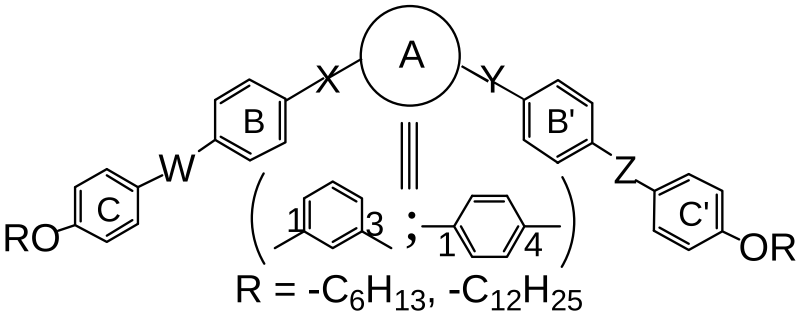

Fig. 40 The structure of the linear and bent-core isomers

Table 13 The explanation of the isomers with different central units

System	Central unit	W	X	Y	Z	T_b
L1	1,4-phenylene	-COO-	-COO-	-OOC-	-OOC-	N 329° I
E1	1,3-phenylene	-COO-	-COO-	-OOC-	-OOC-	$SmCP_A$ 119° I

T_b clearing temperatures in Celsius

We have considered the bent-shaped molecule **E1** and the corresponding linear isomer **L1** for the systematic comparative conformational analysis including single molecules and molecular dynamics simulations on clusters. The systems are defined in Fig. 40 and Table 13.

5.2 Computational details

As described in the chapter 3, the *ab initio* and DFT calculations were carried out using the program package Gaussian98 and molecular dynamics (MD) simulations have been carried out with an implemented AMBER program using gaff force field. MD studies were performed on the isolated molecules in vacuum at 300K with a simulation time of 1 ns. A time step of 1 fs was used in all simulations. Non-bonded interactions were calculated with a cut-off radius of 10000 pm. The MD simulations on the clusters were performed with 64 monomers. For the treatment of the clusters a total simulation time of 1.5 ns and a time step of 2fs were used at 300 K including heating phases. Last 200ps of the equilibration phases were taken into account for the analysis of the MD data at 300 K. The MD simulations were carried out with n, p, T ensemble. The effect of pressure was shown by the MD simulations at 300K with different pressure conditions of 1, 100, 200, 300, 400 and 500 bars. The SHAKE algorithm was used for all atoms. The non-bonded interactions in the clusters were calculated with a cut-off radius of 1000 pm. The MD results were analyzed in a similar manner as described in the chapter 3.

5.3 DFT results

5.3.1 Relaxed rotational barriers – ϕ_1

The conformational flexibility of the core part of the linear and bent-shaped molecules can be illustrated by the relaxed rotational barrier related to the torsion angle $\phi_{1.}$ This is shown in Fig. 41.

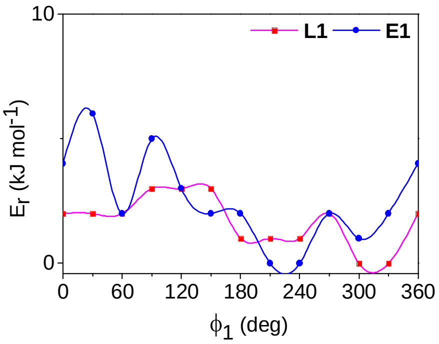

Fig. 41 Relaxed rotational barriers (DFT) related to the torsion angle ϕ_1 for the systems E1 and L1.

The relaxed rotational barriers were calculated with hexyloxy groups as terminal chains for the two systems. The considered two systems show almost same flexibility of the core part over the whole range of ϕ_1 with barriers lower than 10 kJ mol$^{-1.}$ There was no significant effect of the shape on the barriers related to ϕ_1.

5.3.2 Dipole moments, polarizabilities, bending angles and ESP group charges

The dependency of the dipole moment (μ), polarizability (α) and the bending angle (γ) with constraints to the torsion angle ϕ_1 for the systems was shown in Fig. 42. The one-fold scans of the dipole moments related to the torsion angle ϕ_1 indicate a larger range for **E1** (1–7 Debye) and show a smaller one for **L1**) (0-5 Debye). The energy weighted dipole moments ($\bar{\mu}$) including conformations with a relative energy lower than 10 kJ mol^{-1} show the sequence $\bar{\mu}$ (**E1**): 3.6 D > $\bar{\mu}$ (**L1**): 2.4 D.

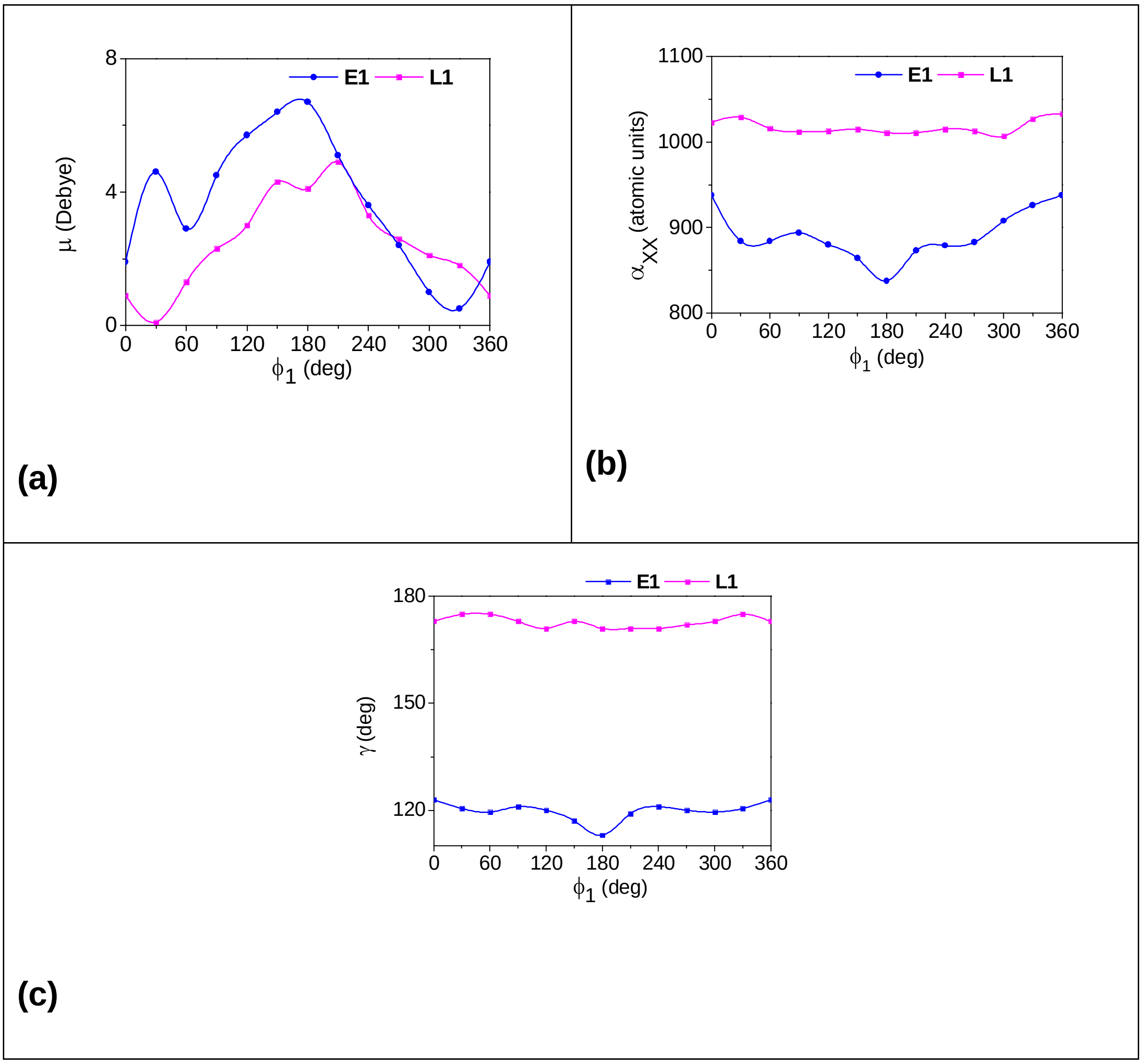

Fig. 42 One-fold scans (DFT) related to the torsion angle ϕ_1: [(a): dipole moments μ, (b): diagonal components α_{xx} of the polarizability. (c): bending angles γ].

The dipole moments and their components for the most stable conformations of the two molecules are given in Table 14.

Table 14 Dipole moments (μ) and their components, diagonal components of the polarizability (α_{XX}, α_{YY}, α_{ZZ}), bending angle (γ) and the molecular length values (L_C, L_T) for the most stable conformations of the systems.

System	μ_x	μ_y	μ_z	μ	α_{XX}	α_{YY}	α_{ZZ}	γ	L_C	L_T
E1	**0.00**	**-0.78**	**0.00**	**0.78**	**916**	**514**	**294**	**120**	**27.9**	**55.1**
L1	**0.02**	**-2.03**	**0.04**	**2.03**	**1023**	**391**	**335**	**173**	**30.6**	**59.9**

Dipole moments in Debye, polarizability in a.u. (1 a.u. is approximately 1.649 10^{-41} C^2 m^2 J^{-1}), bending angle in degree, lengths in Å.

The dipole moment (μ) shows a larger conformational dependency than α_{xx} especially for **L1**. From the diagonal elements of the polarizability (see Table 14) it follows that α_{XX} is the essential component which is oriented to the long axis of the molecule. The dependence of α_{XX} related to ϕ_1 is illustrated in Fig. 42b. The trends in the curves confirm the sequence of α_{XX} for the most stable conformers α_{XX} (**E1**) < α_{XX} (**L1**) (Table 14). These findings are supported by the energy weighted values $\bar{\alpha}_{XX}$ including conformations lower than 10 KJ mol^{-1} $\bar{\alpha}_{XX}$ (**E1**) :891 < $\bar{\alpha}_{XX}$ (**L1**) : 1017.

In the considered systems, α_{XX} values of the most stable conformers can be correlated with the core (L_C) and the total (L_T) lengths (Table 14). The one-fold scan of the bending angle γ related to the torsion angle ϕ_1 is given in Fig. 42c. In some way, the curves of the dependency of γ are comparable with those ones of α_{XX} (Fig. 42b) for the corresponding systems.

Moreover, from the electrostatic potential group charges (q/ESP) a global pattern of the charge distribution at the aromatic rings of the molecules was calculated. The q/ESP values for the systems at the centers of the aromatic rings are illustrated in Fig. 43.

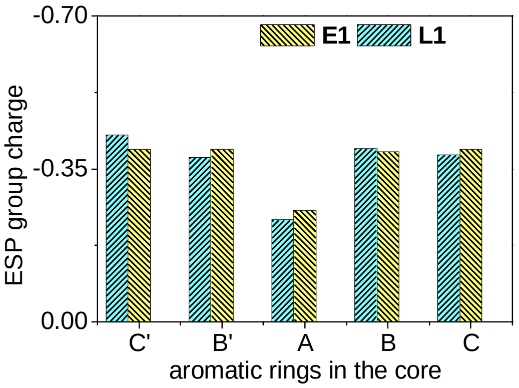

Fig. 43 Electrostatic potential group charges (q/ESP) on the centers of the rings for the systems.

The charges at the connecting groups show no significant changes for the systems which are not drawn in Fig. 43 due to clarity. It is remarkable that **E1** has a symmetrical charge distribution on the bent-core and the **L1** does not have the same. It results that different shape creates a small disturbance on the electron density distribution on the core part of the mesogens. However, the difference in the ESP group charges between the two systems is not much with in the DFT method. The total charge on the central unit of the **E1** isomer is somewhat higher than the **L1**. The higher charge on the central unit (A) gives rise to lower clearing temperature of the isomers (see Table 13).

5.4 MD results - monomers

5.4.1 Trajectories of torsion angle - ϕ_1

MD simulations were performed on the isolated molecules with dodecyloxy terminal chains in vacuum at 300K of the compounds. The trajectories of the torsion angle ϕ_1 were shown for the two systems at 300 K in Fig. 44. The MD results on the isolated molecules support the conformational findings from the relaxed rotational barriers within the DFT method (Fig. 41). The trajectories of the torsion angle ϕ_1 illustrate the flexibility of the core part of the considered molecules. In isolated molecules there is no significant difference in the conformational flexibility between linear and bent-shaped isomers.

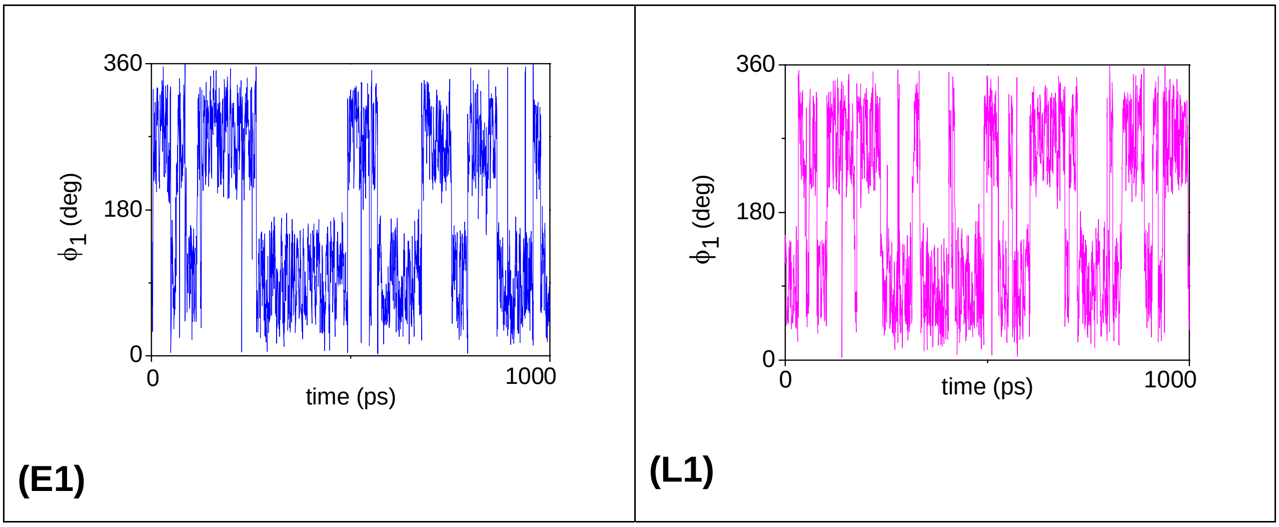

Fig. 44 Trajectories of the torsion angle ϕ_1 for the isolated molecules at 300 K. (**E1**: bent-core, **L1**: linear)

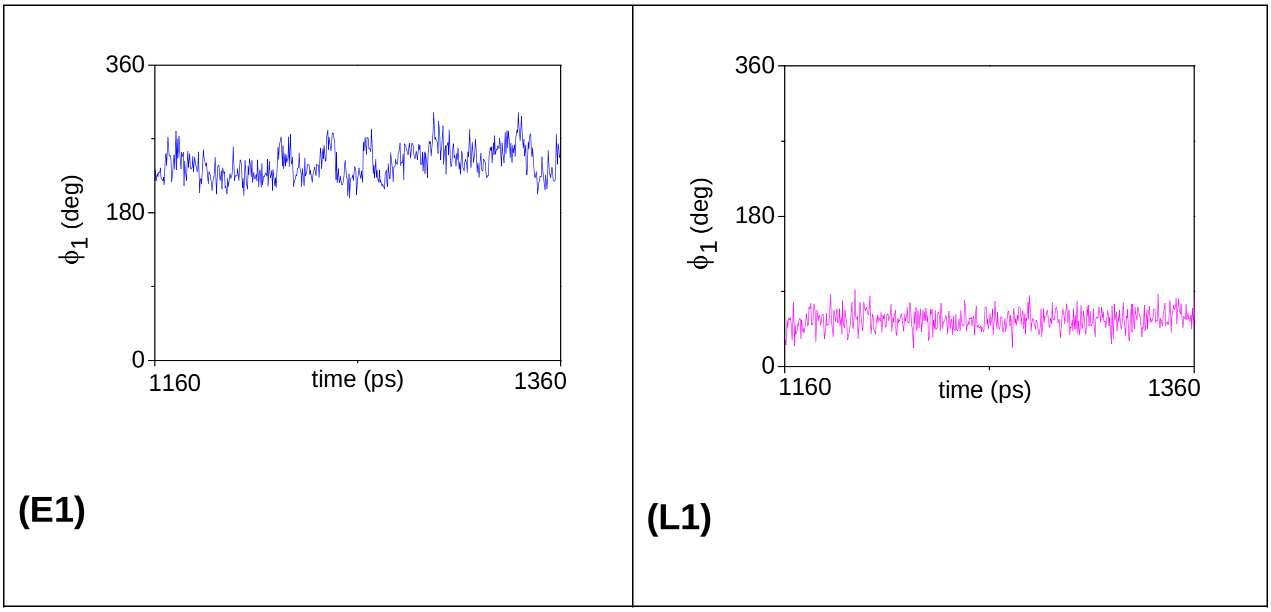

Fig. 45 Trajectories of the torsion angle ϕ_1 for molecules in the cluster environment of the systems at 300 K.

In order to investigate the flexibility of the core part of the molecules in the aggregate state, MD simulations on clusters with 64 monomers were performed. At 300 K the MD results on clusters similar trajectories of ϕ_1 for a molecule in the cluster environment were generated (Fig. 45).

The conformational degree of freedom for the core of the isomers in the clusters was significantly reduced. Obviously, the environment of the other molecules leads in all cases to the effect that only small areas of ϕ_1 are preferred but the values are different for the systems. A comparison of the trajectories of the isolated molecules in Fig. 44 and the corresponding ones of a molecule in the cluster environment in Fig. 45 indicates a large aggregation effect regarding the conformational behavior of the considered isomers. The different central units in the linear and bent-core molecules have less influence on the conformational behavior of the isolated molecules but favor diverse core arrangements of the corresponding monomers in the clusters.

5.4.2 Bending angle and molecular length

The bending angle was calculated for the bent-core molecule **E1** within the MD procedure. The full width at half maximum (FWHM) values and maximal frequency (γ_{max}) of bending angle were presented. The results are summarized in Table 15. The linear isomer **L1** has been also considered in the calculation of bending angle to see the difference in the full width at half maximum values (FWHM). The γ_{max} values from the MD run show a different trend than the γ values obtained from the most stable structures of the DFT calculation (Table 14). In the cluster environment the γ_{max} values differs from the results in vacuum at 300 K. Generally, the bending angle γ_{max} of the molecules in the clusters are larger than in vacuum. This can be explained by the larger conformational degree of freedom of an isolated molecule in the gas phase which causes that conformers with small bending angles are also realized. The effect of pressure on the FWHM and γ_{max} values was also given in the

Table 15. By increasing the pressure a small change in the FWHM and γ_{max} values was obtained.

Table 15 Full width at half maximum (FWHM) values and bending angles of maximal frequency (γ_{max}) for the isolated systems at different pressures.

Pressure (bar)	**FWHM (deg)**		**γ_{max} (deg)**	
	System		**System**	
	L1	**E1**	**L1**	**E1**
Vacuum	**13.0**	**23.4**	**167**	**116**
1	**5.08**	**5.13**	**174**	**120**
100	**5.78**	**4.78**	**174**	**119**
200	**4.73**	**5.63**	**172**	**119**
300	**5.34**	**5.22**	**174**	**119**
400	**3.82**	**5.15**	**174**	**118**

Table 16 Molecular lengths for the systems in the cluster environment at 300 K and different pressure conditions.

Pressure (bar)	**Core length (L_C) / Å**		**Total length (L_T)/ Å**	
	System		**System**	
	L1	**E1**	**L1**	**E1**
1	**30.47** **(30.6)**	**25.24** **(27.9)**	**57.17** **(59.9)**	**43.69** **(55.1)**
100	**30.42**	**25.16**	**56.05**	**43.48**
200	**30.33**	**25.07**	**55.02**	**42.79**
300	**30.26**	**24.98**	**54.07**	**42.96**
400	**30.03**	**24.79**	**52.04**	**42.32**
500	**29.96**	**24.56**	**52.69**	**42.51**

DFT values in parentheses for comparison

The length of the molecules was given as the core (L_C) and total (L_T) lengths which were calculated as mean values from their trajectories within the MD run. The results are given in Table 16. The results in Table 15 show that molecules in the cluster environment have larger L_T values than those ones in vacuum. This can be attributed to a smaller rate of conformations with folded dodecyloxy chains in the aggregated state. By increasing the pressure a decrease in the core and total lengths of the molecules was observed. The pressure effect of shortening on L_T values is larger for the linear isomer than in the bent-core isomers. The reduced length of the alkoxy side chains were obtained for the **E1** in comparison with DFT results (all trans orientation of carbon atoms in the side chain), see Table 16. This indicates that the shape of the molecules leads also in the clusters to essentially different preferred arrangements of the alkoxy side chains.

5.5 MD results - clusters

5.5.1 Radial atom pair distribution function

The structure formation of the molecules in the clusters can be analyzed by the calculation of the radial atom pair distribution function g(r). The g(r) values were related to the reference atom C2 located in the central aromatic ring of the linear and bent-shaped molecules. The results for the clusters within three different pressure conditions at 300 K were illustrated in the Fig. 46. From the results the order of structure formation in the cluster is **E1** > **L1**. Moreover, the g(r) curve shows distinct behavior for the linear and bent shaped systems. The increasing of the pressure from 100 to 500 bar leads to a shift in the first g(r) peak to a lower value in the bent-shaped isomer **E1**. It results that at high pressure of 500 bar, a pressure induced structural change was observed in system **E1**. In the case of the linear isomer **L1** the increasing of the pressure from 1 to 500 bar leads to significant change in the curves of the system **E1**.

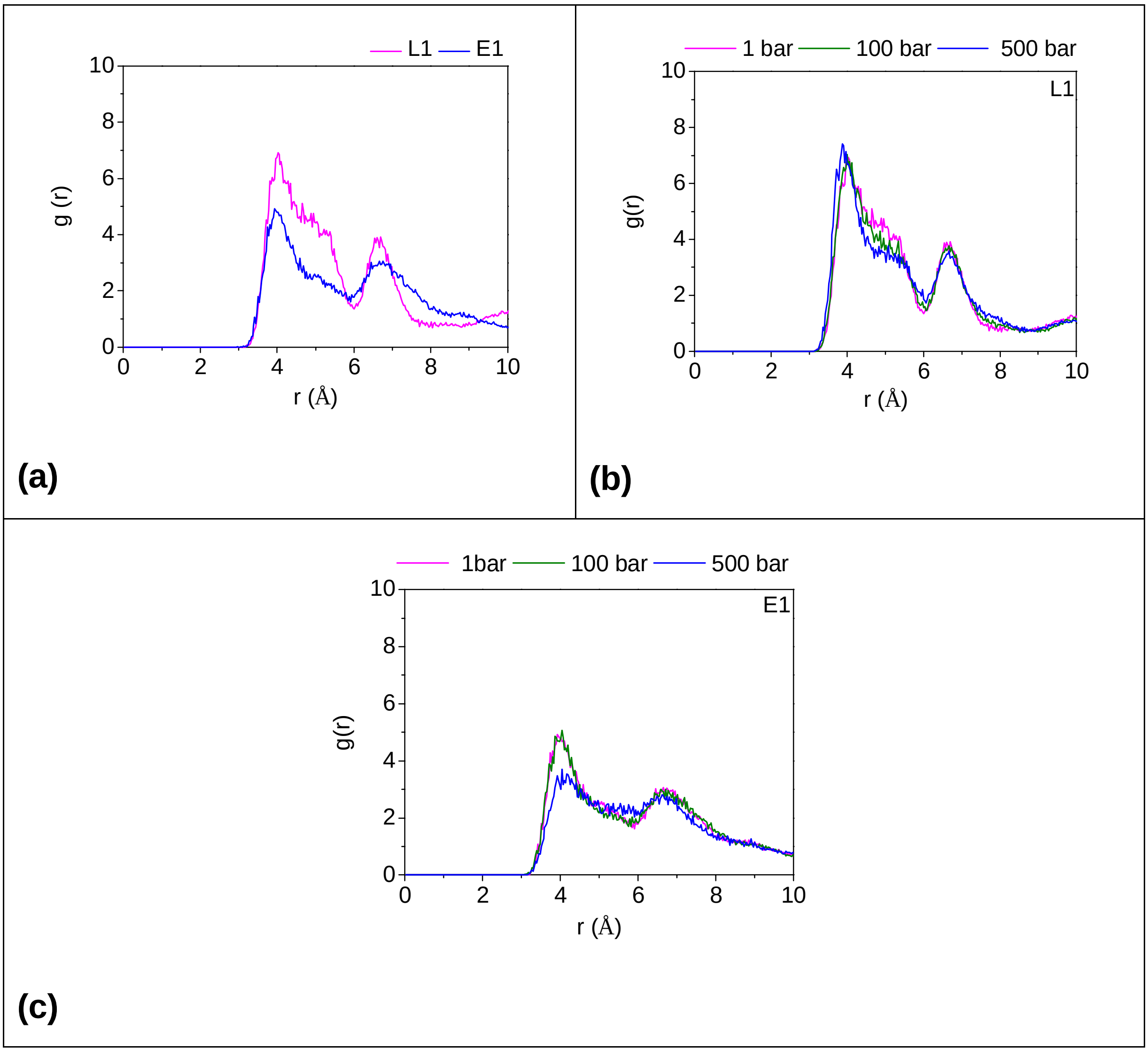

Fig. 46 Radial atom pair distribution functions g(r) for systems **L1** and **E1** at 300K and different pressure (a): **L1** and **E1** at 1 bar; (b): **L1**, (c): **E1**)

5.5.2 Density/pressure plots

Further information about the packing of the molecules can be obtained from the density calculations of the MD run on the clusters. We have presented the density value of the clusters from the final snapshots of MD results with various pressure conditions for the two systems. The results are shown in Fig. 47.

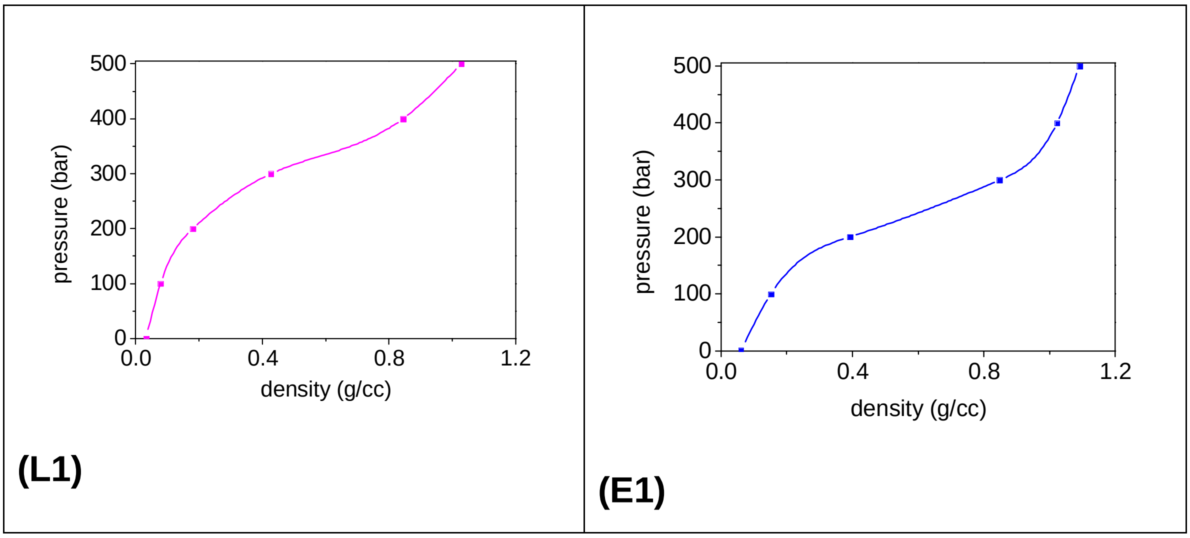

Fig. 47 Density/pressure plot for the linear and bent-core systems

From the Fig. 47, the results show that the bent-shaped system has a larger density than the corresponding linear system. The density of both systems increases with rising pressure. At 500 bar, the bent shaped system **E1** has a higher density than the corresponding linear isomer **L1**. The largest deviations in the density values between the linear and the bent-shaped clusters were found in the range of 200 – 400 bar.

5.5.3 Diffusion coefficients

The mobility of the molecules in the clusters has been investigated by diffusion coefficients which were calculated using the Einstein model within the molecular dynamics run. The D values for the systems were calculated from the MD runs at 300 K at different pressure. For all pressure conditions, the last 200 ps of the equilibration steps were considered for comparison which correspond to total simulation periods of 1160-1360 ps (1bar) and 1360-1560 ps (100,200,300,400 and 500 bar), respectively. The D values are summarized in Fig. 48. A diffusion plot shows that the linear isomer has higher diffusion values than the bent-shaped one. A near linear D/p correlation was obtained for **L1**. In the bent shaped system, the diffusion values become almost constant at high pressure conditions (400, 500 bars). A significant difference was observed on the diffusion values by different shape of the systems **E1** and **L1**.

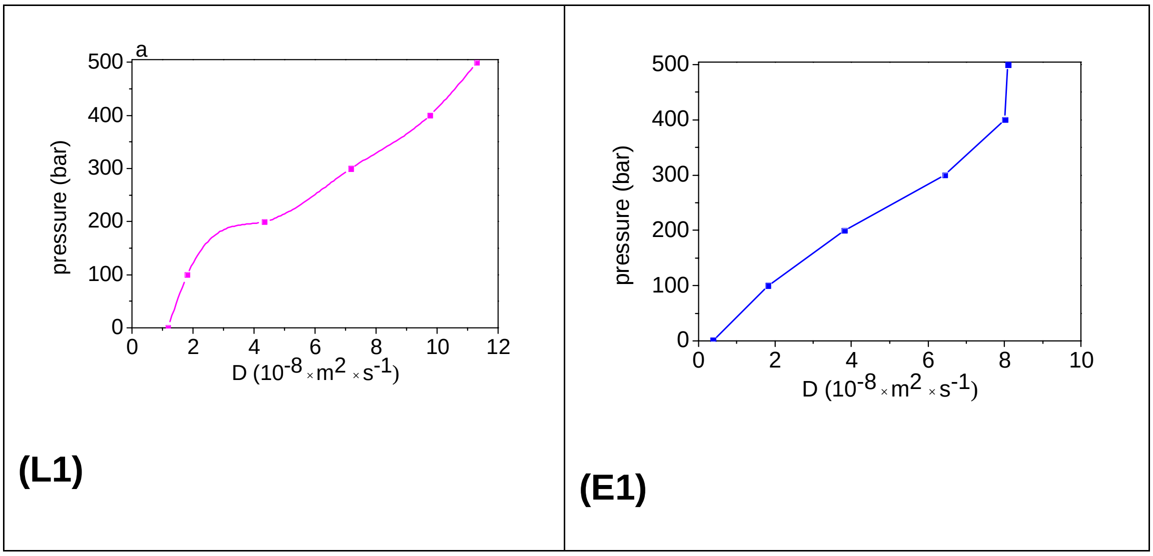

Fig. 48 Diffusion coefficients D of the clusters of systems **L1** and **E1** at 300 K at different pressure conditions.

Chapter 6 Cyclic urea - a new central unit in bent-core compounds

A new class of five-ring bent-core molecules with a cyclic urea group as a central unit was synthesized [94]. A significant difference was found in the mesophase behavior of such molecules by increasing the number of carbon atoms in the central ring (A) of the systems (Fig. 49) Therefore, systematic density functional theory (DFT) calculations and molecular dynamics simulations (MD) were performed on such bent-core mesogenic molecules. The theoretical investigations were based on conformational properties and intermolecular interactions. Such investigations can give some insights to the role of different central units on the various mesogenic behavior of such mesogens. We have also discussed the flexibility of the systems with different central units such as 1,3-phenylene unit, 2,7-napthalene unit and 3,4'-biphenyl units by two-fold scans.

6.1 Systems and explanations

The explanation of the systems and their mesophase behavior is given in the Fig. 49 and Table 17.

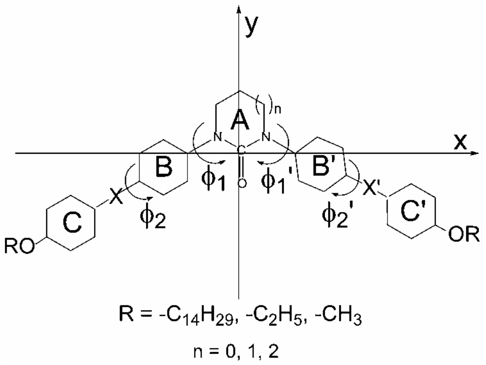

Fig. 49 The main structure of the systems with explanation of the coordinate system and significant torsion angles

Table 17 Explanation of the systems and their mesophase behavior ($R = -C_{14}H_{29}$ for the terminal chains)

System	n	X	X'	Mesophase behavior [94]
U1	**0**	**-OOC-**	**-COO-**	**Cr 189° SmC 314° SmA 329° I**
U2	**1**	**-OOC-**	**-COO-**	**Cr 198° (M1 186°) SmCP$_A$ 200° SmA 208° I**
U3	**1**	**-COO-**	**-OOC-**	**Cr 144° M2 143° SmCP$_A$ 174° Iso**
U4	**2**	**-OOC-**	**-COO-**	**Cr 107° (SmCP$_A$ 97°) SmA 159° Iso**

M1, M2 – mesophases not classified; transition temperatures in Celsius.

6.2 Computational details

As described in the chapter 3, the *ab initio* and DFT calculations were carried out using the program package Gaussian98 and molecular dynamics (MD) simulations were performed with an implemented AMBER program using GAFF force field. MD studies were limited to the isolated molecules in vacuum at 300K with a simulation time of 1 ns. A time step of 1 fs was used in all simulations. Non-bonded interactions were calculated with a cut-off radius of 10000 pm.

6.3 DFT results

6.3.1 Rotational barriers – ϕ_1

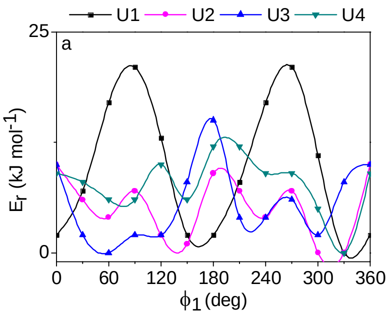

Fig. 50 The relaxed rotational barriers related to ϕ_1 (DFT, R= $-CH_3$)

The relaxed rotational barriers were calculated with respect to torsion angle ϕ_1 (Fig. 50) for the four different mesogenic molecules. The barriers were obtained by a partial optimization procedure with systems containing methoxy terminal chains to reduce the computational effort. The Fig. 50 shows that the system **U1** has a high energy barrier of about 20 kJ mol^{-1} and other systems give energy barriers of about 10 kJ mol^{-1}. It indicates that the system **U1** has a lower conformational flexibility of the wings than the other systems **U2**, **U3** and **U4** which can be explained by the higher strain in the central unit in the case of system **U1** in comparison to the other systems **U2**, **U3** and **U5**. In a limited way an even-odd effect is seen in the barriers of ϕ_1 on the molecules **U1**, **U2** and **U4**.

6.3.2 Two-fold potential energy surface scans

The investigations of the effect of the central unit (A) and direction of the ester linkage groups (X, X') on the conformational behaviour of the systems are completed by Ramachandran-like plots with respect to the torsion angles ϕ_1 and ϕ_1' including 30° steps. The results are illustrated in Fig. 51 for systems including five-, six- and seven-membered central rings with both C-C linkage groups (**U1**, **U2** and **U4**) and C-O linkage groups (**U3**). The findings from the Ramachandran-like plots support the results on the conformational flexibility of the systems obtained by one-fold PES scans related to the torsion angle ϕ_1. Systems **U1** and **U4** show lesser conformational flexibility than the systems **U2** and **U3**. Moreover, the Ramachandran-like plots illustrate that the stationary points (minima, maxima and saddle points) result in different areas of the maps for systems. The two-fold scans are symmetric **(U1)** but asymmetric otherwise **(U2**, **U3**, **U4)**. The flexibility of the wings with respect to the N-C bond in cyclic urea systems is between that one related to the C-O and the C-C bonds in the ester systems [80]. The less flexible system **U1** forms only smectic phases and high flexible systems **U2**, **U3** and **U4** form the SmCP phases.

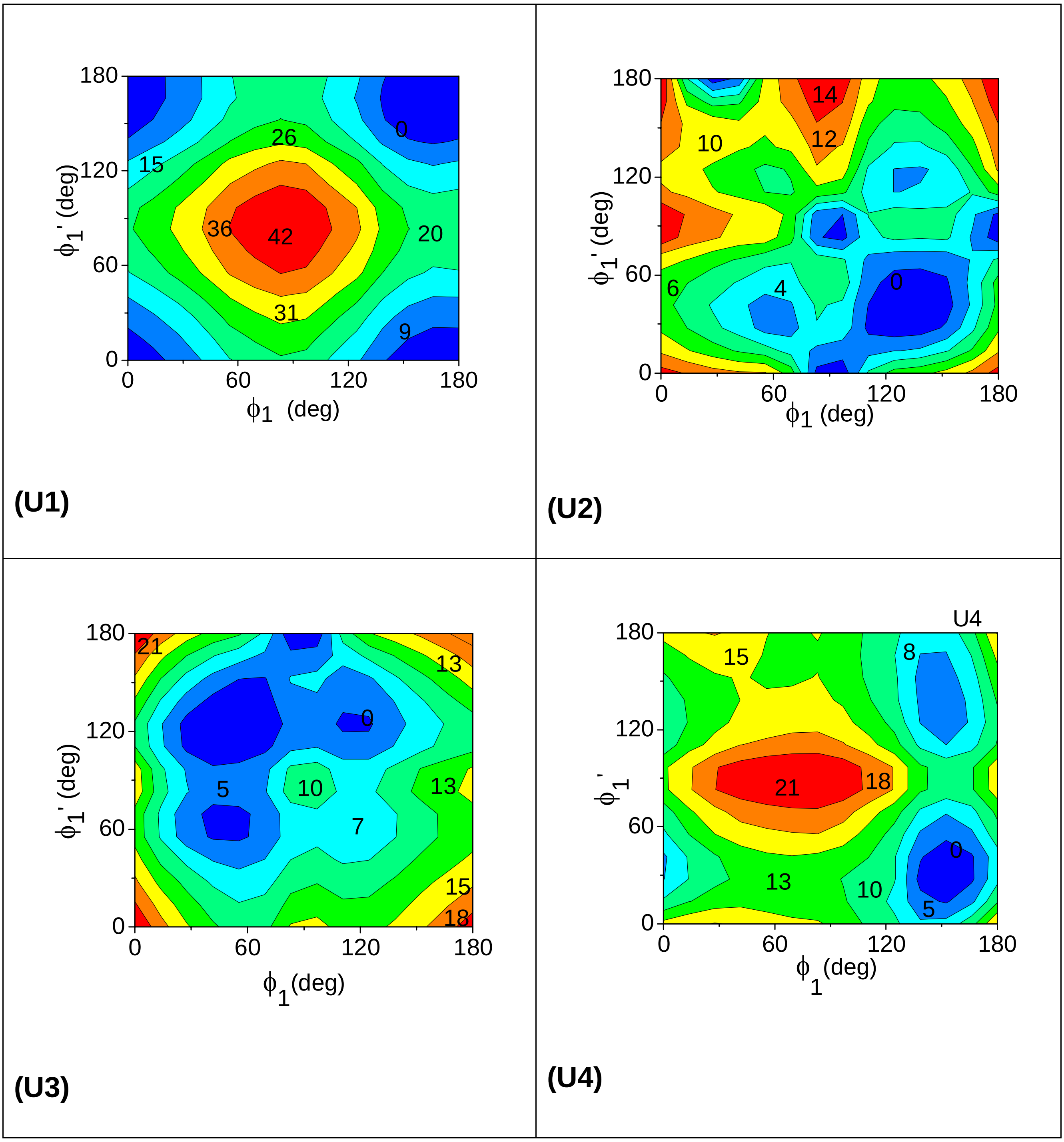

Fig. 51 Two-fold potential energy surface scans (HF) related to the torsion angles ϕ_1 and ϕ_1' (energy values in kJ mol^{-1}).

6.3.3 Dipole moment, bending angle and diagonal component of polarizability

The dipole moment μ and the diagonal component α_{XX} of the polarizability for the most stable conformations of the considered systems are given in the Table 18. The values were obtained for the systems with ethoxy terminal chains in order to reduce the computational effort. The values of the dipole moments show that the cyclic urea central unit reduces the total dipole moments of the molecules (systems **U1**, **U2** and **U3**) in comparison to other type of bent-core molecules [see Tables 2, 9 in chapters 3 and 4].

Table 18 Dipole moment and polarizability values of the systems with ethoxy terminal chains (DFT).

System	μ	α_{XX}	α_{YY}	α_{ZZ}
U1	**0.36**	**715.70**	**396.30**	**194.31**
U2	**1.52**	**628.84**	**431.51**	**230.72**
U3	**3.10**	**662.37**	**376.84**	**260.02**
U4	**1.51**	**659.13**	**441.22**	**243.12**

An increase in the total dipole moment was observed by changing the direction of the connecting groups (X, X') in **U3.** The diagonal component α_{XX} of the polarizability is higher in the systems **U1** and **U4** than in the system **U2**. In a limited way, an even odd effect has been observed in the values of the diagonal component α_{XX} values.

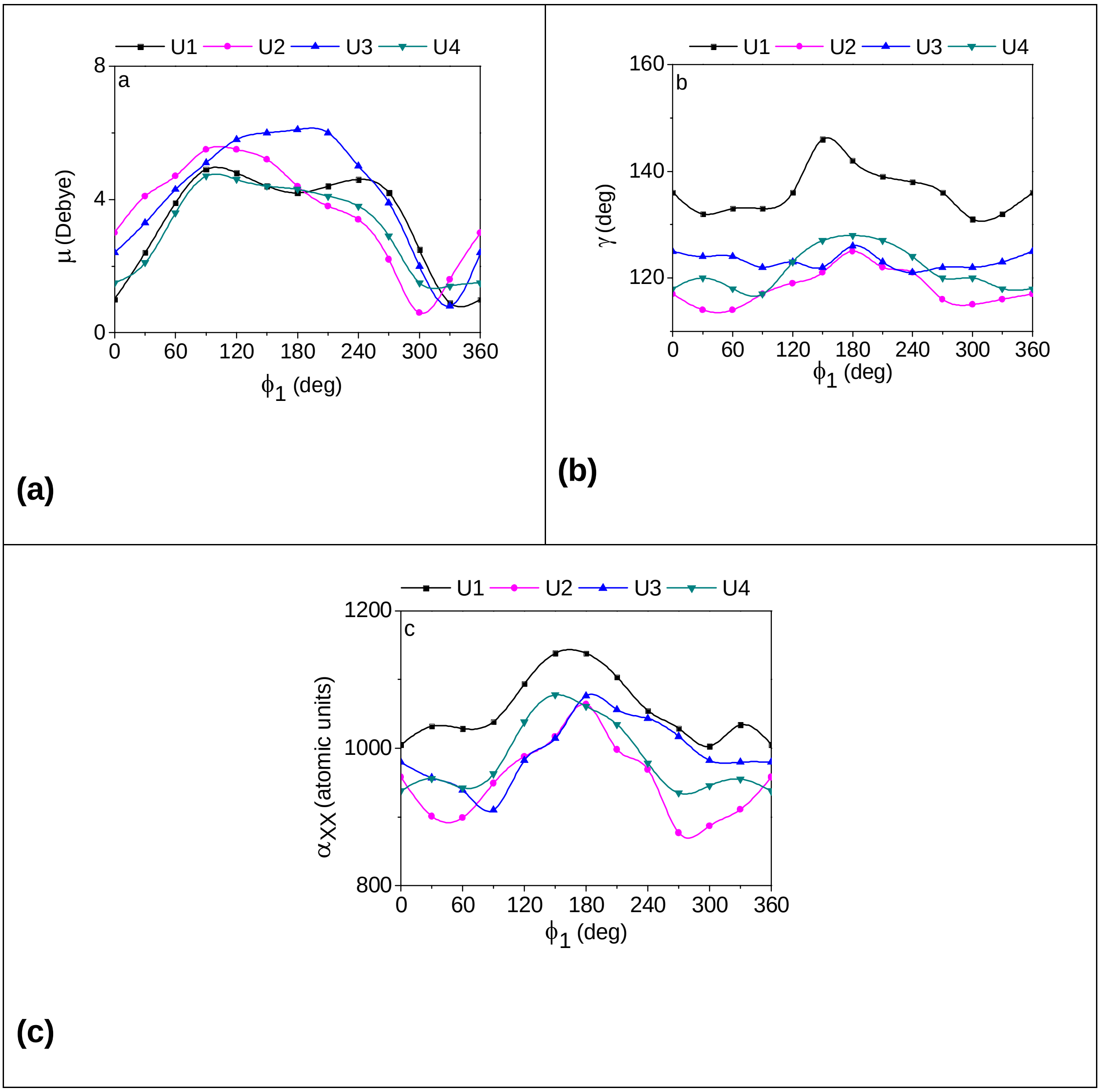

Fig. 52 One-fold scans (DFT) related to the torsion angle ϕ_1.for the systems with R= -CH3) [(a): dipole moment μ, (b): bending angle γ, (c): diagonal element of the polarizability α_{xx}).

The dependency of the dipole moment related to torsion angle ϕ_1 was given in Fig. 52a. The five-membered system **U1** shows smaller dependency than the six- and seven-membered systems (**U3**, **U4**). The dependency of bending angle (γ) related to torsion angle ϕ_1 was illustrated in Fig. 52b. The systems **U1** and **U4** show a larger dependency than **U2** and **U3**. Generally, larger bending angle values were obtained for the five- membered **U1** system and lower one for six- membered systems **U2** and **U3**. The dependency of diagonal element α_{xx} related to torsion angle ϕ_1 was shown in Fig. 52c which indicates nearly same trend as the bending angle (γ).

6.3.4 ESP group charges

The total electrostatic potential (ESP) group charges (q/ESP = -ρ) on the rings of the bent-core give a global pattern of the electron density distribution on the wings of the molecule. For the calculation of ESP group charges on the rings A, B, B', C and C', the heavy atoms were only considered. The ESP charge results were illustrated in Fig. 53. In a limited way, the ESP charge patterns on the aromatic rings correlate with the meso phase behavior. The larger ESP group charge on the central unit correlates with lower clearing temperatures of the systems (Fig. 53). This correlation is in agreement with clearing temperatures of bent and linear isomers in chapter 5.

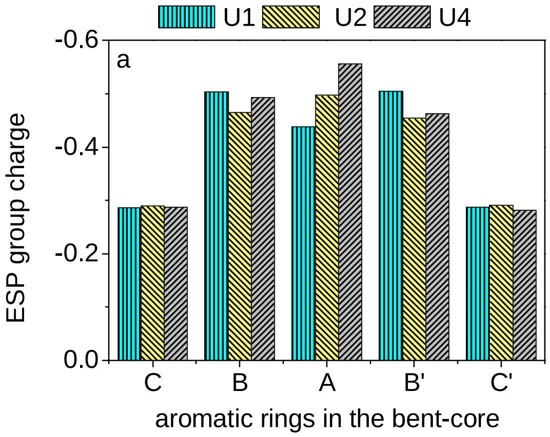

Fig. 53 Electrostatic potential group charges on the centers of the rings for the systems **U1**, **U2** and **U4** (DFT).

Moreover, there is no alternation of charge distribution on the aromatic rings in the bent-core of the systems. Generally, the conformational studies on such systems show that the flexibility of the molecules depends on the central unit (A) and the connecting groups (X, X'). The system **U1** shows a lower conformational flexibility, smaller dipole moment and larger bending angle (γ) values which results that the molecule shows rod like mesogenic characters. So it forms only SmA and SmC phases without any polar order. The systems **U2** and **U3** show a moderate bending angle (γ) which supports the formation of polar SmCP phases. In other words from the strain on the central unit (A) of such compounds decrease in the following sequence: **U1**> **U2** > **U4**. This has a major influence on the mesophase clearing temperatures. In some way, the ESP group charge distribution on the bent-core systems **U1**, **U2** and **U4** correlated with their mesophase behavior. It results that systems **U2** and **U4** has an asymmetrical ESP charge pattern on the rings of bent-core and form tilted SmCP phases. The system **U1** with symmetrical ESP charge pattern form a SmC and SmA phases without any polar order (SmCP phase) (see Table 17).

6.4 MM results - dimers

The interaction energy between the bent-core molecules was calculated. The dimerisation energy was calculated as $\Delta E_D = E_{dimer} - 2E_{monomer}$. The calculations were done by molecular mechanics within AMBER force field. The molecules have been shifted by each other in two different directions considering stacking and inplane arrangements.

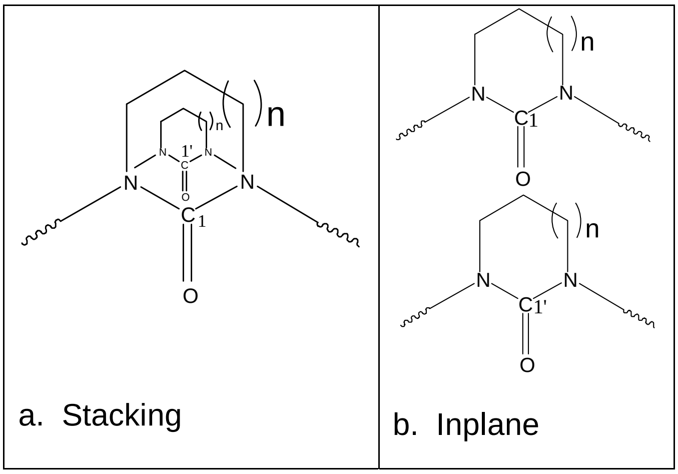

a. Stacking

b. Inplane

Fig. 54 Two different arrangements of the dimers

The equilibrium distance R_{eq} (C1→C1') between the bent-core molecules in two different arrangements was calculated for the systems **U1**, **U2**, **U3** and **U4**. The results were presented in the Fig. 54. The results show that the order of the R_{eq} distance in the inplane arrangement is **U1** < **U2** ≅ **U3** ≅ **U4** and in the stacking arrangement is **U1** < **U2** ≅ **U3**< **U4**. It results that higher R_{eq} values were obtained in both arrangements for the seven membered system **U4** and lower values for the five-membered one **U1**. The values for the six- membered system **U2** is in between **U1** and **U4**. Different orientation of the ester linkages in the connecting groups (X, X') does not change the R_{eq} values in the considered arrangements which are shown by the results of the systems **U2** and **U3**. However higher values of the dimerisation energy were obtained by C-C linkage to the central unit in comparison to C-O linkage (Figs. 55b and 55d). The intermolecular distances in the systems **U1**, **U2** and **U4** have been significantly altered by different central units in the inplane and stacking arrangement of the models.

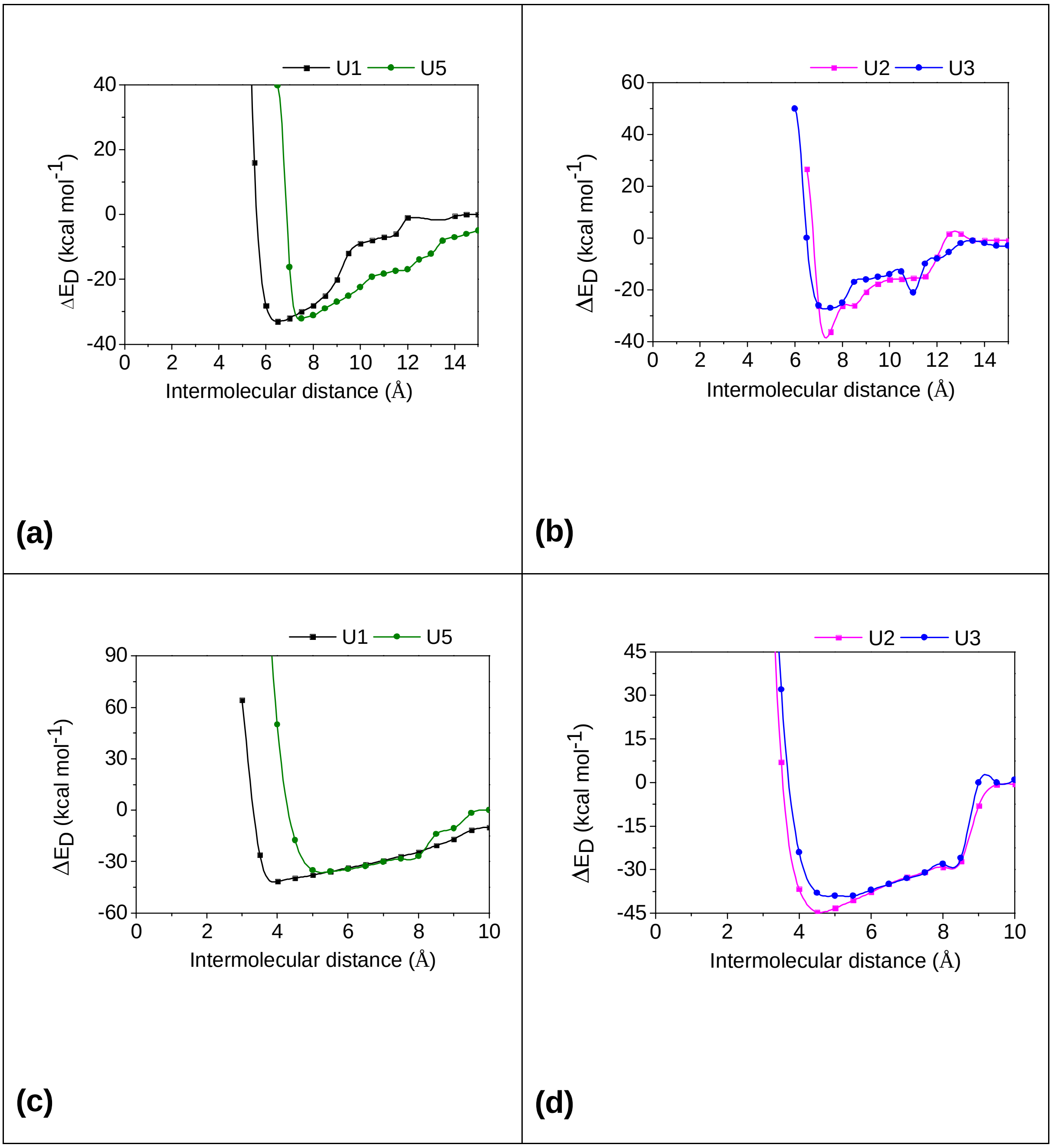

Fig. 55 Dependency of the dimerisation energy related to intermolecular distances for the systems **U1**, **U2**, **U3** and **U4**.

(a, b: inplane, c,d: stacking)

6.5 MD results - monomers

6.5.1 Trajectory of the torsion angle - ϕ_1

The MD simulations were performed on the isolated molecules with $C_{14}H_{29}O$- side chains in vacuum at 300 K.

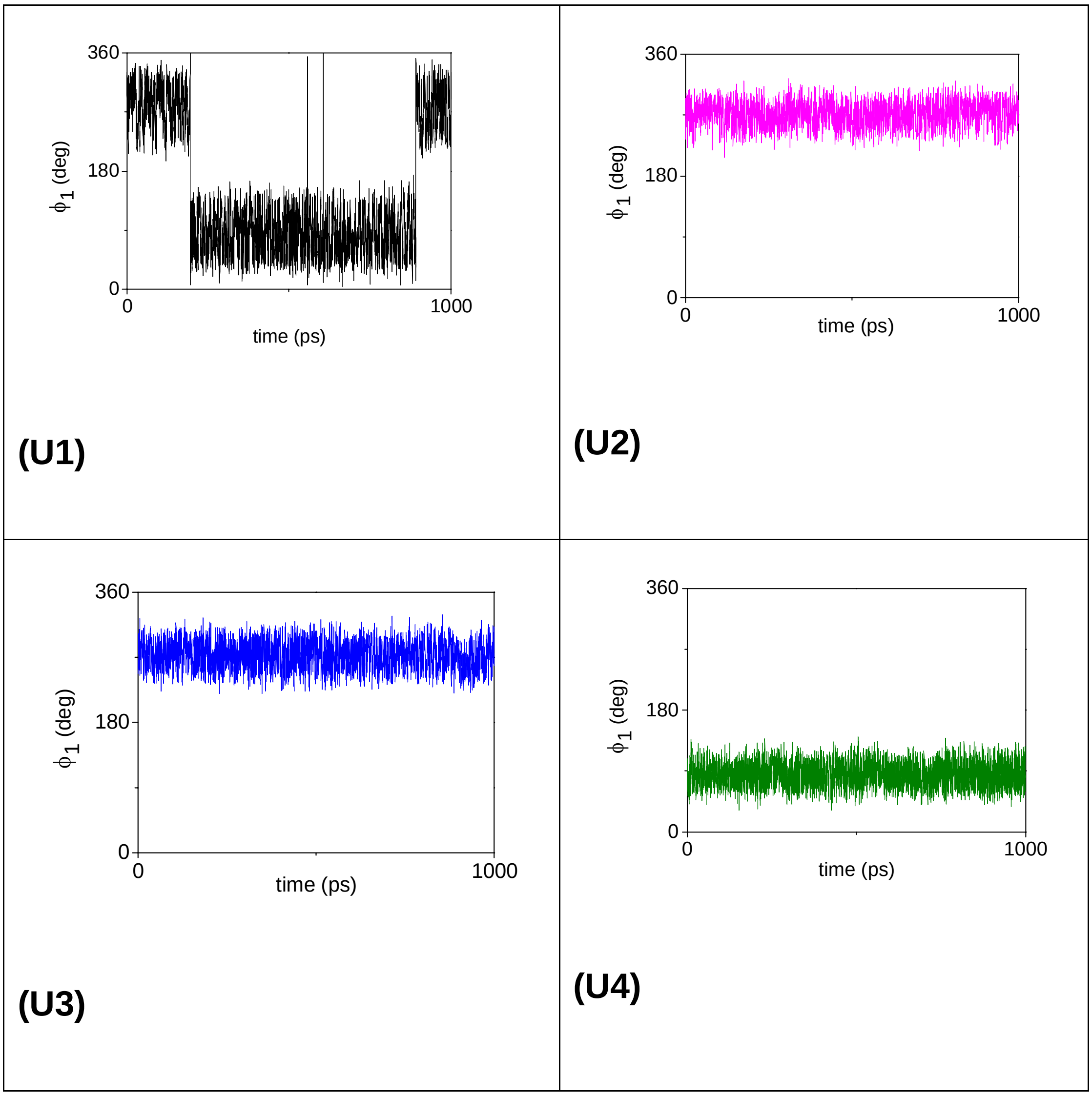

Fig. 56 Trajectories of the torsion angle ϕ_1 of the monomers **U1**, **U2**, **U3** and **U4**.

In Fig. 56, the trajectories of the torsion angle ϕ_I for the four systems were shown. The trajectories of the torsion angle ϕ_I for the systems **U1**, **U2**, **U3** and **U4** are in a limited way comparable with DFT results (see Fig. 50). The preferred different values of the torsion angle ϕ_1 for the systems depend on the central unit (A).

6.5.2 Bending angle and molecular length

The bending angle (γ) has been calculated for four systems from the MD results at 300 K. The full width at half maximum and γ_{max} values of the bending angles were calculated from the MD run. The system **U1 (U2)** shows larger (smaller) FWHM, γ_{max}, L_C, L_T values (Table 19).

Table 19 The full width at half maximum (FWHM), γ_{max} and molecular length (L_C and L_T) values for the systems

System	FWHM/deg	γ_{max}/deg	Molecular length / Å	
			L_C	L_T
U1	**15.4**	**139.2**	**23.94**	**29.19**
U2	**12.9**	**115**	**21.64**	**7.62**
U3	**14.1**	**122.7**	**22.57**	**14.07**
U4	**13.9**	**117.5**	**22.33**	**15.24**

The values of systems **U2** and **U3** were different which is caused by different orientation of the connecting groups (X, X'). The system **U1** shows higher L_T and Lc values than the other systems.

6.6 Two-fold scans of different central units

In order to show influence of the different central units on the conformational flexibility of the bent-core molecules, The two-fold scan of three different systems with 1,3-phenylene, 2,7-naphthalene and 3,4'-biphenyl central units were calculated. The considered three systems were explained in the Fig. 57 and Table 20.

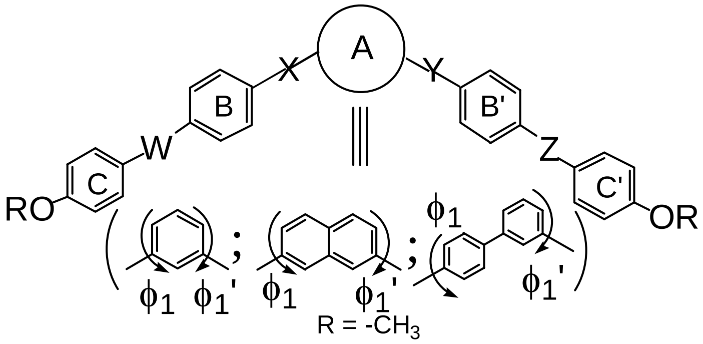

Fig. 57 The main structure of the considered three systems

Table 20 Explanation of the central unit and connecting groups for the three systems

System	Central unit	W	X	Y	Z
E1	1,3-phenylene	-COO-	-COO-	-OOC-	-OOC-
N1	2,7-naphthalene	-COO-	-COO-	-OOC-	-OOC-
B1	3,4'-biphenyl	-COO-	-COO-	-OOC-	-OOC-

System **E1** has been discussed in detail in the chapter. All the calculations were carried out with on the HF/STO-3G level. The Ramachandran-like plots with respect to the torsion angles ϕ_1 and $\phi_{1'}$ including 30^o steps for the three systems were shown in Fig. 58.

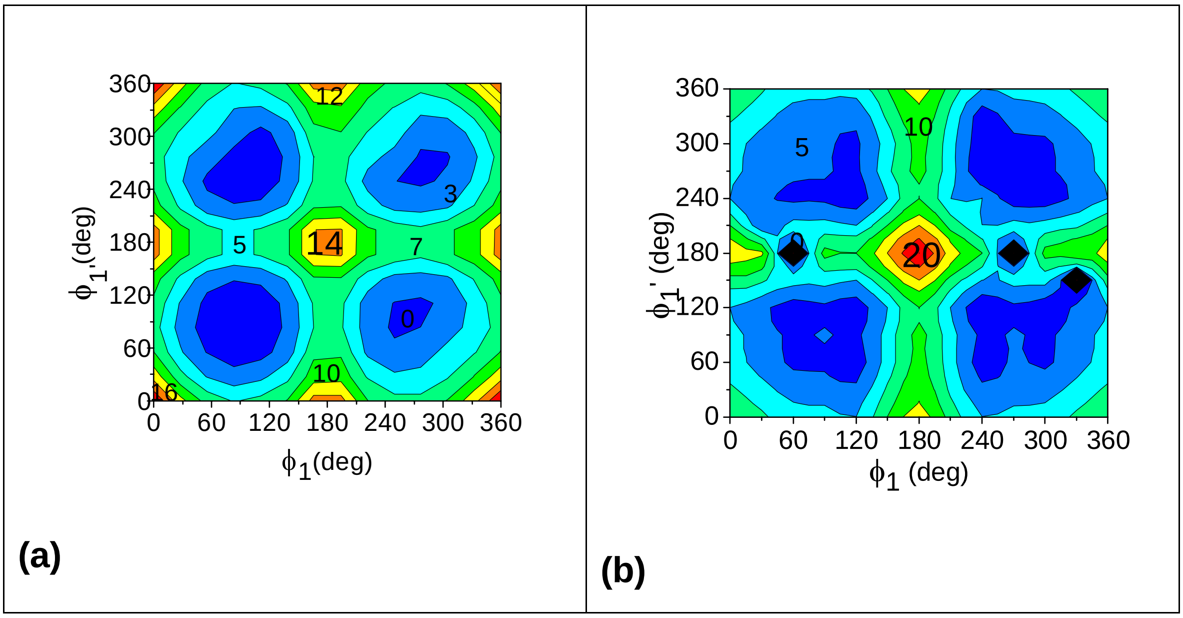

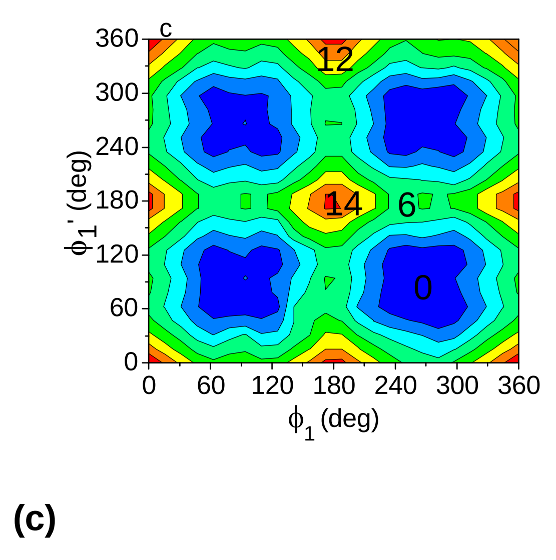

Fig. 58 The two-fold scans for the systems a. **E1**, b. **N1**, c. **B1**

In three systems the orientation of the ester connecting groups is the same with respect to the central unit A. The findings from the Ramachandran-like plots show that the conformational flexibility of system **N1** is low in comparison to **E1** and **B1**. Moreover, the Ramachandran-like plots illustrate that the stationary points (minima, maxima and saddle points) result in different areas of the maps for the systems **E1**, **N1** and **B1**.

Chapter 7 Hydrogen bonding in bent-core compounds

In this chapter four different hydrogen bonded bent-core systems were investigated. In the systems **H1** and **H2**, the hydrogen bonding can occur between the two bent-cores [95]. In the systems **H3**, **H4**, the hydrogen bonding is used to build up a bent-core structure [96]. In order to get some basic information about the stability of hydrogen bonding and polarity of such molecules, we have made systematic investigations on the monomers by *ab initio* and DFT calculations as well as MD simulations on the dimers. We have also analyzed the proton transfer process on such systems because the dynamics of hydrogen bonding is important in such ferroelectric and antiferroelectric materials [97-98].

7.1 Systems and explanations

The explanation of the systems and their mesophase behavior is given in the Fig. 59 and Table 21.

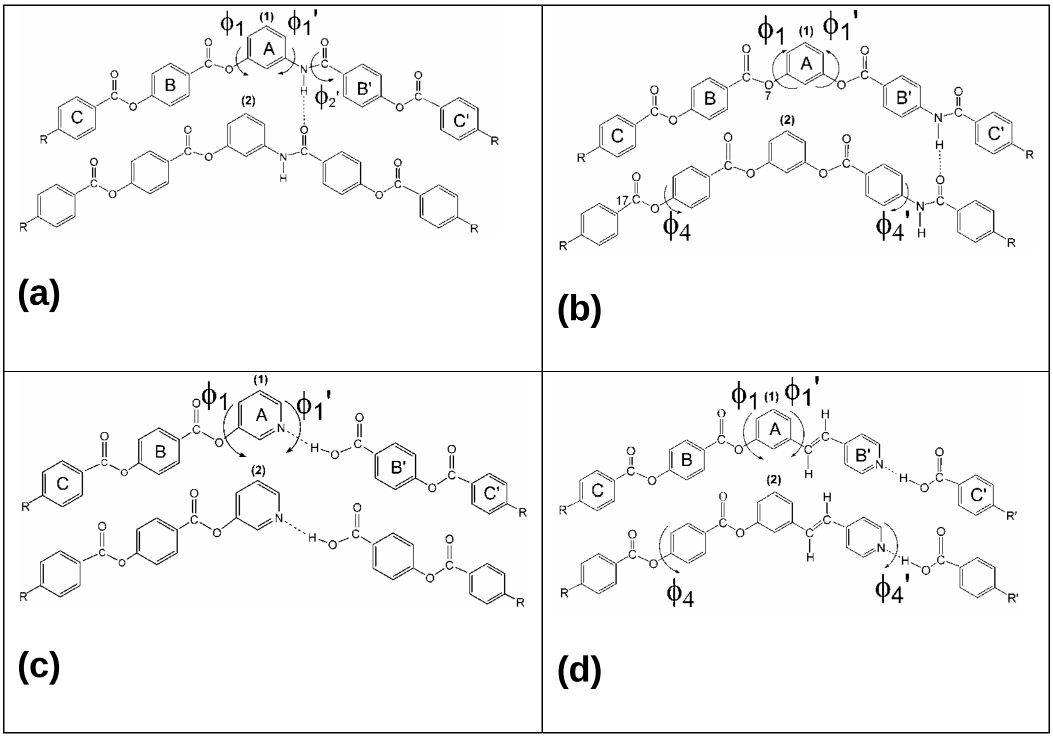

Fig. 59 The structures of the hydrogen bonded systems with explanation of

the significant torsion angles (R, R'- alkoxy terminal chains)

a : **H1**-**H1**, b: **H2**-**H2**, c: **H3**-**H3**, d: **H4**-**H4**

Table 21 Mesophase behavior of the systems **H1**, **H2 H3** and **H4**.

System	Mesophase behavior	R	R'
H1	**Cr 120° SmCP 161° Iso**	**-$OC_{12}H_{25}$**	**-**
H2	**Cr 126° SmCP 165° I ↓**	**-$OC_{12}H_{25}$**	**-**
H3	**Cr 108° SmA 131° N 145° I**	**-$OC_{14}H_{29}$**	**-$OC_{18}H_{37}$**
H4	**Cr 82° SmCP 142° I**	**-$OC_{14}H_{29}$**	**-$OC_{18}H_{37}$**

transition temperatures in Celsius

7.2 Computational details

As described in the chapter 3, the *ab initio* calculations were carried out using the program package Gaussian98 and molecular dynamics (MD) simulations were performed with an implemented AMBER program using gaff force field. MD studies were limited to the dimer of such molecules in vacuum at 300K with a simulation time of 1 ns. A time step of 0.5 fs was used in all simulations. Non-bonded interactions were calculated with a cut-off radius of 10000 pm.

7.3 HF and DFT - results

7.3.1 Rotational barriers – ϕ_1' and ϕ_4'

The relaxed rotational barriers were calculated with respect to torsion angle ϕ_1' (Fig. 60a) for the system **H1** related to C-N bond. The barriers were obtained by a partial optimization procedure for systems with terminal methoxy chains to reduce the computational effort. The Fig. 60a results that the system **H1** shows a more structured curve with respect to C-N bond in comparison to C-O barrier (**E1** – see chapter **4**) but the energy of the barrier 12 kJ mol^{-1} is in the sequence with C-O (**E1**) < C-N (**H1**) < C-C (**E4**) [see chapter 3 and 4].

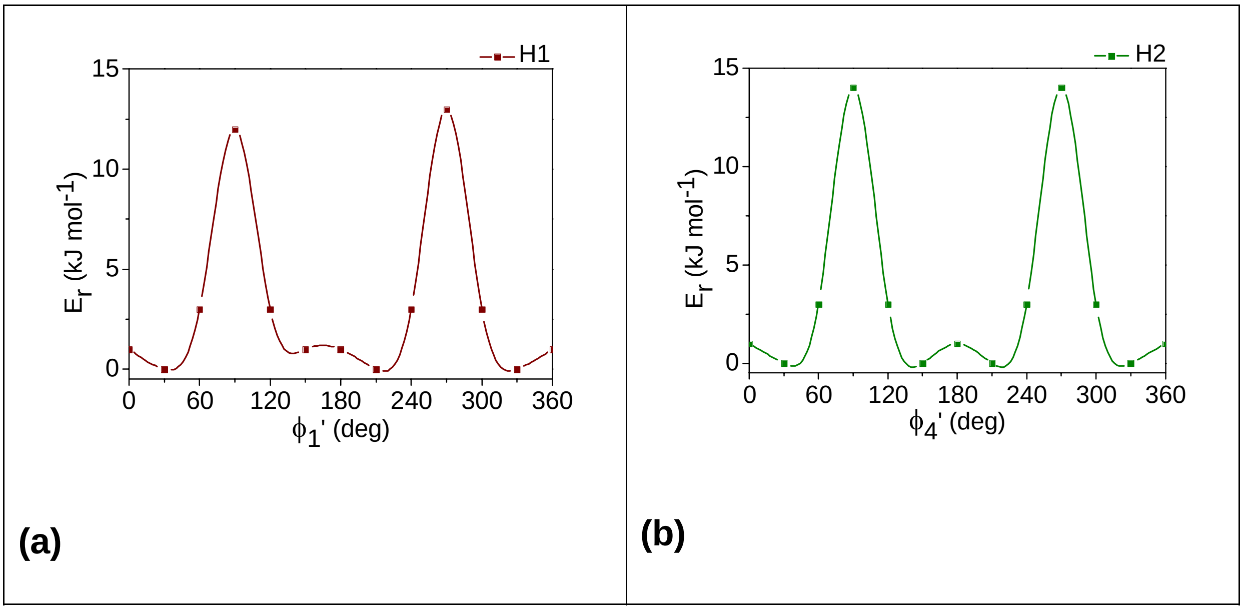

Fig. 60 The relaxed rotational barriers for the systems **H1** and **H2** related to torsion angles ϕ_1'and ϕ_4'. (HF, R= -OCH$_3$)

The relaxed rotational barriers for the single molecules are presented Fig. 60 for the systems **H1** and **H2**.

The rotational barrier related to torsion angle ϕ_4' for the system **H2** is similar to the ϕ_1' barrier of system **H1** with multi minima points. The calculated hydrogen bond energy for the systems **H3** and **H4** is -53.4 and -60.4 kJ mol^{-1} respectively (B3LYP/6-31G(d)).

7.3.2 Two-fold potential energy surface scans

The investigations of the effect of the ester, amide, hydrogen bonding linkages on the conformational behaviour of the systems are shown by Ramachandran-like plots with respect to the torsion angles ϕ_1 and ϕ_1' (**H1**, **H3**) and ϕ_4 and ϕ_4' (**H2**, **H4**) including 30°steps. The results are illustrated in Fig. 61 for systems **H1**, **H2**, **H3** and **H4** including C-O and C-N linkage groups (**H1**, **H2**) and C-O linkage, N→H hydrogen bonding linkages (**H3**, **H4**). The findings from the Ramachandran-like plots support the results on the conformational flexibility of the systems obtained by one-fold PES scans related to the torsion angle $\phi_1^{'}$ and $\phi_4^{'}$ for the systems **H1** and **H2**. The systems **H1** and **H2** show lower conformational flexibility than the systems **H3** and **H4**. Moreover, the Ramachandran-like plots illustrate that the stationary points (minima, maxima and saddle points) result in different areas of the maps for systems. The two-fold scans are symmetric for **H1**, **H2** but asymmetric for **H3**, **H4**. The flexibility of the wings with respect to the C-N bond in the systems **H1** and **H2** is between that one related to the C-O and the C-C bonds in the ester systems [see chapter 4]. The two-fold scan for a system with one hydrogen bonding linkage gives barriers up to 14 and 12 kJ mol^{-1} which is comparable with the two-fold energy map constructed by C-O linkages.

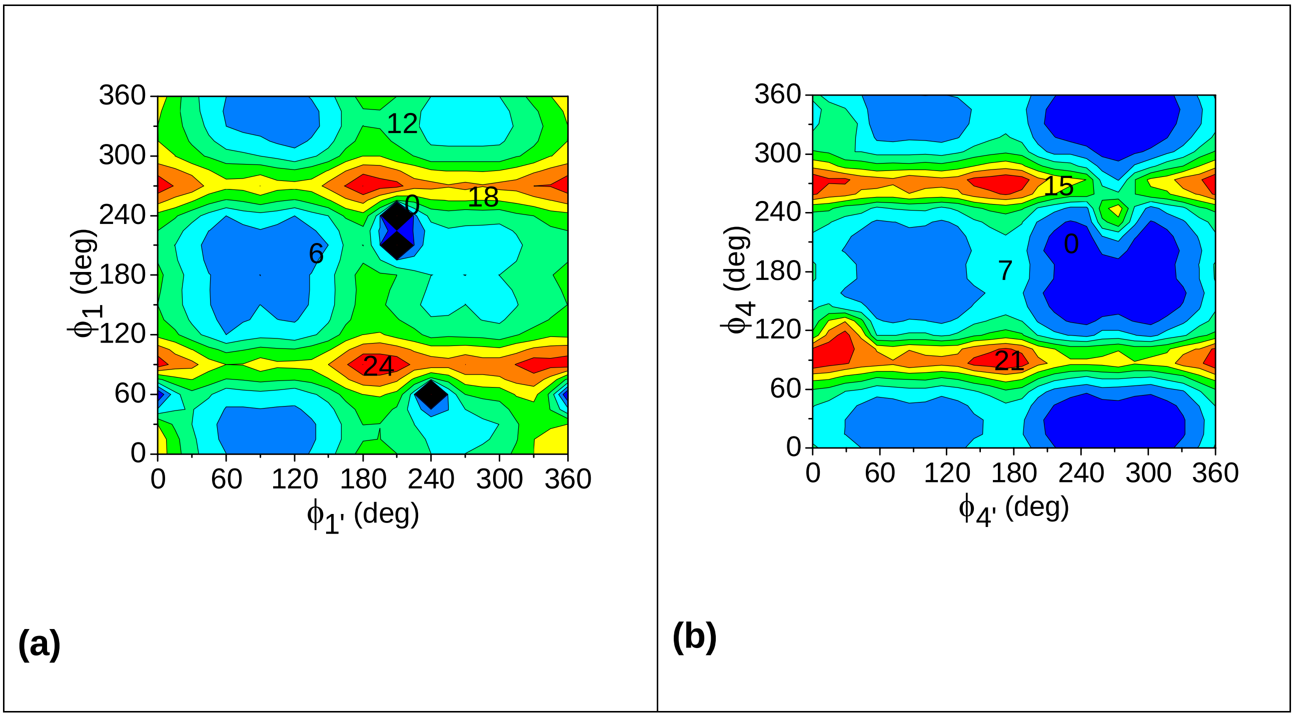

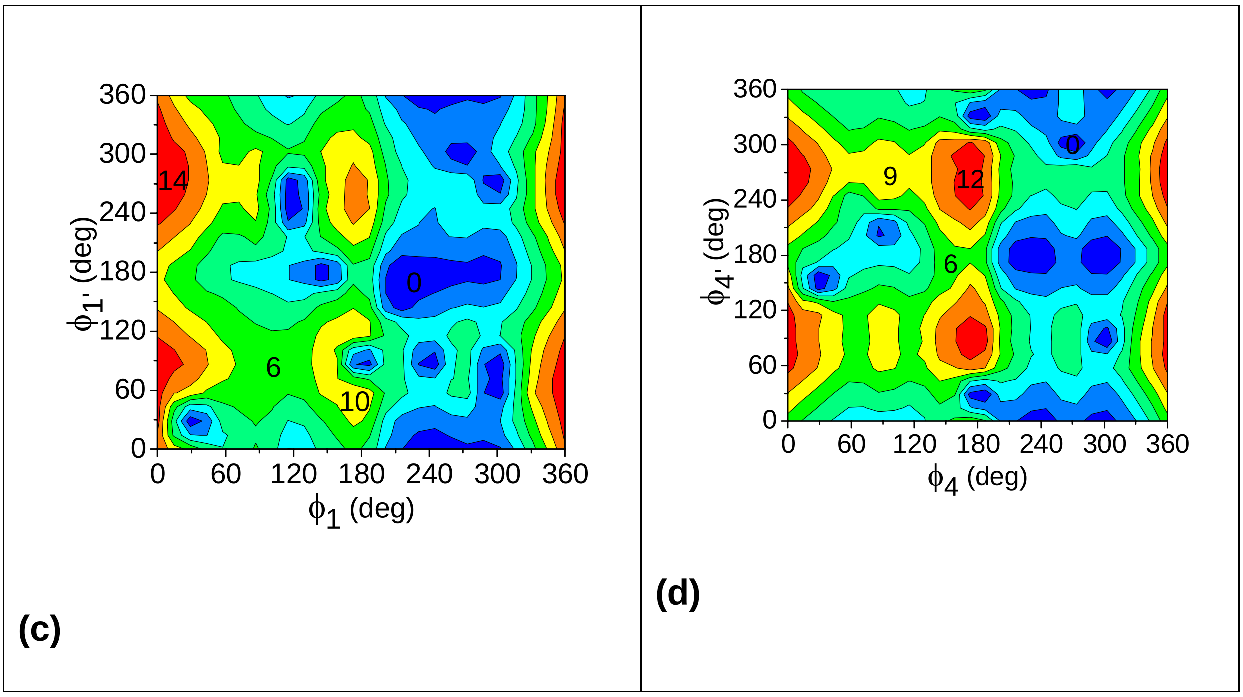

Fig. 61 Two-fold potential energy surface scans (HF) related to the torsion angles ϕ_1, ϕ_1' and ϕ_4, ϕ_4'. a: **H1**, b: **H2**, c: **H3**, d: **H4** (energy values in kJ mol^{-1}).

7.3.3 Dipole moments, bending angles and polarizabilities

The dipole moment, diagonal components of polarizability and bending angle values of the most stable conformations for the considered systems are given in the Table 22. The values were obtained for the systems with terminal hexyloxy chains. The dipole moments values for the most stable conformations of systems **H1**, **H2** show that replacement of a -COO- by a -CONH- group increase the total dipole moment of the molecule by about 10 Debye [μ (**E1**) = 0.77 D]. However, a decrease in the value of diagonal component α_{xx} was observed in comparison to ester connecting group [α_{xx} (**E1**) = 916 atomic units].

Table 22 The dipole moment, polarizability and bending angle values of the most stable conformations for the systems **H1**, **H2**, **H3** and **H4** (DFT, R= -OC_6H_{13}).

System	μ_x	μ_y	μ_z	μ	α_{xx}	α_{yy}	α_{zz}	γ
H1	1.12	-11.54	4.24	12.34	773.32	609.24	360.26	117
H2	1.31	-10.84	2.61	11.23	785.12	587.22	380.49	121
H3	-5.05	-5.39	-1.10	7.47	864.79	497.54	337.46	133
H4	-7.55	-3.77	-2.73	8.84	965.62	537.27	280.13	120

Dipole moment in Debye; polarizability in atomic units; bending angle in degree

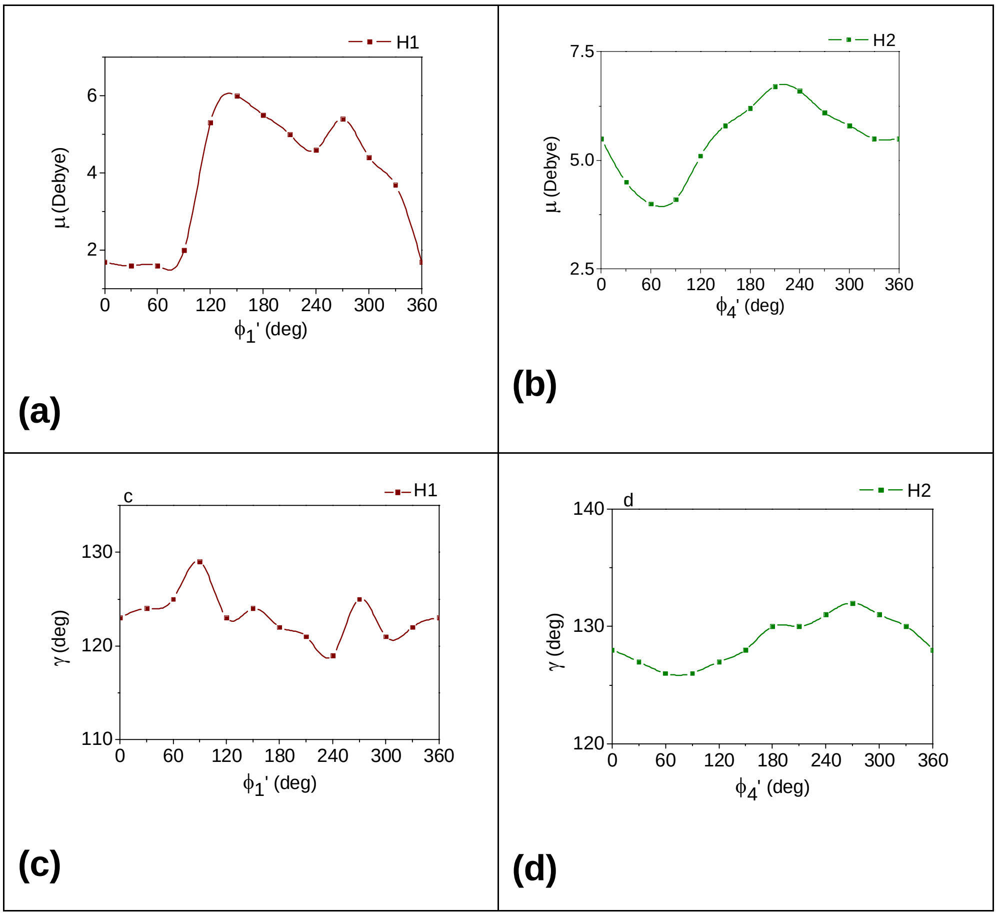

Fig. 62 Dependency of dipole moment (a, b) and bending angle values (c, d) for the systems **H1** and **H2** (HF, R= -OC_6H_{13})

By changing the position of the amide linkage group a decrease in the total dipole moment value of about 1 Debye was observed (**H2**). From the values of systems **H3** and **H4**, hydrogen bonding within the bent-core increases the μ_x component values in comparison to **H1**, **H2** systems. By changing the position of the hydrogen bonding an increase in the μ_x component was observed. The values confirm the significant influence of hydrogen bonding on the dipole moment values. The dependency of dipole moment with respect to torsion angle ϕ_1 for the system **H1** and the dependency with respect to torsion angle ϕ_4 for the system **H2** were shown in Fig. 62. The lower dependency of bending angles was observed in the systems **H1**, **H2** in comparison to other type of bent-core molecules (see Chapters **3** and **4**). The γ values of the most stable conformations are about 120° except system **H3**. The hydrogen bond linkage between the rings A and B' (**H3**) increase the bending angle (see Table 22).

7.3.4 ESP group charges

The total electrostatic potential group charges (q/ESP = -ρ) on the rings of the bent-core give a global pattern of the electron density distribution on the wings of the bent-core molecules. For the calculation of ESP group charges on the rings A, B, B', C and C', the heavy atoms were only considered. The ESP group charge results were illustrated for the systems **H1**, **H2** in Fig. 63a. The change in the position of the amide connecting groups causes a decrease of total electron density of the central aromatic ring (**H2**). The electron density distribution in the systems **H3** and **H4** is shown in Fig. 63b. The four systems show almost same electron density pattern on the aromatic rings in the bent-core with the sequence ρ (C, C') > ρ (B, B') > ρ (A) (see Fig. 63). This charge distribution is similar to the system **E1** in chapter **4**.

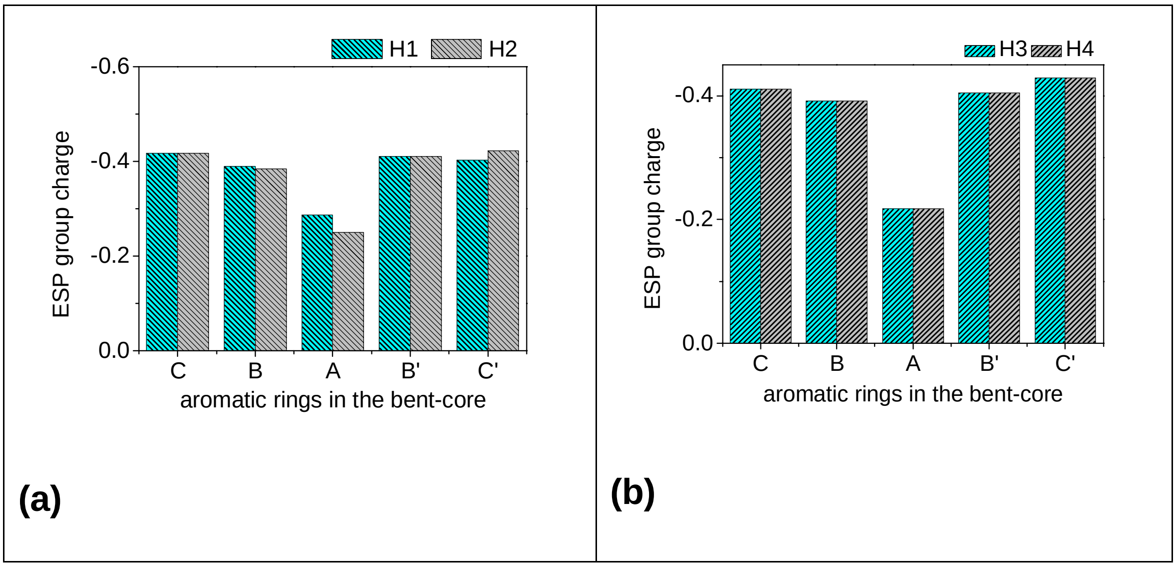

Fig. 63 Electrostatic potential group charges (DFT) on the centers of the rings for the systems **H1**, **H2, H3** and **H4**.

7.3.5 Proton transfer on the bent-core units

The proton transfer is an interesting phenomenon in ferroelectric and antiferroelectric materials. The system **H4** forms a SmCP phase and **H3** forms only a SmA phase. However, we have considered both systems for comparison. The proton transfer process was calculated on HF/STO-3G level by increasing the O-H bond length was with the step size of 0.1Å from 1 to 2Å using a partial optimization procedure. A simple representation of systems **H3** and **H4** was shown in Fig. 64.

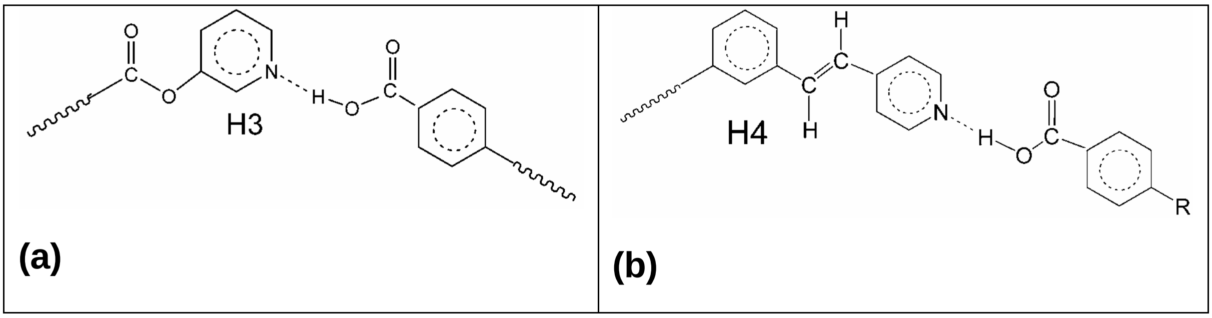

Fig. 64 Systems **H3** and **H4** (simplified)

The energy change during the proton transfer process (O–H---N) was illustrated in Fig. 65. The O-H---N is more stable than the O---H–N by around 180 kJ mol^{-1} for both systems. The larger energy difference in the proton transfer process may be due to overestimation of HF/STO-3G method with small basis set.

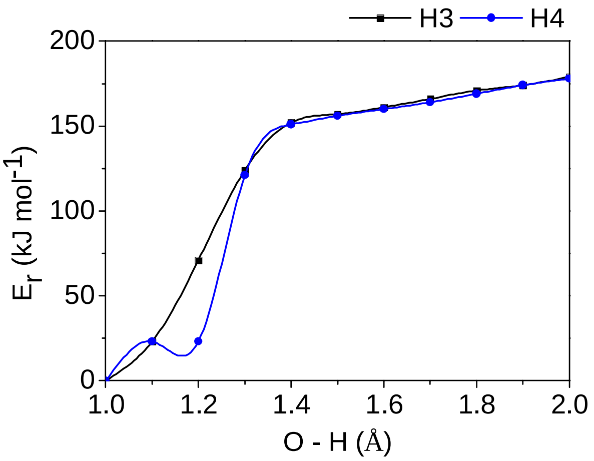

Fig. 65 O–H→N proton transfer process for the system **H3** and **H4**.

7.4 MD results – Dimers

7.4.1 Trajectory of torsion angles

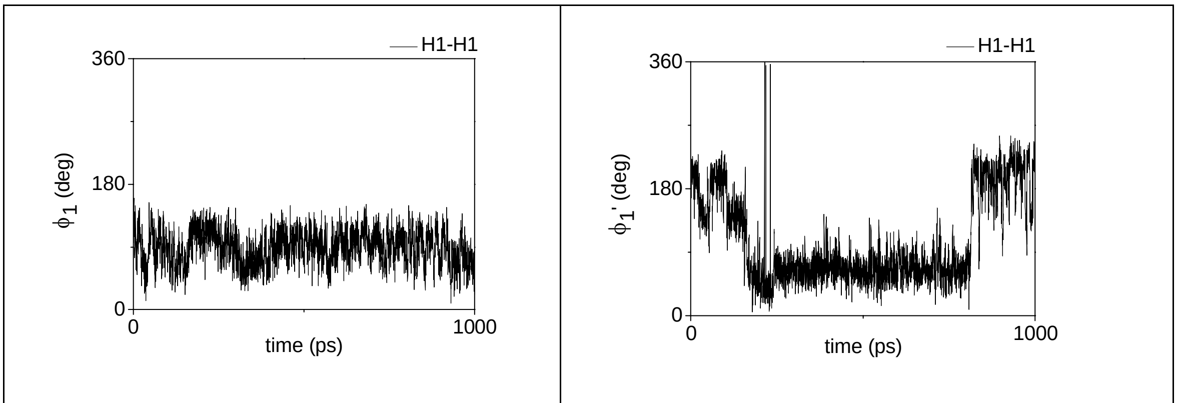

(a) C-O

(b) C-N

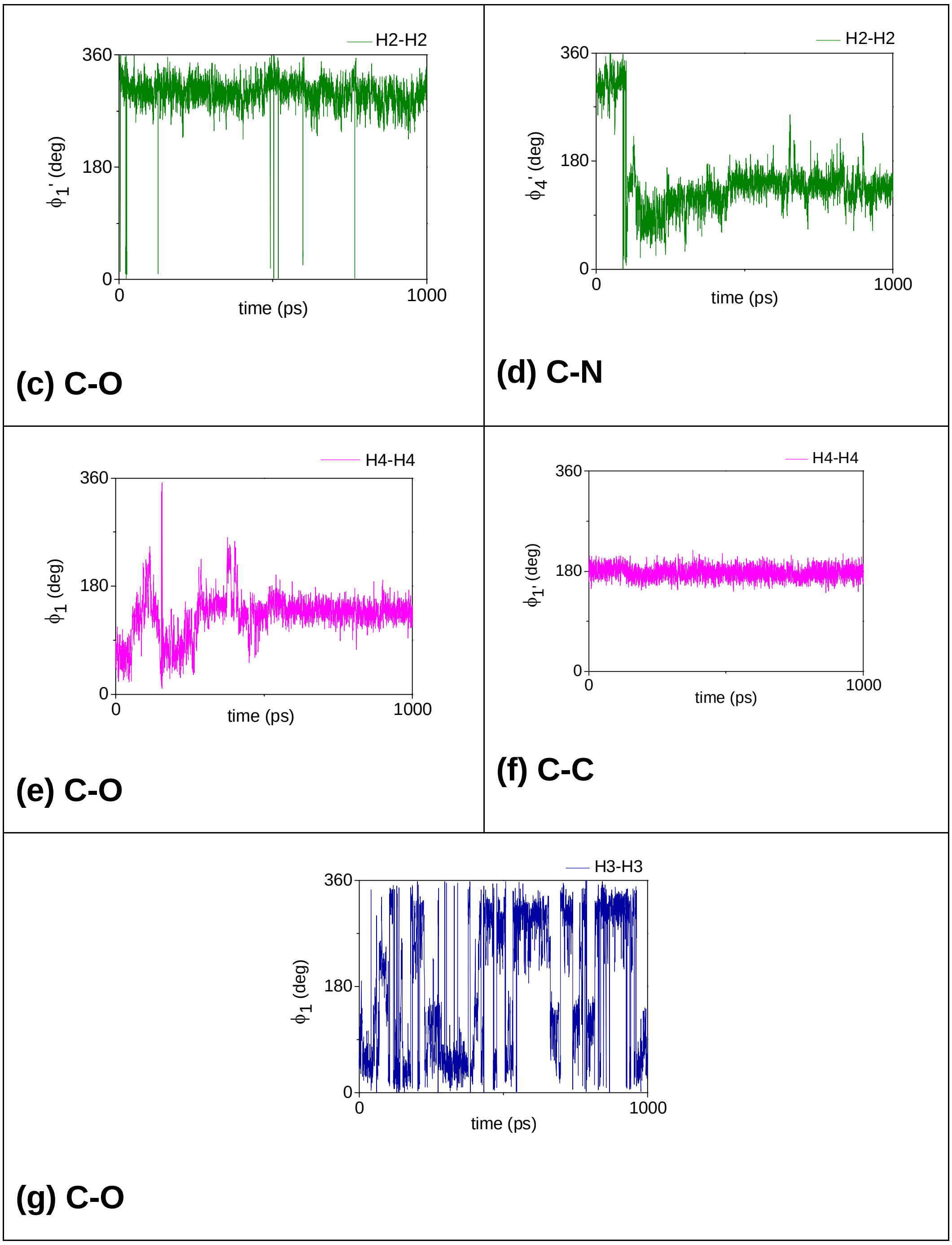

Fig. 66 Trajectories of significant torsion angles for the systems **H1-H1**, **H2-H2**, **H3-H3** and **H4-H4**.

The MD simulations were carried out on four different systems on a dimer level in vacuum with cutoff value of 10000 pm. The trajectories of the torsion angles were presented from the last 1 ns of the MD run with total 2ns time period. The Figs. 66a and 66b illustrate the trajectories of torsion angles around C-O bond (ϕ_1) and C-N bond (ϕ_1'). The considerable coupling effect has been observed on the flexibility of the C-O bond (ϕ_1) in the system **H1-H1** by the neighboring amide connecting group (ϕ_1') and the adjacent molecule. In the case of system **H2-H2** the position of the amide group is the linkage between rings B' and C'. However, a coupling effect on the flexibility of the C-O bond retains. For the system **H3-H3**, the trajectory around the bond C-O related to torsion angle ϕ_1 was shown in Fig. 66g. The hydrogen bonding is not stabilized during the MD run in vacuum. Therefore, the high flexibility of the C-O bond was observed. In Fig. 66e and 66f, the trajectory of torsion angles ϕ_1 and ϕ_1'for the system **H4-H4** were shown. In this system the neighboring CH=CH unit cause a considerable coupling effect on the flexibility of the C-O bond as the amide connecting groups.

In order to estimate the stability of the hydrogen bonding, we have calculated the trajectory of the corresponding N-O distance for the considered four systems. In the systems **H3-H3** and **H4-H4**, the hydrogen bonding was not stabilized during the MD run in vacuum. In the case of systems **H1-H1** and **H2-H2** it was stabilized.

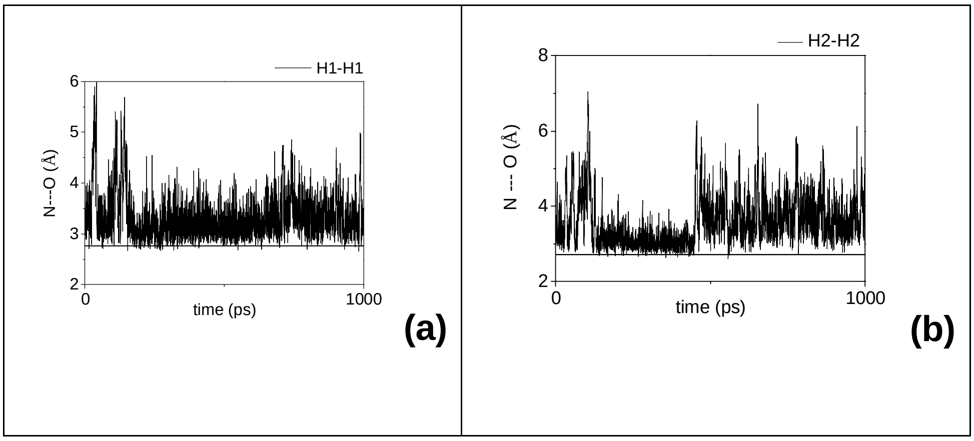

Fig. 67 The trajectories of the N-O distances (O-H---N) for the systems **H1-H1** and **H2-H2**.

The trajectories of the corresponding N-O distances were given in Fig. 67 for the systems **H1-H1** and **H2-H2**. For the system **H1-H1** the N-O distance retains near the value of 2.8 Å. In the case of system **H2-H2 t**he N-O distance is fluctuating to higher values during the MD run (Fig. 67). The results support that the type of hydrogen bonding in **H1-H1** (A, B’ linkage) is energetically more stable than that one in the **H2-H2** (B’, C’ linkage).

Chapter 8 Ferroelectric, antiferroelectric and B_7 mesophase model

In this chapter ferroelectric (FE), antiferroelectric (AF) structural models will be discussed for the various systems in terms of the energy by molecular mechanics calculations with AMBER force field. We have proposed a structural model for one of the interesting banana (B) mesophase B_7 [3, 5, 7and 99]. From the investigations of various types of bent-core molecules some new bent-core structures have been proposed.

8.1 Systems and explanations

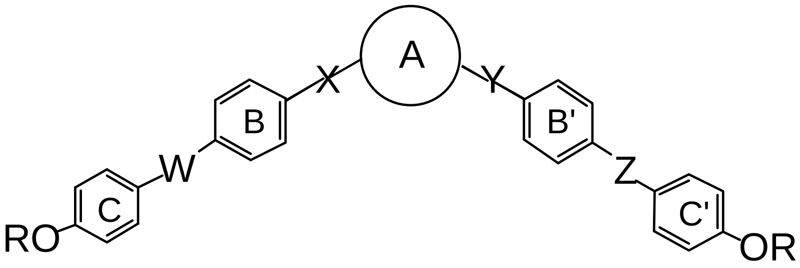

Fig. 68 The general structures of the considered systems.

We have considered totally eight systems **S1**, **S4**, **S12** (please see chapter 3) **E1**, **E3** (please see chapter 4) **U2**, **U3** and **U4** (please see chapter 6) which are already discussed in the previous chapters. Within the molecular mechanics calculations the terminal alkoxy chains of the mesogenic bent-core compounds were considered ($C_8H_{17}O$- alkoxy chains - for the systems **S1**, **S4**, and **S12**, $C_{12}H_{15}O$- alkoxy chains - for the systems **E1**, **E2** and $C_{14}H_{29}O$- alkoxy chains - for the systems **U2**, **U3** and **U4**).

8.2 Computational details

As described in the chapter 3, molecular mechanics calculations were carried out with an implemented AMBER program using gaff force field. The ferroelectric, antiferroelectric models were prepared on basis of reference [3]. The molecular mechanics calculations were performed with the cut-off radius value of 20Å using full optimization procedure and periodic boundary conditions. Totally, 32 molecules were considered in the ferroelectric and antiferroelectric models in a 4 × 4 × 2 ordered arrangement. The optimized conformations of the monomers were used as starting structures for the layers. The intermolecular distances between the molecules in the inplane and stacking orientations were used from the optimized values for the dimers of the corresponding systems. The proposed helical structural model of the B7 meso phase was created within AMBER program. The SEQUENCE command was used to create the helical arrangement of the bent-core molecules of system **S12**. The energy value and direction of the dipole moment were compared with the corresponding antiferroelectric and ferroelectric structural models.

8.3 The energies of the structural models

The energy of the ferroelectric and antiferroelectric models for the different systems was presented in Table 23. The FE and AF models for the system **S1** (P-8-O-PIMB: simplified explanation of the system) were shown in Fig. 69.

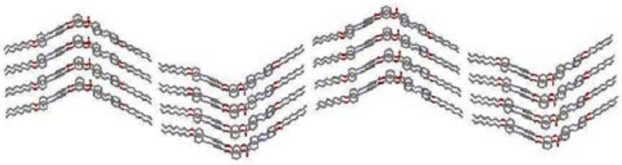

Fig. 69 Starting structure for the minimization of antiferroelectric model of the system **S1** (hydrogen atoms are not shown)

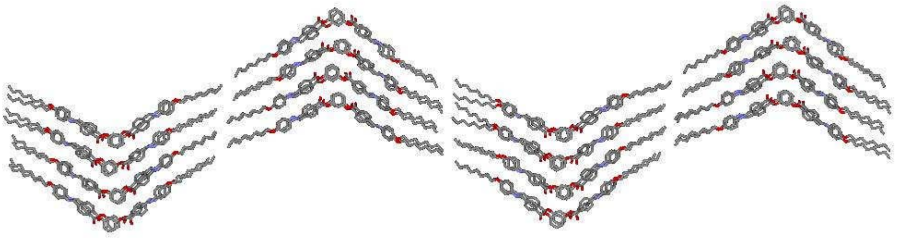

Fig. 70 Minimized structure for the antiferroelectric model of the system **S1** (hydrogen atoms are not shown)

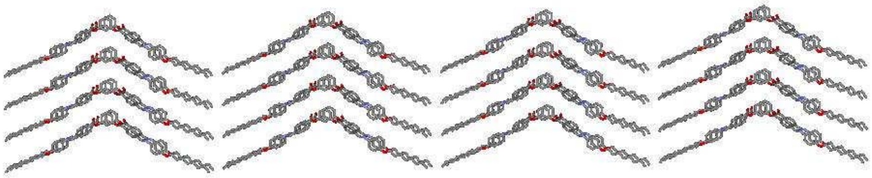

Fig. 71 Starting structure for the minimization of the ferroelectric model of the system **S1** (hydrogen atoms are not shown)

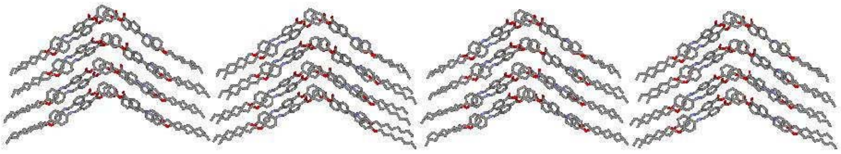

Fig. 72 Minimized structure of the ferroelectric model of the system **S1** (hydrogen atoms are not shown)

It is remarkable that the stability of the alternative arrangements of the clusters for the systems rather different. The ΔE ($\Delta E = E_{FE} - E_{AF}$) values differ in sign and amount (Table 23).

Table 23 The energy values of the antiferroelectric and ferroelectric models for the different systems calculated by AMBER

System	AF	FE	$\Delta E = E_{FE} - E_{AF}$	Mesophase [3,91,94]
S1	**-17183**	**-17192**	**- 9**	**$SmCP_A$**
S4	**-25706**	**-25589**	**117**	**$SmCP_A$**
S12	**-19288**	**-19455**	**- 167**	**$SmCP_F$**
E1	**-44547**	**-44760**	**- 213**	**$SmCP_F$**
E3	**-17727**	**-17894**	**- 167**	**$SmCP_A$**
U2	**-17183**	**-16999**	**184**	**$SmCP_A$**
U3	**-25739**	**-25664**	**75**	**$SmCP_A$**
U4	**-15970**	**-15832**	**138**	**$SmCP_A$**

The energy values in kJ mol^{-1}.

A small energy difference between the two polar states was observed only in the system **S1** and a large energy difference between them was found for the system **E1**. In some way the energy difference between the two states can give some insight about the switching possibility of the molecules between the FE and AF electric states and these energy calculations can support the triangular wave experiments which are traditional experimental methods for determining ferroelectric and antiferroelectric states of such materials [3]. Moreover, the results confirm that the energy difference between the two states essentially depends on the molecular structure

8.4 A proposed helical model for the B7 mesophase

One of the interesting mesophase formed by bent-core molecules is the B7. The optical texture of the B7 mesophase is given in Fig. 73.

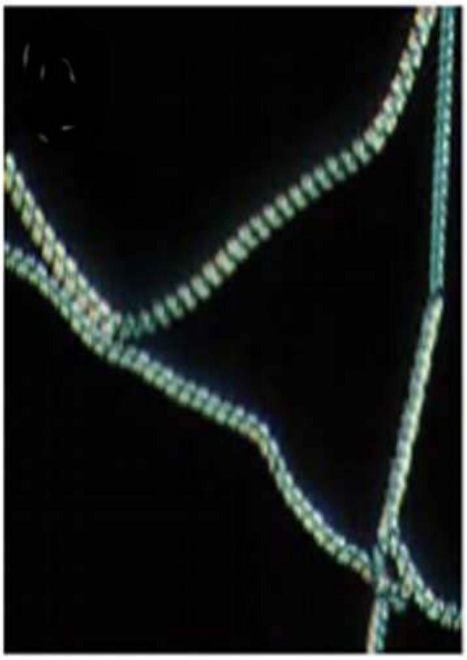

Fig. 73 A typical helical growth of B7 mesophase texture [3,5-7]

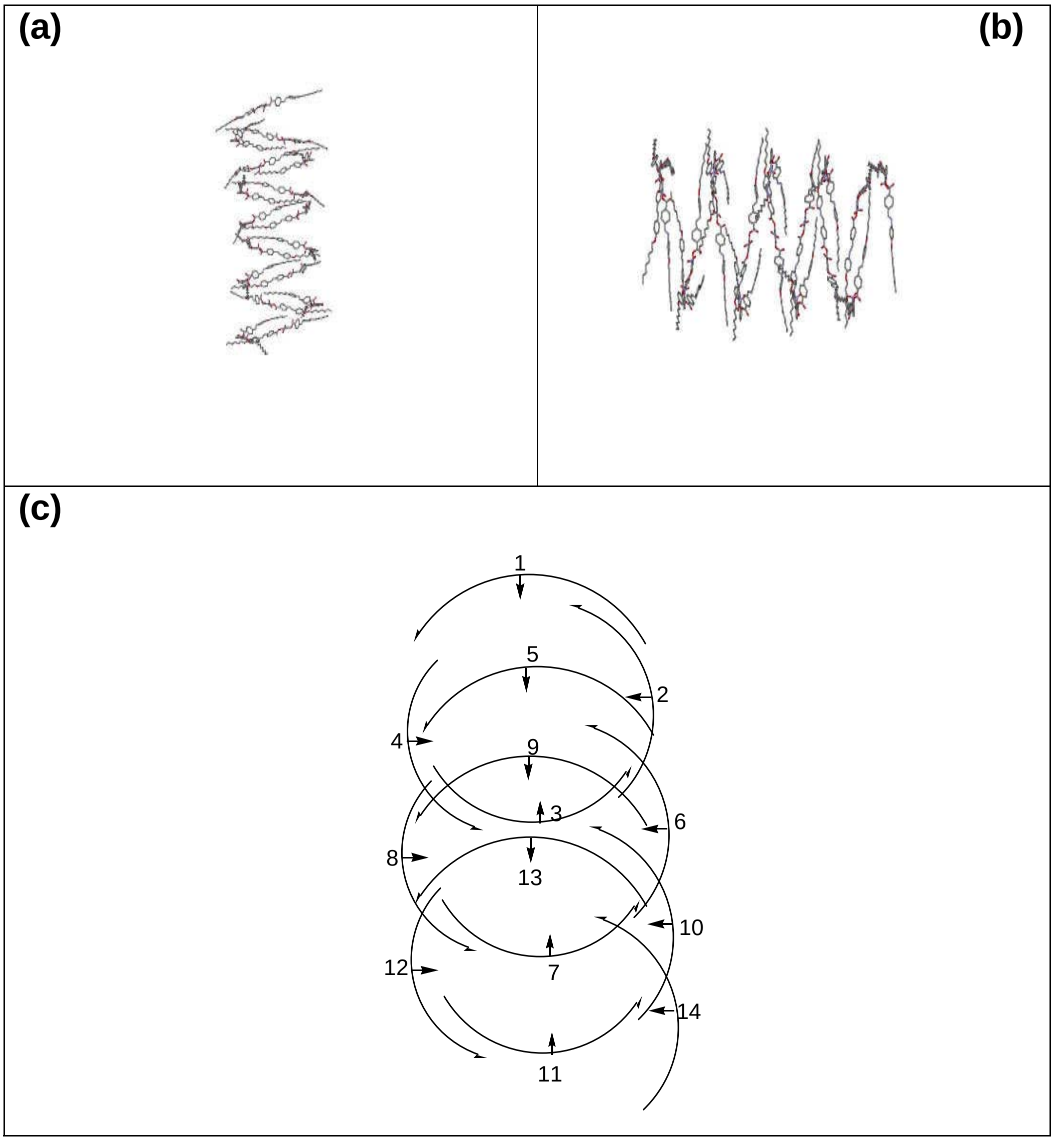

Fig. 74 A helical structure by bent-core molecules: (a,b): different views, (c): direction of the dipole moment in the bent-core molecules is indicated by arrows.

The interest on these mesophases comes by its extraordinary optical textures. [3,5-7]. We have considered the **S12** system for this helical model which forms the B7 mesophase. The energy calculations support that the FE state is more stable than the AF state for this system by 167 kJ mol^{-1}. There was an undulated layer structural model proposed for this mesophase to explain the splay polarization in literature [99]. In the Fig. 73, the typical optical texture of B_7 mesophase is shown. The proposed helix model for the B_7 mesophase was given in the Fig. 74. The direction of the dipole moments in the molecules within the helix was indicated by the direction of the arrows which is shown in Fig. 74c. The proposed helical model structure of the system **S12** is energetically (847 kJ mol^{-1}) less stable than the most stable ferroelectric model structure of that system. However, essentially the model has been proposed on the basis of to explain the possiblility of helical arrangement of the bent-core molecules and third type of the polarization which is different from the polarization of classical AF and FE polar states.

8.5 Proposed new bent-core structures

8.5.1 Halogen bonding in bent-core mesogens

The hydrogen bonding and halogen bonding are becoming useful concepts in supramolecular chemistry. Halogen bonding is the noncovalent interaction between halogen atoms (Lewis acids) and neutral or anionic Lewis bases. This interaction occurs in presence of electron poor halogen atom and electron rich Lewis base. A first indication of the relative strength of the hydrogen and halogen bonding came from solution calorimetry which is a simple and convenient tool to study weak intermolecular interactions [100, 101]. A complex formation enthalpy (ΔH_f) of 31.4 kJ mol^{-1} was measured for the dimer between 1-iodoperfluorohexane and 2,2,6,6-tetramethylpiperidine [103] and a prototype hydrogen-bonded complex (triethylamine/n-butanol) gave ΔH_f 23 kJ mol^{-1} [104, 105]. K.E. Riley *et al* [100] reported that the interaction energy of the halogen bonding is 2.39 kcal mol^{-1} in iodobenzene-formaldehyde complex ($distance_{I---O}$ is 3.2 Å, $angle_{I---O-C}$ is 110°) by MP2/6-31+G** level of theory calculations. Recently linear shaped mesogenic molecules with halogen bonding [102] and bent-core molecules with hydrogen bonding were reported [95 ,96]. The stability of halogen bonding and hydrogen bonding is comparable. Therefore, the bent-core structures with halogen bonding were proposed. This is just an attempt to design such a type of molecules. The proposed new bent-core model structures were given in Fig. 75.

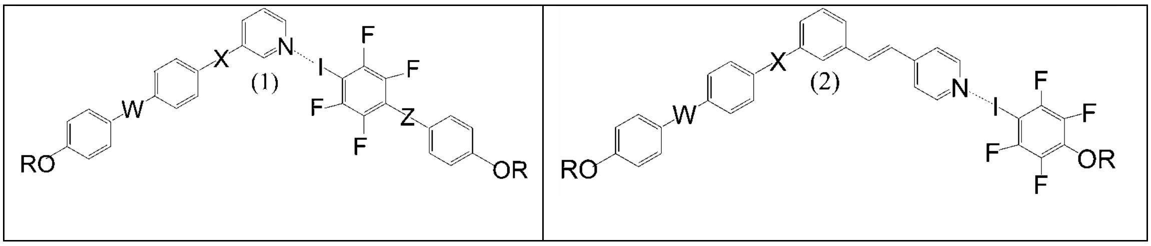
(1)
RO
W
X
N
I
F
F
F
F
Z
OR
(2)
RO
W
X
N
I
F
F
F
F
OR

Fig. 75 Bent-core molecules containing halogen bonding, in the models **(1)**, **(2)**. In which W, X, Y and Z are the ester connecting groups and -OR indicates the terminal alkoxy chains.

9 Summary

In this work various types of five-ring bent-core molecules have been investigated including different central units, various linkage groups, substitutions on the central and external phenyl rings and hydrogen bonded systems (Fig. 76). The conformational and polar properties of isolated bent-core molecules were carried out by *ab initio* calculations on the HF/STO-3G (Hartree Fock) standard and DFT (density functional theory) studies on the B3LYP/6-31G(d) level.

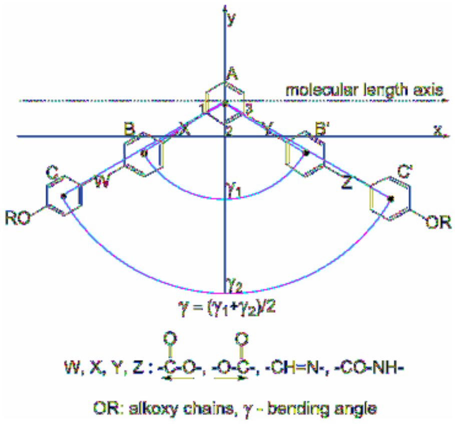
y
A
molecular length axis
1
2
3
B
X
Y
B'
x
C
W
Z
C'
RO
OR
γ_1
γ_2
$\gamma = (\gamma_1+\gamma_2)/2$
W, X, Y, Z : -C(=O)-O-, -O-C(=O)-, -CH=N-, -CO-NH-
OR: alkoxy chains, γ - bending angle

Fig. 76 The general structure of five-ring bent-core mesogens with explanation of the coordinate system, bending angle γ and connecting groups (W, X, Y, Z) and terminal chains (–OR).

Relaxed rotational barriers, dipole moments, polarizabilities, molecular lengths, bending angles and electrostatic potential (ESP) group charges as well as the influence of an external electric field were mainly obtained from DFT studies. Two-fold potential energy surface (PES) scans were performed within the HF/STO-3G method to reduce the computational effort on the large bent-core molecules. The applicability of the HF method with the small basis set on the bent-core system was checked. Investigations on alternative arrangements (stacking and inplane) on dimers of banana-shaped molecules were carried out by molecular mechanics calculations using the AMBER force field. Moreover, molecular dynamics (MD) simulations were performed on monomers and clusters of bent-core molecules with up to 128 monomers. The aggregation effect on such molecules was studied in more detail by a comparison of significant properties of the isolated molecule in the gas phase and a molecule in cluster environment. The effect of temperature, size and pressure on the aggregation behavior of the clusters was studied. The bending angle (γ) is a significant parameter of bent-core systems (see Fig. 76). A simple model was used to define the bending angle for the five-ring bent-core mesogens.

Comparison with X-ray structure

Both the most stable HF and DFT conformers of the 4,6-dichloro substituted compound (**S4**) show twisted conformations. This is in agreement with the X-ray structure of this compound and supported by a superposition of the three structures. The bending angles (γ) of the HF and DFT structures are smaller than that one from the solid state X-ray structure. The average structure from MD on clusters is in a better agreement with X-ray results than the HF and DFT findings. This is due to the including of neighboring effects in the cluster environment.

Polar Substitution

Overall twelve different substituted bent-core molecules with polar substituents at the central and outer phenyl rings were investigated. The substituents at the central 1,3-phenylene unit has the larger effect on the bending angle values than the bent-core systems with polar substituents on the external phenyl rings which is shown by the results of the bent-core molecule **S12** with nitro substitution in the 2 position of the central ring (A) and the dichloro substituted system **S4**. The calculated bending angle for the system **S4** is in agreement with nuclear magnetic resonance (NMR) measurements in the liquid crystalline state. The chlorine in the 4,6-positions (**S4**) and nitro group in 2 position (**S12**) of the central 1,3-phenylene unit reduce the conformational flexibility of the bent-core molecules. The total dipole moment of the molecules was reduced by the 2 nitro substitution (**S12**). The fluorine **S5** (chlorine **S8**) substitution on the external phenyl rings adjacent to the alkoxy chains of the bent-core molecules increase (decrease) the flexibility of the terminal alkoxy chains which was shown by relaxed rotational barriers in comparison to the unsubstituted system. The intermolecular distances are significantly altered by dichloro substituents (**S4**) in the central ring (A) both in stacking and inplane directions. The MD results of the clusters on the 4,6-chlorine substituted (**S4**) and 2-nitro substituted **(S12)** system were compared with the unsubstituted system **S1**. The long range order is increased in system **S12** and reduced in system **S4**. The chlorination in 4,6-positions (**S4**) can induce significant perturbations in the conformations of monomers and influence the aggregation of the bent-core molecules. The effect is more distinct in the curves of the radial atom-pair distribution functions g(r) at clearing temperature.

Different orientations of ester connecting groups

The different orientation of ester linkage groups on bent-core molecules with 1,3-phenylene unit was studied in a systematical way on the ten bent-core isomers. The relaxed rotational barriers related to C-O and C-C bonds of ester connecting groups are obtained by B3LYP/6-31G(d) level calculations. The C-O linkage increase and C-C linkage decrease the flexibility of the bent-core molecules. The flexibility of the terminal alkoxy chains in the ten isomers can also be changed by the different orientation of ester connecting groups in the W, Z positions (see Fig. 76). No coupling effect has been observed by different orientation of ester connecting groups on the flexibility of neighboring connecting groups. The total dipole moments of the molecules were altered from 1 Debye to 8 Debye. A good correlation was obtained between the calculated dipole moments and the experimental static dielectric constants values by Kirkwood model in the bent-core isomers. In the presence of an external electric field, a significant increase of the total dipole moment of the bent-core molecules was obtained. In a limited way, a correlation between the ESP group charges on the rings and mesophase properties were observed in the ten isomers. If the electron density (ρ) on the central ring is smaller than that one of the external rings [ρ (A) < ρ (C, C’)] there is a tendency to form smectic phases. The opposite case [ρ (A) > ρ (C, C’)] can be seen as an indicator of favoured formation of columnar phases. The intermolecular distance is not altered by changing the direction of ester connecting groups in bent-core molecules.

Remarkable size and pressure effects were observed in clusters with 64 and 128 molecules with respect to their aggregation behavior.

Bent-core vs. linear isomers

The difference between mesogenic isomers with central 1,3-phenylene (bent) and 1,4-phenylene (linear) units was analyzed from single molecule to clusters. No difference was found on the conformational flexibility between the linear and bent-core isomers. The bent-core isomer shows a symmetrical electron density distribution and linear isomer shows asymmetrical electron density distribution. A small difference on the electron density distribution on the aromatic rings was observed. The order of structure formation in the clusters with 64 monomers is larger in the **E1** than in the **L1** system. The increase of the pressure from 1 to 500 bars leads to a significant change in the g(r) curves of the linear and bent-core isomers.

Cyclic urea - a new central unit

Four different new types of bent-core molecules with a cyclic urea central unit have been investigated. A five-membered (**U1**), two six-membered (**U2**, **U3**) and a seven-membered (**U4**) with central cyclic urea units were included. Systems **U2** and **U3** differ by the alternative orientation of ester linkage groups. The relaxed rotational barrier related to N-C bond shows a lesser flexibility in the system **U1** in comparison to other three systems. A certain even-odd effect has been observed on the flexibility and the values of the dipole moment. Moreover, the bending angle of **U1** (γ=140°) is significantly larger than for the other systems. This can be seen as a hint that **U1** forms only smectic phases without any polar order. In the considered systems, the higher ESP group charges on the central unit (A) correlates with low clearing temperatures of the systems. Results of the two-fold scans on bent-core systems with central 1,3-phenylene, 3,4’-biphenylene, 2,7-napthalene units indicate that the flexibility of bent-core molecules with a central 2,7-napthalene unit is rather less.

Hydrogen bonding

In order to estimate the stability and flexibility of the bent-core molecules with hydrogen bonding, we have considered four different bent-core systems **H1**, **H2**, **H3** and **H4**. In the systems **H1** and **H2**, the hydrogen bonding occurs between two bent-core units (**H1**---**H1, H2**---**H2**) through amide linkage groups. In **H3** and **H4**, the hydrogen bonding is used to build up the bent-core structure by pyridine and carboxylic acid units. The systems **H3** and **H4** differ from each other by the position of hydrogen bonding linkages in Y (**H3**) and Z (**H4**) positions (see Fig. 76). The flexibility related to the amide linkages (C-N) is lower (higher) than that one of a C-O (C-C) bond of ester linkage groups. Amide and ethylene linkage groups of such molecules have high coupling effects on the flexibility of the neighboring connecting groups. The two-fold scans related to ester and hydrogen bonding linkage groups show that the connection by hydrogen bonding indicates nearly the same conformational degree of freedom as O-C linkage. MD results on the four dimers show that the hydrogen bonding is less stable for the systems **H3-H3**, **H4-H4** in comparison to **H1-H1** and **H2-H2**.

Ferroelectric, antiferroelectric and B7 phase model

Molecular mechanics (AMBER) calculations on cluster with 32 monomers were performed for eight different bent-core systems including ferroelectric (FE) and antiferroelectric (AF) starting structural models. The energy difference $\Delta E = E(FE)-E(AF)$ for the alternative arrangement of the molecules differ in its sign and amount for the clusters of the systems **S1**, **S4**, **S12**, **E1**, **E3**, **U2**, **U3** and **U4**. In some way, the energy difference (ΔE) between the two states gives some basic hints about the switching possibility between them as well as the most possible polar state. The negative sign of the ΔE values shows the FE state is more stable than the AF state. Moreover, a helical structural model was proposed for the interesting B7 mesophase. The bent-core system with a nitro substitution in the 2 position of the central 1,3-phenylene unit (**S12**) was considered for the helical model. The helical model is significantly less stable than the corresponding ferroelectric model which is observed from the molecular mechanics optimization procedure. However, in some way the proposed model is suitable to explain another possibility of polarizations in such molecules. The concept of halogen bonding was considered on the bent-core mesogenic molecules.

Bibliography

1 (a). G. W. Gray: Molecular structure and properties of liquid crystals, Academic press Inc: New York, 1962. (b). G. W. Gray and P. A. Winsor: Liquid crystals and plastic crystals, John Wiley & Sons: New York, 1974, vol.1.

2 J. -C. Dubois, P. Le. Barny, M. Manzac and C. Noel: Hand book of liquid crystals; edited by D. Demus, J. Goodby, G.W. Gray, H. -W. Spiess and V. Vill, Wiley-VCH, Weinheim, 1998.

3 G. Pelzl, S. Diele and W. Weissflog: *Adv. Mater*., **11** (1999) 707.

4 J. W. Goodby, D. W. Bruce, H. Hird, C. Imrie and M. Neal: *J. Mater. Chem*., **11** (2001) 2631.

5 R. Amaranatha Reddy and C. Tschierske: *J. Mater. Chem.,***15**, (2005), 907.

6 M. B. Ros, J. L. Serrano, M. R. de la Fuente, and C. L. Folcia: *J. Mater. Chem*.,**15** (2005) 5093.

7 H. Takezoe, and Y. Takanishi: Jap. *J. Appl. Phys*., **45** (2006) 597.

8 D. Vorlander: Ber. *Dtsch. Chem. Ges*.,**62** (1929) 2831.

9 D. Vorlander and A. Apel: *Ber. Dtsch. Chem. Ges*., **65** (1932) 1101.

10 T. Akutagawa, Y. Matsunaga and K. Yasuhara: *Liq. Cryst*., **17** (1994) 659.

11 T. Niori, T. Sekine, J. Watanabe, T. Furukawa and H. Takezoe: *J. Mater. Chem*., **6** (1996) 1231.

12 D. R. Link, G. Natale, R. Shao, J. E. Maclennan, N. A. Clark, E. Korblova and D. M. Walba: *Science* **278** (1997) 1924.

13 D. Kruerke and G. Heppke: presented at Gordon Conf. Liquid Crystals, 1997, New Hampsure; Banana-shaped Liquid Crystal Workshop, 1997, Berlin.

14 T. Sekine, T. Niori, J. Watanabe, T. Furukawa, S. W. Choi and H. Takezoe: *J. Mater. Chem*., **7** (1997) 1307.

15 T. Sekine, T. Niori, M. Sone, J. Watanabe, S. W. Choi, Y. Takanishi and H. Takezoe: Jpn. *J. Appl. Phys*., **36** (1997) 6455.

16 H. Nadasi, “Bent-core mesogens-substituent effect and phase behaviour”, Martin-Luther-University Halle-Wittenberg, Dissertation, 2003.

17 J. P. Bedel, J. C. Rouillon, J. P. Marcerou, M. Laguerre, H. T. Nguyen and M. F. Achard: *Liq. Cryst*., **27** (2000) 1411.

18 W. Weissflog, H. Nadasi, U. Dunemann, G. Pelzl, S. Diele, A. Eremin and H. Kresse: *J. Mater. Chem*., **11** (2001) 2748.

19 R. Amaranatha Reddy and B. K. Sadashiva: *Liq. Cryst*., **30** (2003)1031.

20 H. Nadasi, W. Weissflog, A. Eremin, G. Pelzl, S. Diele, B. Das and S. Grande: *J. Mater. Chem*.,**12** (2002) 1316.

21 H. N. Shreenivasa Murthy and B. K. Sadashiva: *Liq. Cryst*., **29** (2002) 1223.

22 G. Dantlgraber, D. Shen, S. Diele, and C. Tschierske*: Chem. Mater*., **14** (2002) 1149.

23 D. A. Coleman, J. Fernsler, N. Chattham, M. Nakata, Y. Takanishi, E. Körblova, D. R. Link, R -F. Shao, W. G. Jang, J. E. Maclennan, O. Mondainn-Monval, C. Boyer, W. Weissflog, G. Pelzl, L -C. Chien, J. Zasadzinski, J. Watanabe, D. M. Walba, H. Takezoe and N. A. Clark, *Science* **301** (2003) 1204.

24 A. Eremin, H. Nadasi, G. Pelzl, S. Diele, H. Kresse, W. Weissflog and S. Grande: *Phys. Chem. Chem. Phys*., **6** (2004) 1290.

25 T. Imase, S. Kawauchi and J. Watanabe: *J. Mol. Struct*. ,**560** (2001) 275.

26 K. Fodor Csorba, A. Vajda, G. Galli, A. Jakli, D. Demus, S. Holly and E. Gacs-Baitz: Macromol. *Chem. Phys*., **203** (2002) 1556.

27 Y. D. Ronald, K. Foder Csorba, J. Xu, V. Domenici, G. Prampolini and C. A. Veracini: *J. Phys. Chem. B*., **108** (2004) 7694.

28 V. Domenici, L. A. Madsen, E. J. Choi, E. T. Samulski, C. A. Veracini: *Chem. Phys. Lett.,* **402** (2005) 318.

29 I. Cacelli and G. Prampolini: *Chem. Phys*., **314** (2005) 283.

30 M. P. Neal, A. P. Parker, C. M. Care: *Mol. Phys*., **91** (1997) 603.

31 P. J. Camp, M. P. Allen, A. J. Masters: *J. Chem. Phys*., **111** (1999) 21, 9871.

32 J. L. Billeter, R. A. Pelcovits: *Liq. Cryst*., **27** (2000)1151.

33 J. Xu, R. L. B. Selinger, J. V. Selinger, R. Shashidhar: *J. Chem. Phys*., **115**, (2001) 9, 4333.

34 R. Memmer: *Liq. Cryst*., **29** (2002) 483.

35 P. K. Maiti, Y. Lansac, M. A. Glaser, N. A. Clark: *Phys. Rev. Lett*., **88** (2002) 65504.

36 T. C. Lubensky, L. Radzihovsky*: Phys. Rev. E.,* **66** (2002) 031704.

37 S. J. Johnston, R. J. Low, M. P. Neal: *Phys. Rev. E*. ,**66** (2002) 061702.

38 Y. Lansac, P. K. Maiti, N. A. Clark: *Phys. Rev. E.* ,**67** (2003) 011703.

39 A. Dewar, P. J. Camp: *Phys. Rev. E*., **70** (2004) 70, 011704.

40 A. Dewar, P. J. Camp: *J. Chem. Phys*., **123** (2005)123, 174907.

41 S. Orlandi, R. Berardi, J. Steltzer, C. Zannoni: *J. Chem. Phys*., **124** (2006) 124, 124907.

42 N. Duff, J. Wang, E. K. Mann and D. J. Lacks: *Langmuir*., **22** (2006) 9082.

43 W. J. Hehre, R. F. Stewart and J. A. Pople: *J. Chem. Phys*., **51** (1969) 2657.

44 A. J. P. Devaquet, R. E. Townshend and W. J. Hehre: *JACS*, 98:**14** (1976) 4068.

45 R. Hoffmann: *J. Chem. Phys*., **39** (1963) 1397.

46 Z. Huckel: *Zeitschrift fur Physik*., **70** (1931) 203.

47 S. Huzinga: *J. Chem. Phys*., **42** (1965) 1293.

48 P-Q. Lowdin: Advances in quantum chemistry., **5** (1970) 185.

49 I. Mayer: *Chem. Phys. Lett*., **97** (1983) 270.

50 C. C. J. Roothaan: *Rev. Mod. Phys*., **23** (1951) 69.

51 J. C. Slater: *J. Phys. Rev.,* **36** (1930) 57.

52 W.J. Hehre, L. Radom, P.v.R. Schleyer and J. Pople: in *ab initio* molecular orbital theory, John Wiley & Sons, New York, 1986.

53 P. Hohenberg, W. Kohn: *J. Phys Rev*., **136** (1964) B864.

54 W. Kohn, L. Sham: *J. Phys Rev*., **140**, (1965) A1133.

55 A. D. Becke: *Phys Rev A*., **38** (1988) 3098.

56 C. Lee, W. Yang, R. G. Parr: *Phys Rev B*., **37**(1988) 785.

57 R. M. Dreizler, E. K. U. Gross: Density Functional Theory; Springer: Berlin, 1990.

58 R. G. Parr, W. Yang: Density-Functional Theory of Atoms and Molecules; Oxford University Press: New York, 1989.

59 R. G. Parr, W. Yang: *Annu Rev Phys Chem*., **46** (1995) 710.

60 W. Kohn, A. D. Becke, R. G. Parr: *J. Phys Chem*., **100** (1996) 12974.

61 A. R. Leach: Molecular modeling – principles and applications, Pearson education limited, Second edition, England, 2001.

62 N. H. March: Electron Density Theory of Atoms and Molecules; Academic: London, 1992.

63 E. S. Kryachko, E. V. Ludena: Energy Density Functional Theory of Many-Electron System; Kluwer: Dordrecht, 1990.

64 M. J. Frisch, G. W. Trucks, H. B. Schegel, G. E. Scuseria, M. A. Robb, J. R. Cheeseman, V. G. Zakrzewski, J. A. JR. Montgomery, R. E. Stratmann, J. C. Burant, S. Dapprich, J. M. Millam, A. D. Daniels, K. N. Kudin, M. C. Strain, O. Farkas, J. Tomasi, V. Barone, M. Cossi, R. Cammi, B. Mennucci, C. Pomelli, C. Adamo, S. Clifford, J.Ochterski, G. A. Peterson, P. Y. Ayala, Q. Cui, K. Morokuma,D. K. Malick, K. Raghavachari, J. B. Foresman, J. Cioslowski, J. V. Ortiz, B. B. Sefanov, G. Liu, A. Liashenko, P. Piskorz, I. Komaromi, R. Gomperts, R. L. Martin, D. J. Fox, T. Keith, M. A. AL-Laham, C. Y. Peng, A. Nanayakkara, C. Gonzalez, M. Chahacombe, P. M. W. Gill, B. G. Johnson, W. Chen, M. Wong, J. L. Andres, C. Gonzalez, M. Head-Gordon, E. S. Replogle and J. A. Pople: 1998, *Gaussian, Inc*, Pittsburgh, PA.

65 T. Clark: A Handbook of Computational chemistry, John Wiley & Sons, New York, 1985.

66 A. R. Leach: Molecular Modeling Principles and Applications Longman, Essex, 1996.

67 P. Kollman: *Ann. Rev. Phys. Chem.,* **38** (1987) 303.

68 N. L. Allinger: *Encycl. Comput. Chem*., **2** (1998) 1013.

69 D.A. Case, T.A. Darden, T.E. Cheatham, III, C.L. Simmerling, J. Wang, R.E. Duke, R. Luo, K.M. Merz, B. Wang, D.A. Pearlman, M. Crowley, S. Brozell, V. Tsui, H. Gohlke, J. Mongan, V. Hornak, G. Cui, P. Beroza, C. Schafmeister, J.W. Caldwell, W.S. Ross, and P.A. Kollman: (2002) AMBER 7, University of California, San Francisco.

70 (a). A. D. MacKerell, D. Bashford, M. Bellott, R. L. Dunbrack, J. D. Evanseck, M. J. Field, S. Fischer, J. Gao, H. Guo, S. Ha, D. Joseph-McCarthy, L. Kuchnir, K. Kuczera, F. T. K. Lau, C. Mattos, S. Michnick, T. Ngo, D. T. Nguyen, B. Prodhom, W. E. Reiher, B. Roux, M. Schlenkrich, J. C. Smith, R. Stote, J. Straub, M. Watanabe, J. Wiorkiewicz-Kuczera, D. Yin, M.

Karplus, *J. Phys. Chem. B.*, 102 (1998) 3586. (b). A. D. Jr. MacKerell, B. Brooks, C. L. Brooks III, L. Nilsson, B. Roux, Y. Won, M. Karplus, In *The Encyclopedia of Computational Chemistry;* P. v. R. Schleyer et al., Eds.; John Wiley & Sons: Chichester, Vol. 1 (1998) 271. (c). B. R. Brooks, R. E. Bruccoleri, B. D. Olafson, D. J. States, S. Swaminathan, M. Karplus: *J. Comput. Chem.*, **4** (1983)187.

71 W. R. P. Scott, P. H. Hunenberger, I. G. Ironi, A. E. Mark, S. R. Billeter, J. Fennen, A. E. Torda, T. Huber, P. Kruger, W. F. van Gunsteren: *J. Phys. Chem. A.,* **103** (1999) 3596.

72 T. A. Halgren: *J. Comp. Chem*., **17** (1996) 616.

73 S. Ananda Rama Krishnan, W. Weissflog, G. Pelzl, S. Diele, H. Kresse, Z. Vakhovskaya, and R. Friedemann: *Phys. Chem. Chem. Phys*., **8** (2006) 1170.

74 P. Auffinger, E. Westhof: *Encycl. Comput. Chem*., **3** (1998)1628.

75 H. J. C. Berendsen, D. P. Tielemen: *Encycl. Comput. Chem*., **3** (1998)1639.

76 R. M. Whitnell, K. B. Wilson: *Rev. Comput. Chem*., **4** (1993) 67.

77 W. F. van Gunsteren, H. J. C. Berendsen: *Angew. Chem. Int. Ed. Eng*. **29** (1990) 992.

78 W. W. Evans, G. J. Evans: *Adv. Chem. Phys*., **63** (1985) 377.

79 M. P. Allen and D. J. Tildesley: Computer Simulations of Liquids, Clarendon Press, Oxford, 1987

80 J. M. Haile: Molecular dynamics simulations, John Wiley & Sons, Inc, New York, 1997

81 S. Ananda Rama Krishnan, W. Weissflog and R. Friedemann: *Liq. Cryst*. **7** (2005) 847.

82 D. A. Case, T. E. Cheatham, T. Darden, H. Gohlke, R. Luo, K. M. JR. Merz, A. Onufriev, C. Simmerling, B. Wang, R. J. Woods: *J. Compt. Chem*., **26** (2005) 1668

83 A. Jakalian, B. L. Bush, D. B. Jack and C. L. Bayly: *J. Comput. Chem*., **21** (2000) 132.

84 R. Friedemann, S. Naumann and J. Brickmann: *Phys. Chem. Chem. Phys*., **3** (2001) 4195.

85 P. Monecke, R. Friedemann, S. Naumann and R. Csuk: *J. Mol. Model*., **4**, (1998) 395.

86 C. L. Brooks, M. Karplus and B. M. Pettitt, in Proteins: A theoretical perspective of dynamics, structures and Thermodynamics; Advances in chemical physics LXXI; John Wiley & Sons: New York, 1988.

87 J. G. Kirkwood: *J. Chem. Phys*., **7** (1939) 919.

88 H. Hartung, A. Stettler and W. Weissflog: *J. Mol. Struct*., **31** (2000) 526.

89 J. P. Bedel, J. C. Rouillon, J. P. Marcerou, M. Laguerre, H. T. Nguyen,

and M. F. Achard: *J. Mater. Chem*., **12** (2002) 2214.

90 H. Toriumi and E. T. Samulski, in Ordered Fluids & Liquid Crystals, Eds. Griffin, A.C. Johnson, J.F. Plenum: Press New York, London 1984 *4*, pp. 597-613.

91 W. Weissflog, G. Naumann, B. Kosata, M. W. Schroder, A. Eremin, S. Diele, H. Kresse, R. Friedemann, S. Ananda Rama Krishnan, G. Pelzl: *J. Mater. Chem*., **15** (2005) 4328.

92 J. G. Kirkwood: *J. Chem. Phys*., **5** (1939) 911.

93 H. Kresse, H. Schlacken, U. Dunemann, M. W. Schröder and G. Pelzl: *Liq. Cryst*., **29** (2002) 1509.

94 B. Glettner, S. Hein, R. Amaranatha Reddy, U. Baumeister and C. Tschierske: “Cyclic ureas as novel building blocks for bent-core liquid crystals”, *Chem. Comm*., accepted.

95 S. Findeisen: *"Influence of hydrogen bonding on the aggregation of bent-core molecules"*, Martin-Luther-University Halle-Wittenberg, Dissertation, 2007.

96 N. Gemino, M. B. Ros, J. L. Serrano and M. R. de la Fuente: *Angew. Chem. Int. Ed.*, **43** (2004) 5235.

97 J. Sworakowski: *Ferroelectrics*, **128** (1992) 295.

98 S. Horiuchi, T. Hasegawa, Y. Tokura: *J. Phys. Soc. Jpn.*, **75** (2006) 051016.

99 (a). A. Jakli, D. Kruerke, H. Sawade and G. Heppke: *Phys. Rev. Lett*. **86** (2001) 5715. (b). D.A. Coleman, J. Fernsler, N. Chattham, M. Nakata, Y. Takanishi, E. Korblova, D. R. Link, R. -F. Shao, W. G. Jang, J. E. Maclennan, O. Mondainn-Monval, C. Boyer, W. Weissflog, G. Pelzl, L. -C. Chein, J. Zasadzinski, J. Watanabe, D. M. Walba, H. Takezoe, N. A. Clark: *Science* **301** (2003) 1204.

100 P. Metrangolo, H. Neukirch, T. Pilati, G. Resnati: *Acc.Chem.Res*., **38** (2005) 386.

101 P. Auffinger, F. A. Hays, E. Westhof, P. Shing Ho, *PNAS*, 101.48, 16789.

102 E. Corradi, S. V. Meille, M. T. Messina, P. Metrangolo, G. Resnati: (2000) *Angew. Chem. Int. Ed.* **112,** 1852–1856.

103 E. M. Arnett, L. Joris, E. Mitchell, T. S. S. R. Murty, T. M. Gorrie, P. v. R. Schleyer: *JACS*. 1970, 92, 2365.

104 K. E. Riley, K. M. Jr. Merz: *J. Phys. Chem. A*., **111**(9), 1688, 2007.

105 P. Metrangolo, C. Prasang, G. Resnati, R. Liantonio, A. C. Whitwood, D. W. Bruce: *Chem. Comm*., 3290, 2006.

Abbreviations and symbols

B_n	banana-mesophases, n-used to designate the sub type of B-phases
B-factor	indicator of thermal motion of molecules
Col	columnar phase
C.T.K	Clearing temperature in Kelvin
d	layer distance
D	diffusion coefficient
DFT	density functional theory
E_r	relative energy
ESP	electrostatic potential
FWHM	full width at half maximum
g(r)	radial atom pair distribution function
g(o)	Orientational correlation function
HF/SCF	Hartree-Fock / self consistent field
K	Boltzmann’s constant
L_C	core length
L_T	total length of the molecule
L_{MD}	total length of the molecule from MD results
$\overline{L}_{MD}$	Average total length of the molecule from MD results
L_{MM}	total length of the molecule from MM calculations
$\overline{L}_{MM}$	Average total length of the molecule from MM calculations
MC	Monte Carlo
MD	molecular dynamics
MM	Molecular Mechanics
N	nematic phase

n, p, T	n – number of particles, p – pressure, T – temperature
PES	potential energy surface
RMSD	root mean square deviation
SmA	non-tilted smectic phase
SmC	tilted smectic phase
SmCP	tilted smectic phase with polar order
$\mathrm{SmC_sP_A}$	synclinically tilted antiferroelectric smectic phase with polar order
$\mathrm{SmC_sP_F}$	synclinically tilted ferroelectric smectic phase with polar order
$\mathrm{SmC_AP_A}$	anticlinically tilted antiferroelectric smectic phase with polar order
$\mathrm{SmC_AP_F}$	anticlinically tilted ferroelectric smectic phase with polar order
μ	dipole moment
$\bar{\mu}$	energy weighted dipole moment
γ	bending angle or bent-core angle
α	polarizability
α_{XX}, α_{yy}, α_{zz}	diagonal elements of polarizability
ε_0	dielectric constant
ρ	electron density
Φ, ϕ	torsion angles
ΔE_D	dimerisation energy

Curriculum Vitae

Ananda Rama Krishnan Selvaraj

EDUCATION

1992 – 1994	High School, Govt. Boys Hr.Sec. School Vridhachalam – India
1994 – 1996	Higher secondary, Neyveli Lignite Corporation Boys.Hr.Sec.School Neyveli - India
1996 – 1999	Bachelor of Chemistry Poompuhar College, Bharathidhasan University Tiruchirapalli – India.
2000 – 2002	Master of Chemistry, National Institute of Technology Tiruchirapalli – India
2002	Research fellow in Indian Institute of Sciences, Bangalore, India
2003 – 2004	Research Assistant, Raman Research Institute Bangalore, India
2004 – 2007	Doctoral thesis, Institute of Chemistry / Organic Chemistry Martin-Luther-Universität Halle-Wittenberg

PERSONAL INFORMATION

Name	Ananda Rama Krishnan Selvaraj
Date of birth	October 12th, 1978
Place of birth	Vridhachalam, India
Nationality	Indian
Martial status	Single

Place:Halle (Saale); Date: 08.08.2007

Erklärung

Hiermit versichere ich, dass ich die vorliegende Arbeit selbständig verfasst habe und keine anderen als die von mir angegebenen Quellen und Hilfsmittel verwendet habe. Diese Dissertation wurde bisher an keiner anderen Hochschule oder Universität vorgelegt.

Halle (Saale), den 08.08.2007